Diamond anvil cell and high-pressure physical investigations

A. Jayaraman

Bell Laboratories, Murray Hill, New Jersey 07974

The present status of high-pressure research with the diamond anvil cell (DAC) is reviewed in this article, mainly from an experimental aspect. After a brief description of the different types of DAC's that are currently in vogue, the techniques used in conjunction with the DAC in modern high-pressure research are presented. These include techniques for low- and high-temperature studies, x-ray diffractometry, spectroscopy with the DAC, and other measurements. Results on selected materials, with a view to illustrating the physics behind high-pressure phenomena, are presented and discussed. These include metal-semiconductor transitions, electronic transitions, phonons and high-pressure lattice dynamics, and phase transitions. A whole section is devoted to the behavior of condensed gases, principally H_2, D_2, O_2, N_2, and rare-gas solids. The concluding section briefly deals with speculations on ultra-high-pressure research with the DAC in the future.

CONTENTS

I. INTRODUCTION

Research at high pressure is very much dependent upon techniques, and every advance in the latter has resulted in a phenomenal expansion in our knowledge concerning the behavior of matter at high pressures. The Bridgman era (roughly from 1910 to 1950) was dominated by the so-called Bridgman anvil and the piston-cylinder device, both of which were invented and developed by Bridgman for electrical resistance and compressibility measurements up to 100 kilobar.[1] In the post-Bridgman era, Drickamer and his co-workers developed the ultra-high-pressure supported anvil devices for resistance, Mössbauer, x-ray diffraction, and optical absorption studies, and pioneered ultra-high-pressure research of the solid state. They extended the pressure range to several hundred kbar and discovered many new phenomena concerning the behavior of solids at high pressure (Drickamer, 1965, 1966). Concurrently, improved versions of the piston-cylinder device,

[1]Pressure is expressed in this article in kbar (kilobar) $=10^3$ bar and Mbar (megabar) $=10^6$ bar. Another unit of pressure currently in vogue is GPa (gigapascal) $=10^4$ bar (10 kilobar). One bar $=10^5$ N m^{-2} (pascal) $=0.9869$ atm $=1.0197$ kg cm^{-2}.

the belt apparatus, and the multiple-anvil devices became powerful tools in the hands of the high-pressure researcher for the study of phase transitions and material synthesis at high pressure and high temperature. Also, the extension of high-pressure techniques to very low temperatures had considerable success, and scores of new superconductors (elements that became superconducting at high pressure) were added to the list of superconducting elements and compounds.

Thus while a lot of new results at high pressure were accumulating, a rather quiet revolution in high-pressure generation techniques had taken place over a span of 15 years, resulting in the development of the diamond anvil cell (DAC). The DAC is fast becoming the most powerful ultra-high-pressure device, helping physicists and chemists discover new states of matter and understand the basic physics underlying ultra-high-pressure phenomena. The DAC has put the geophysicist nearer to the center of the Earth, for it is now possible to combine laser heating of the material in the DAC to simulate pressure and temperature conditions prevailing deep down in the Earth's interior (Bassett, 1979). Today a DAC capable of generating megabar pressures can fit into the palm of the hand and a variety of sophisticated measurements can be performed on materials of microscopic dimensions. For instance, optical absorption and reflectivity measurements, and Raman and Brillouin scattering studies to several hundred kilobar have become possible. Powder and single-crystal x-ray diffraction studies are becoming routine investigations with the DAC. The principle underlying the DAC, pressure calibration, and the capabilities of the DAC for physical and structural studies have been briefly reviewed by Block and Piermarini (1976) in *Physics Today*. Since the publication of the above there have been new developments. This article is a review on the DAC, its usefulness for physical investigations at high pressure, and new results.

Although it has been known that diamond is the hardest substance known to man and is quite transparent to x rays and light, its value for generation and containment of high pressure was not realized until 1950, when Lawson and Tang (1950) used a drilled three-carat single-crystal diamond (in a split-bomb configuration) with a miniature piston, for performing high-pressure x-ray diffraction studies. After the above attempt, the use of diamond for pressure generation was almost forgotten until 1959, when two different versions of the DAC, conceived independently, appeared on the scene; one for high-pressure x-ray powder diffraction study by Jamieson, Lawson, and Nachtrieb (1959) at the University of Chicago and the other for infrared absorption measurements by Weir *et al.* (1959) at the National Bureau of Standards (NBS). The former used a clamped DAC in 90° configuration (x-ray beam normal to the stress direction), while Weir *et al.* used the 180° transmission geometry (light beam coincident with the stress axis) and a spring-loaded lever-arm system integral with the DAC apparatus for applying thrust to the diamonds. Both the 180 °C transmission geometry and the spring-loaded lever-arm system have become essential features of the modern DAC, except for single-crystal x-ray diffractometry, where a screw-clamped DAC is preferred for the sake of compactness.

Since the original 1959 NBS version, development of the DAC for powder (Piermarini and Weir, 1962) and single-crystal x-ray diffraction (Weir, Block, and Piermarini, 1965), the introduction of the metal gasket technique for hydrostatic pressure generation (Van Valkenburg, 1965), the ruby fluorescence technique (Barnettt, Block, and Piermarini, 1973) for pressure calibration, the evolution of the pressure scale based on the R-line shift (Piermarini *et al.*, 1975; Piermarini and Block, 1975), introduction of new pressure transmitting media for hydrostatic pressures to 100 kbar (Piermarini, Block, and Barnett, 1973), generation of pressures of half a megabar in the gasketed anvil, and many innovative changes in the mechanical design (Piermarini and Block, 1975), all pioneered by the group at the NBS, have turned the DAC into a fine quantitative tool for modern physical research.

II. TECHNIQUES

A. Diamond cells

1. Generic types

The basic principle of the DAC is very simple. A sample placed between the flat parallel faces of two opposed diamond anvils (see Fig. 1) is subjected to pressure when a force pushes the two opposed anvils together. However, variations in the DAC arise from different ways in which the force-generating and the anvil-alignment mechanisms can be designed. Accordingly, five types of DAC's have evolved and these are illustrated in Figs. 2—6.

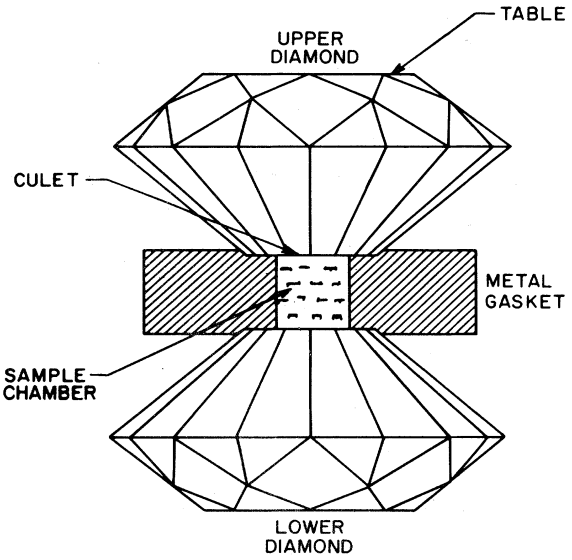

FIG. 1. Opposed diamond anvil configuration, with a metal gasket for sample confinement in a pressure medium; the basic part of the DAC.

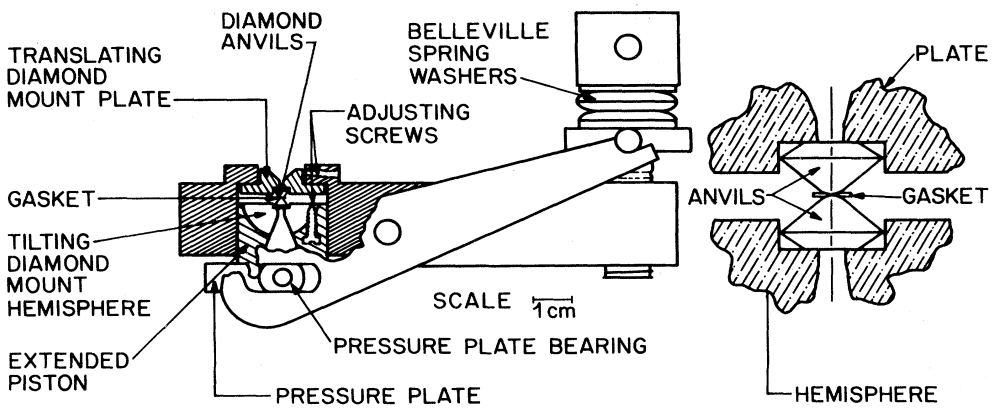

FIG. 2. Sectional view of the National Bureau of Standards ultrahigh-pressure DAC developed by Piermarini and Block (1975). On the right is the enlarged view of the anvils. Lower diamond set on hemispherical mount for alignment.

a. NBS cell

Figure 2 shows the DAC introduced by Piermarini and Block (1975) and represents a recent design of the NBS. The main body of the DAC consists of a rectangular plate 15×6 cm of about 2 cm in thickness, made of 4340 or Vascomax 300 steel, with suitable apertures near one end for the stationary and movable pistons. Force is produced by compressing Belleville spring washers by turns of the screw. The applied load is magnified by a factor of 2 on being transmitted via the lever-arm system to the pressure plate which bears against the extended end of the movable piston. The stationary diamond mount can be translated for centering purposes by three symmetrically situated (120° apart) adjusting screws, and is locked in position by two pulling screws, once centered. The hemispherical mount on the movable piston can be tilted in its socket by adjusting screws to secure parallel alignment of the diamond anvil flats, as determined by the optical interference fringe pattern. The diamond mounts are hardened to RC 55—60 and have suitable apertures for entry and exit of optical, x-ray, and other radiations through the diamonds. Pressures as high as 500 kbar have been reached with this DAC.

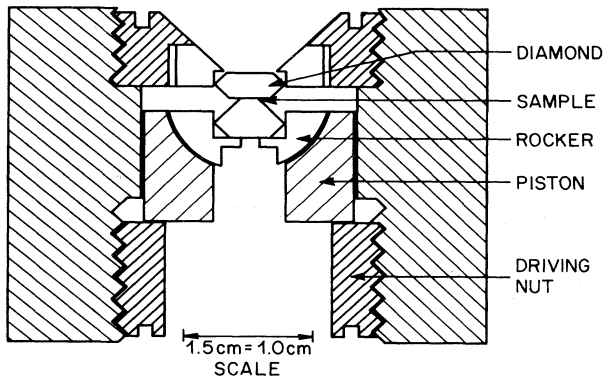

FIG. 3. Bassett-type cell with half-cyclindrical rockers for diamond alignment (after Bassett, Takahashi, and Stook, 1967).

b. Bassett cell

The DAC shown in Fig. 3, introduced by Bassett, Takahashi, and Stook (1967) has a threaded gland to apply force on the diamond anvils. The stainless-steel block (5 cm to a side) comprising the main body of the DAC has suitable apertures for the stationary piston and the sliding one, and the latter is held by a key in a slot to prevent its rotation. The rockers provide both angular and translational motion for centering and aligning the diamonds. The highest pressure attainable depends on the area of the diamond flat, and pressures in the neighborhood of 400 kbar (Jayaraman, 1972) have been reached with 0.3-mm anvil flats in ungasketed operation. The device is simple and has been used extensively for high-pressure x-ray powder diffraction studies (Bassett and Takahashi, 1974), for microscopy, and in phase diagram studies of minerals with laser heating for heating the samples.

c. Mao-Bell cell

In Fig. 4 the DAC developed by Mao and Bell (1978a) at the Geophysical Laboratory in Washington for pressures exceeding a megabar is shown. Like the Piermarini-Block cell, the latter DAC has Belleville spring-loaded lever-arm mechanism for generating the thrust, but has a long (60—70 cm) detachable piston-cylinder assembly. The anvil centering and alignment are accomplished by translating and tilting the two hardened steel (RC 60) or tungsten carbide rockers (half cylinders) in their troughs. The more generously proportioned body and the lever-arm system facilitate generation of larger force, and the long piston-cylinder assembly combined with the tungsten carbide mounts ensures excellent alignment of the diamonds. Mao and Bell (1978b) claimed to have reached 1.7 mbar with $\frac{1}{3}$ carat brilliant-cut diamond anvils, whose culet tips were ground flat or beveled in part to low angles, and pressure generated in a preindented work-hardened stainless-steel gasket.

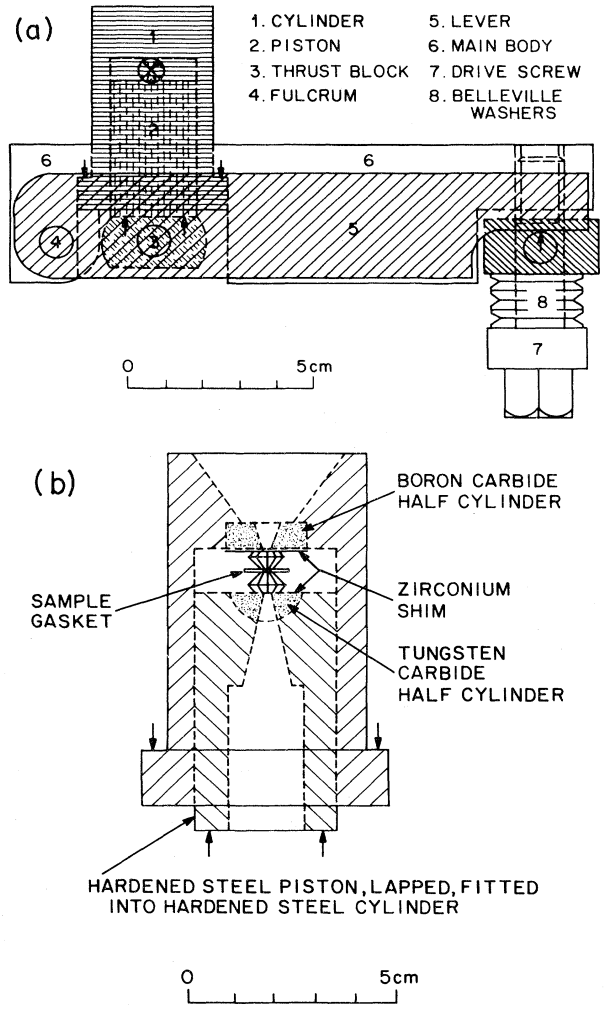

FIG. 4. Mao-Bell cell. A cross-sectional view (Mao *et al.*, 1979). (b) shows the long cylinder-piston assembly with the anvil diamonds set in carbide half cylinders; design features after Mao and Bell (1978a).

d. Syassen-Holzapfel cell

In Fig. 5 the DAC developed by Huber, Syassen, and Holzapfel (1977), based on the Syassen-Holzapfel design, is shown. The thrust for compressing the anvils is generated by a thread-and-knee mechanism. Two threaded rods connecting the front and back sides of the brackets are synchronously turned by a simple gear-set wrench, pulling the lower ends of the brackets together (see Fig. 5). Consequently, the upper ends of the brackets compress the moving piston and generate the pressure. The special geometry of these brackets, levers, and threads results in a large force multiplication, allowing generation of forces in excess of 5 kN on the diamonds. Because of the long piston and good fit combined with the thrust acting strictly parallel to the axis of the instrument, this DAC has excellent alignment stability. The diamond alignment mechanism is similar to the one shown in Fig. 2. The device is capable of generating 500-kbar

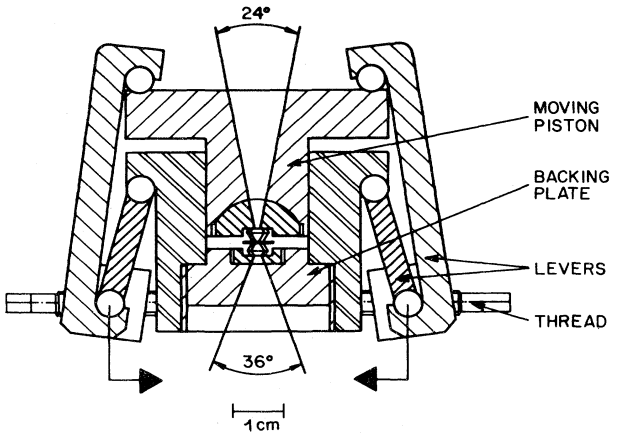

FIG. 5. Syassen-Holzapfel cell; a sectional view. The knee-type lever arms generate the thrust for the piston when the threads are advanced synchronously with a gear-set wrench. The back plate can be modified to accommodate a sapphire backing block to back the diamond for Raman scattering work (Hirsch and Holzapfel, 1981). Top diamond on hemispherical mount for alignment (after Huber, Syassen, and Holzapfel, 1977).

pressure and has been adapted for single-crystal x-ray diffraction, Raman and Brillouin scattering, and other optical studies at high pressure.

e. Merrill-Bassett cell

Figure 6 shows a DAC (Merrill and Bassett, 1974) in which three screws pull the two platens together when tightened, carrying the diamond anvils with them. This device is extremely compact and is particularly useful for single-crystal x-ray diffraction studies, for it can be mounted on an x-ray goniometer head. Suitably shaped Be supports, press-fitted into the steel platens, provide wide-angle access to the incoming and diffracted x-ray beams.

Other DAC's have been designed in which hydraulic pressure pushes the sliding piston, but their usefulness has diminished with the introduction of the ruby scale for pressure calibration. In some DAC's other geometries for optical or x-ray access have been introduced in reponse to certain specific requirements, but by far the most useful geometry is the axial access.

2. Diamonds

Diamonds for the anvil are usually selected from brilliant-cut gem stones. The culet is removed by grinding a flat, octagonal surface with area of approximately 0.45 mm^2 (usually 0.7 mm from side to side of the octagon). The size of the diamond may vary from $\frac{1}{8}$ to $\frac{1}{2}$ carat and the anvil flat from 0.3 to 0.7 mm. Anvil flats similar in area and shape are to be used, although in the Bassett cell (Fig. 3) $\frac{1}{8}$ carat diamonds with dissimilar flats have been employed (0.5—0.3 mm against 1.8 mm). The anvil flat is usually set parallel to the (100) or the

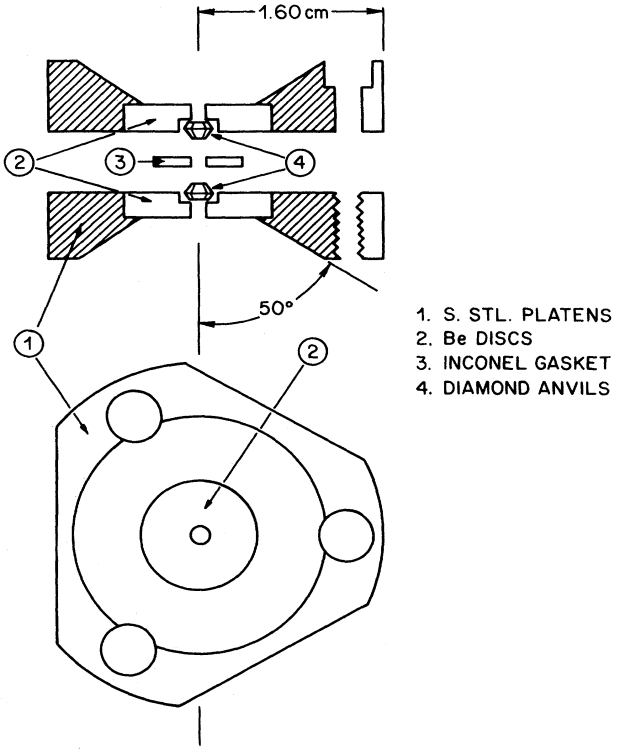

FIG. 6. Merrill-Bassett miniature cell for single-crystal x-ray studies. The diamonds are set in Be backing plates and the thrust applied by tightening the three symmetrically located screws (after Merrill and Bassett, 1974).

(110) plane of the diamond. The octagonal surface opposite to the anvil flat referred to as the table has a diagonal distance of 3.5—4.5 mm (equal to an area of 8—12 mm^2) in larger diamonds and of about 2 mm in $\frac{1}{8}$ carat diamonds. The selection of diamonds and their size depend upon the type of DAC and the nature of the investigation. For instance, diamonds with very low luminescence have to be used in DAC for light scattering studies (Wijngaarden and Silvera, 1980, Hirsch and Holzapfel, 1981), and type-II diamonds usually satisfy this criterion (Adams, Payne, and Martin, 1973; Adams and Sharma, 1977a). On the other hand, a luminescent diamond is no hindrance for x-ray diffraction. In general, larger diamonds are preferred for higher pressures and for larger pressurized volume.

3. Gasketing

The introduction of the gasket into the diamond anvil apparatus is a very important development in the history of the DAC, for it is this discovery which paved the way to make the DAC into a quantitative tool for high-pressure research. The use of a gasket for the containment of a hydrostatic medium was first demonstrated by Van Valkenburg (1965). Figure 7 shows a compressed gasket held between two opposed diamonds. The gasket is prepared by drilling a hole (200 μm in diameter) at the center of the indentation made by the anvil face on a metal foil. The initial thickness of the foil may vary from 0.25 to 0.20 mm and the indented thickness from 0.15 to 0.10 mm. The gasket is seated on the lower diamond flat in the same orientation as it had when taking the indentation. Then the sample and a ruby chip are placed in the hole. This is followed by filling the hole with the fluid and sealing by bringing the upper anvil on the gasket. Inconel X750, tempered 301 stainless steel, and Waspalloy have been used as gasket materials.

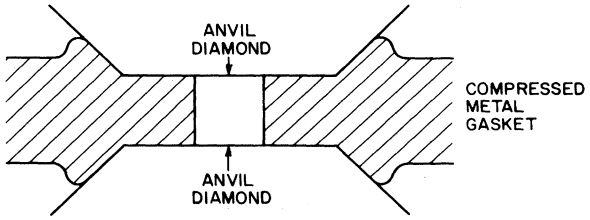

FIG. 7. The shape of a compressed gasket (between two anvil diamonds) supporting the diamond edges.

The gasket, apart from providing containment for the pressure medium, extrudes around the diamonds and acts as a supporting ring, preventing failure of the anvils due to concentration of stresses at the edge of the anvil faces. A further reduction of the stress gradients appears to result by beveling the edges of the diamond anvil, and this is believed to be the key to the successful generation of 1.7 Mbar claimed by Mao and Bell (1978b).

4. Pressure calibration with ruby fluorescence

With the introduction of the ruby fluorescence method in 1972 by Forman *et al.* (1972) a major obstacle with the DAC, namely, pressure calibration, was removed, clearing the way for widespread use of the DAC for high-pressure physical investigation. In earlier years pressure was estimated by force over area, fixed points, and in high-pressure x-ray studies by internal markers such as NaCl or silver. Using well-established freezing points of several liquids and some solid-solid transitions as fixed points, Forman *et al.* (1972) first showed that the R lines of Cr^{3+}-doped Al_2O_3 (ruby lines) shift linearly with hydrostatic pressure in the range of 1—22 kbar, and that the R lines broaden if the ruby experiences nonhydrostatic stresses. Further work by Barnett, Block, and Piermarini (1973) has made the ruby fluorescence technique a very rapid and convenient method for the measurement of pressure. A tiny chip of ruby 5—10 μm in dimension is placed in the pressure medium along with the sample, and the fluorescence is excited by either a He-Cd laser line or any source of strong light. A typical system after Mao and Bell is shown in Fig. 8. The R lines of ruby are quite intense, and the doublet R_1 and R_2 have the wavelengths 6927 and 6942 Å, respectively, at atmospheric pressure. Under pressure these shift to higher wavelengths and the shift is linear with pressure. Piermarini *et al.* (1975) tied the ruby scale to NaCl via the Decker equation of state (Decker, 1971) and showed that it is linear up to 190 kbar. They proposed that $P = 2.746\Delta\lambda$, where P is in kbar and

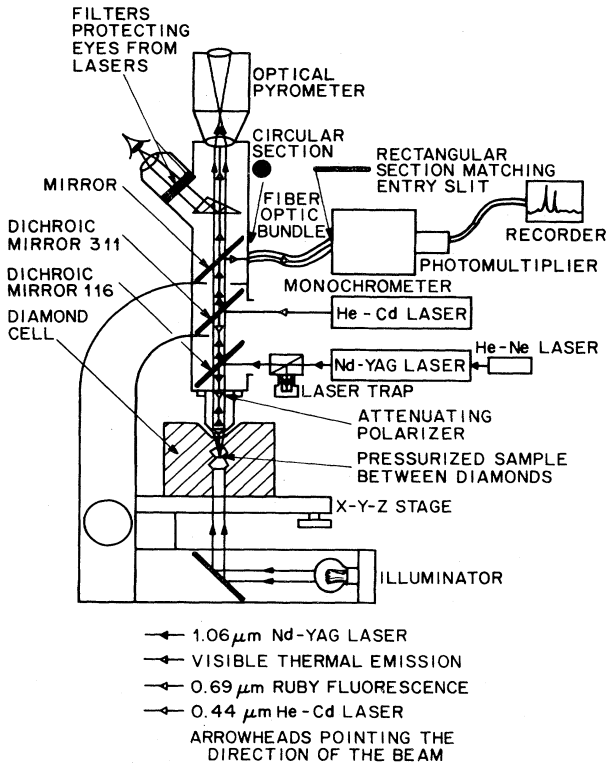

FIG. 8. Block diagram of the laser microoptic system for pressure calibration and laser heating experiments in the DAC. The Nd-YAG laser is for heating and the He-Cd laser for exciting the ruby fluorescence. The dichroic mirrors reflect 95% of the He-Cd laser radiation (after Bell and Mao, 1975).

$\Delta\lambda$ in Å. In a subsequent study (Piermarini and Block, 1975) it was shown that the linearity holds good up to 300 kbar, by determining the B_1-B_2 transition of NaCl (taken to be at 291±5 kbar) and the ruby R line shifts at the same time. The accepted value for the ruby R-line shift is 0.365 Å kbar^{-1} or -0.753 cm^{-1} kbar^{-1}.

The ruby R lines are quite sensitive to temperature and exhibit a positive shift with temperature. However, Noack and Holzapfel (1979) have demonstrated that the linear scale holds good at any temperature down to 4.2 K and that the pressure versus $\Delta\lambda$ slope is exactly the same as that at room temperature.

An important question with regard to the ruby scale is how far it is linear. Piermarini and Block (1975) have used the linear ruby scale (Piermarini *et al.*, 1975) up to 500 kbar and Mao and Bell (1976b) to 1 Mbar. To test the validity of the assumed linearity of the ruby scale, Mao *et al.* (1978) determined the ruby line shift as well as the lattice parameter of Cu, Mo, Ag, and Pd (by high-pressure x-ray diffraction) simultaneously in the pressure range 60 kbar—1 Mbar and used the isothermal equations of state derived from shock-wave experiments to obtain the pressures. From the results they concluded that there is a small positive nonlinearity in the pressure dependence of the wavelength shift of the R lines and that the linear scale underestimates the pressure. They have proposed for the pressure,

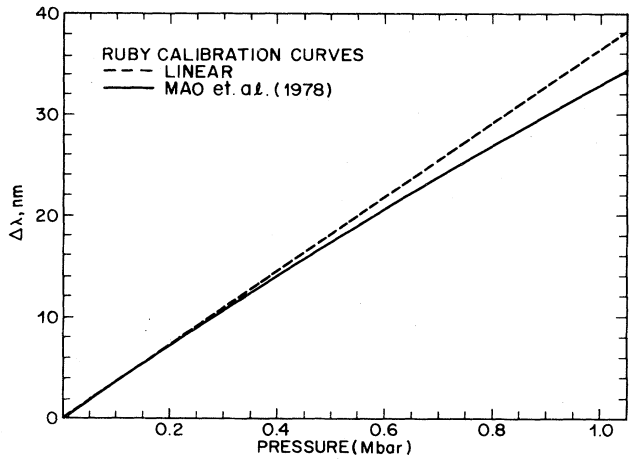

FIG. 9. Ruby fluorescence line (R_1R_2 lines) shifts R with pressure, $\Delta\lambda$ in nm vs pressure in megabar. The pressure according to linear extrapolation is $P(\text{kbar})=3.803\ [(\Delta\lambda/6942+1)^5-1]$ ($\Delta\lambda$ in nanometers) (after Mao *et al.*, 1978).

$$P(\text{Mbar})=3.808[(\Delta\lambda/6942+1)^5-1]\ . \qquad (1)$$

A plot of the ruby line shift $\Delta\lambda$ against pressure is shown in Fig. 9, where the dotted line represents the linear extrapolation according to Piermarini *et al.* (1975) and the solid line is given by Eq. (1). The deviation is negligible below 200 kbar, but at higher pressures a small positive correction to the linear scale appears necessary. The estimate of error in using Eq. (1) at 1 Mbar is stated to be less than 3%.

Ruoff (1979) has questioned the validity of the linear ruby scale on the basis that the pressure for the GaP transition, arrived at in two different ways, is 170—180 kbar and not 220 kbar as indicated by the linear ruby scale. According to Ruoff, the latter scale increasingly overestimates pressure as pressure increases, and the problem stems from the assumptions that are made about the Grüneisen parameter and the state of the shocked material, when reducing the shock data to obtain the isothermal P-V curves. However, Eq. (1) is the only equation (with experimental support) available at present for pressure calibration above 300 kbar. Since it is based on reliable experimental data, its use is recommended until a better pressure scale evolves in the future (see Bean *et al.*, 1982).

5. Pressure media

The hydrostatic limits of several organic fluid pressure media were determined (Piermarini, Block, and Barnett, 1973) by using the ruby line broadening, or by measuring the pressure homogeneity with several ruby chips distributed over the area of the gasket aperture. Accordingly, it was found that a 4:1 methanol-ethanol mixture remains hydrostatic up to 104 kbar at room temperature. A small addition of water in the proportion 16:3:1 H_2O to methanol-ethanol appears to extend the hydrostatic range of the alcohol mixture to 145 kbar. More recently the usefulness of several condensed gases (Mao, Mao, and

Bell, 1982; Liebenberg, 1979) as a hydrostatic pressure medium has been tested using the R line as the probe. The results are shown in Table I for several rare gases which appear attractive in this respect. However, their use requires special filling techniques which are described in a later section.

B. Low temperatures and the DAC

The DAC is cooled either for conducting experiments at low temperatures, or for condensing and trapping He, H, and other gases in the gasket as specimens for study or as a pressure medium. Since the DAC is a small, compact piece of apparatus, direct immersion in a cryogenic fluid is the simplest way to achieve the objectives, and this can be done quite easily with liquid N_2 and O_2, or with other gases that can be condensed at or above liquid-N_2 temperature. However, operation at liquid-He temperatures, or filling with H_2 calls for specially designed cryostats and means for remote sealing the fluid in the gasket. Webb, Gubser, and Towle (1976) have described an apparatus for pressures up to 100 kbar and temperatures down to 0.03 K, which uses a Bassett-type cell in a He^3-He^4 dilution refrigerator. In this, pressure can be changed from outside by applying He^4 gas pressure to a chamber with bellows, which in turn pushes the anvil piston. The apparatus was used to measure the effect of pressure on the superconducting T_c of Al, with a Squid magnetometer to detect the change in the magnetic moment of the sample. Shaw and Nicol (1981) have described a simple DAC for optical spectroscopy to pressures of 100 kbar at temperatures down to 2 K. The cryostat is provided with optical windows and pressure is changed from outside by a helium-driven piston acting on a pivoted clamp.

Mao and Bell (1979a) have developed low-temperature techniques around their DAC for operation at liquid-He temperatures and for filling the gasket with H_2. Their modified DAC for cryogenic temperatures is shown in Fig. 10. The main difference between the present device and the Mao-Bell cell referred to earlier is that force to the thrust block can be applied by advancing the four Belleville spring-loaded precision screws symmetrically into the threaded body of the cylinder block, through a remote control tightening mechanism. This enables the sealing of the condensed gas in the gasket and pressurization up to 150 kbar. Opposing screw directions are used to avoid torque on the remote control tightening mechanism. In Fig. 11 details of the high-pressure cell and in Fig. 12 the cryostat and H_2 filling systems are shown. When the liquefied gas level rises above the anvil gasket

TABLE I. Some pressure media and their useful pressure ranges.

Medium	Freezing Pressure at RT (kbar)	Pressure range of nearly hydrostatic behavior (kbar)	Remarks	Ref.
Methanol:ethanol 4:1	104[a]	~200	Easy filling	Piermarini, Block, and Barnett (1973)
Methanol:ethanol Water 16:3:1	145[a]	~200	Easy filling	Fujishiro *et al.* (1981)
He	118	>600	Cryogenic or high-pressure filling needed	Bell and Mao (1982)
Ne	47	160	Cryogenic or high-pressure filling needed	Bell and Mao (1982)
Ar	12	90	Cryogenic or high-pressure filling needed	Bell and Mao (1982)
Xe		300	Cooling below 165 K needed	Liebenberg (1979)
H_2	57	>600	Cryogenic or high-pressure filling	Mao and Bell (1979b)
D_2	53±2		Cryogenic or high-pressure filling	
N_2	24	130	Cryogenic filling	LeSar *et al.* (1979)
O_2	59	-	Cryogenic filling	Nicol *et al.* (1979)

[a]Glass transition pressure.

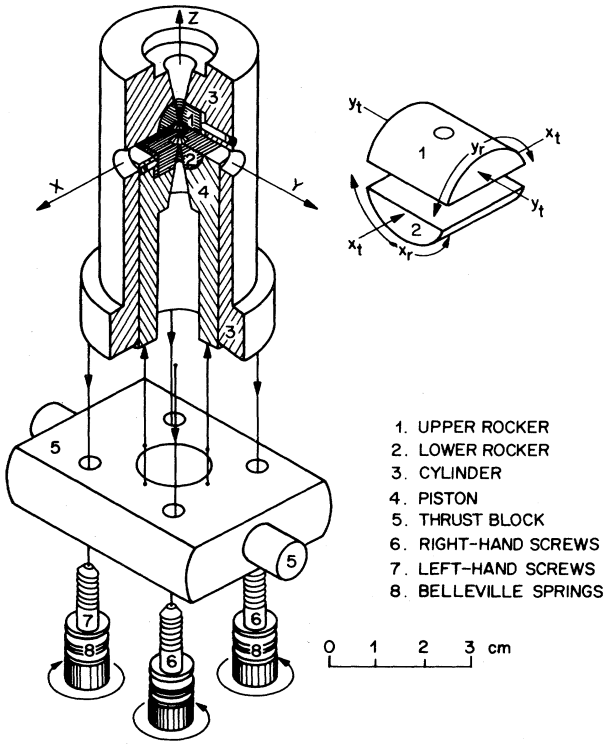

FIG. 10. The DAC for cryogenic experiments, after Mao and Bell (1979a). The gasket is sealed at low temperature, and pressure applied by advancing the four screws. Maximum pressure attainable with the screws is approximately 150 kbar. On the left the WC-supporting half cylinders are shown.

assembly, the liquid is trapped in the gasket hole by forcing the top piston and applying a suitable pressure, viz., 10 kbar in the case of H_2. Then the assembly is withdrawn, while the DAC is still held under pressure and transferred to the lever-arm block for further pressurization and physical investigation at room temperature. The system can be used for optical studies at liquid-He temperatures, with suitable windows in the cryostat.

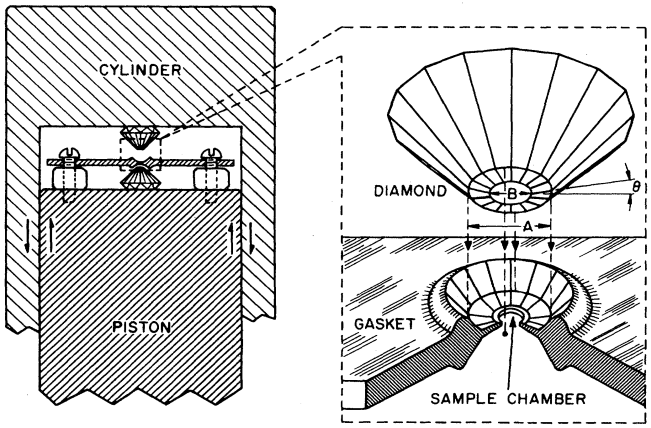

FIG. 11. Details of the diamond anvil region of the DAC shown in Fig. 10 for cryogenic experiments. Diamond anvil slightly bevelled ($A = 370\ \mu$m, $B = 175\ \mu$m, and $\theta = 1.5°$) (after Mao and Bell, 1979a).

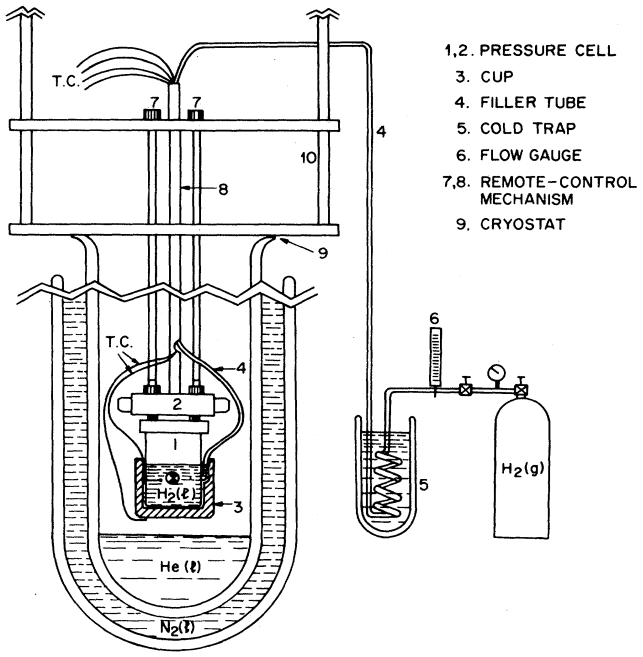

FIG. 12. The DAC shown in Fig. 10 in liquid-He cryostat for filling with liquid hydrogen and for trapping the fluid. The gasket hole is sealed by a remote-control mechanism to tighten the screws via 7.Tc-thermocouple (after Mao and Bell, 1979a).

Diatschenko and Chu (1981) have built a cryogenic press fabricated from Be-Cu, which enables sealing of the desired gas in the gasket of the DAC and pressurization from outside the liquid-He cryostat, through a screw-threaded mechanism. Optical observations can be made while the sample is pressurized, through a built-in telemicroscope system. They were thus able to observe the melting behavior of H_2 between 20 and 300 K. With primary and secondary coils placed close to the diamond anvils, low-temperature electrical measurements and determination of superconducting T_c are possible.

Liebenberg (1979) has devised a very simple technique for filling the gasket with Xe (Fig. 13). In this, the diamond anvil area is sealed off by a wall of indium, and a capillary inserted in the wall brings in the Xe. The DAC is cooled to 165 K and Xe admitted for liquefaction in the gasket area. Liquid Xe is trapped in the gasket hole by pressurizing the DAC. Xenon is found to be hydrostatic to 300 kbar (Liebenberg, 1979). Also, a gas could be in-

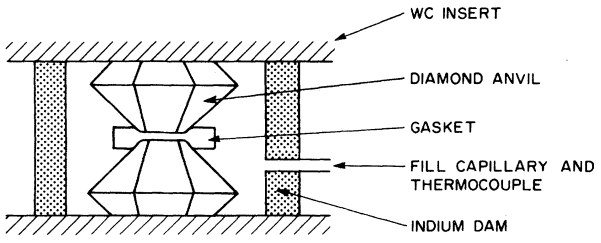

FIG. 13. Indium dam technique for filling and trapping liquid Xe. The diamond flats seal the gasket on applying load. Indium deforms (Liebenberg, 1979) to permit this.

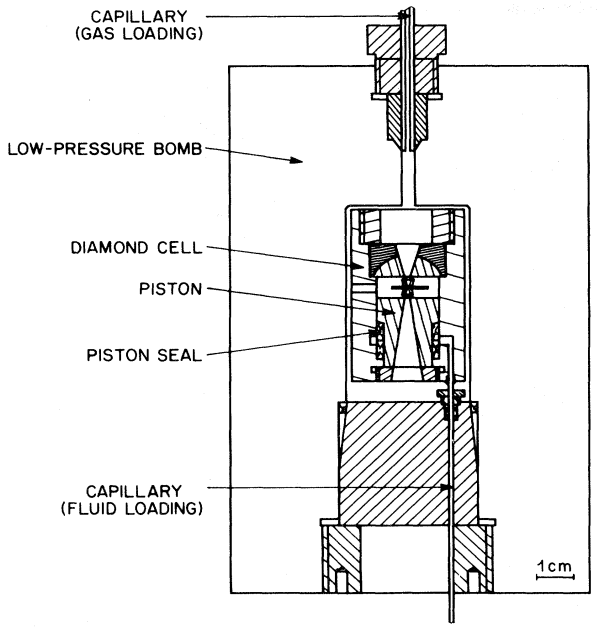

FIG. 14. High-pressure gas loading apparatus for filling the DAC with He or H_2, developed by Besson and Pinceaux (1979). Higher pressures made possible because of higher density attained with compressed gas filling, compared to fluid densities at normal pressures.

troduced through a very fine capillary directly into the hole of a tightly clamped gasket, and the condensed gas trapped by applying additional clamping force to pinch off the capillary (Liebenberg *et al.*, 1978). The latter employed the above method for filling CO_2 and D_2.

Besson and Pinceaux (1979) have invented a high-pressure gas loading technique for filling the gasket with He (see Fig. 14). In this, a high-pressure bomb (made of maraging steel for 5-kbar pressure) with the DAC inside is pressurized to 2 kbar. The gasket of the DAC is sealed by applying 2300-bar He gas pressure to the sliding piston of the DAC through a separate capillary attached to the DAC. The bomb pressure is released to the ambient pressure, maintaining the 300-bar excess pressure on the gasket. Then the cell is withdrawn from the bomb with the capillary still connected and with 300-bar pressure on it, for optical studies. The above technique has been slightly modified by Mills *et al.* (1980) for filling He and D_2 in a Mao-Bell cell. In this, a gear-drive system is used to clamp the Mao-Bell cell from outside the gas-pressure vessel, greatly facilitating the retrieval of the loaded DAC and transfer to the lever-arm system for further pressurization. The advantage of the high-pressure gas filling is that a density higher than the fluid density is obtained. For instance, H_2 gas at 5 kbar is 1.5 times denser than liquid H_2 under ambient pressure, and He gas is 2.3 times denser than liquid He. Denser loadings provide thicker samples and also allow high pressures to be reached before gasket failure due to deformation occurs. When a gas is to be used as a pressure medium, the same procedure is followed.

C. High temperatures and the DAC

There are two approaches for producing high temperatures in the DAC: (1) the sample is heated externally with a resistance heater located immediately around the anvils (Bassett and Takahashi, 1965; Moore, Sorenson, and Devries, 1970; Hazen and Finger, 1981), or (2) the sample is heated internally without raising the temperature of the anvils. The latter can be accomplished with an internal heater, or by coupling electromagnetic radiation to the sample. The problem with the external heating is that it heats up the diamonds as well as other surrounding parts. The diamond begins to oxide in air when heated to 700 °C, and at temperature as low as 800 °C graphitization starts, even when oxidation is prevented by replacing air with an inert atomosphere. Further, the diamond supports lose their strength and hardness at high temperatures. Hence all forms of external heating are limited to ~500 °C. Internal heating can be achieved by using a very fine wire of the sample and passing current through it, as was done by Liu and Bassett (1975) for the determination of the melting point of Fe to 2000 °C and 200 kbar, but the method would be restricted to metals which can be drawn into a fine wire. The possiblity of internally heating the samples by a pulsed ruby or yttrium aluminum garnet (YAG) laser was first demonstrated by Ming and Bassett (1974). The temperature measurements are not, however, accurate, and hence the method of laser heating is suited for only a rough exploration of the high-temperature—high-pressure phase relations.

D. X-ray diffractometry with the DAC

Since the first demonstration by Jamieson, Lawson, and Nachtrieb (1959) that a diamond anvil could be used for high-pressure x-ray powder diffraction, the introduction of axial geometry (Piermarini and Weir, 1962), of techniques for single-crystal studies (Block, Weir, and Piermarini, 1965; Weir, Block, and Piermarini, 1965; Merrill and Bassett, 1974), of Be components in the DAC to enable collection of data over wide angles (Weir, Block, and Piermarini, 1965; Schiferl, 1977; Keller and Holzapfel, 1977; Schiferl, Jamieson, and Lenko, 1978), and the ushering in of the miniaturized DAC (Merrill and Bassett, 1974) have revolutionized high-pressure x-ray diffractometry. Today the DAC is the most widely used tool for high-pressure x-ray powder diffraction as well as in single-crystal studies. Further, gases like N_2, O_2, Ne, Ar, and Xe can be loaded in the gasket and solidified as single crystals for the study of their structure, compressibilities, and pressure-induced phase transitions (Cromer *et al.*, 1981; Schiferl, Cromer, and Mills, 1981; Hazen *et al.*, 1980a, 1980b).

1. Single-crystal diffraction

Figure 15 illustrates a miniature DAC developed by Hazen and Finger (1981) for high-pressure x-ray diffrac-

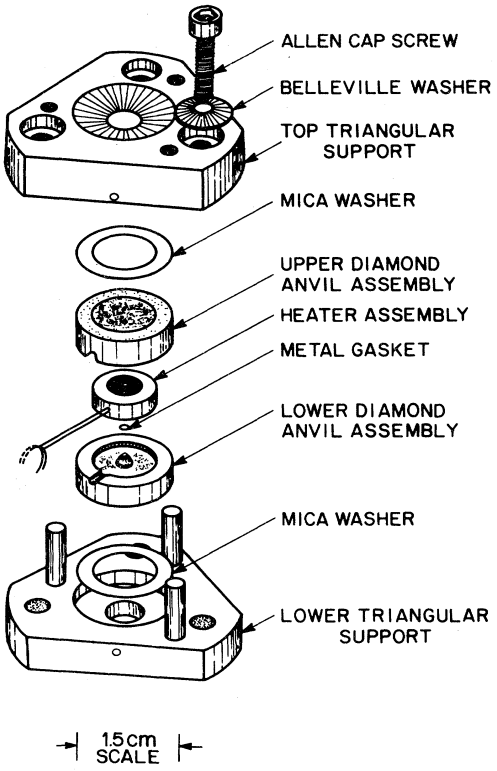

FIG. 15. Miniature DAC for single-crystal x-ray diffraction at elevated temperatures up to 450°C and 30 kbar, developed by Hazen and Finger (1981). The cell is mountable on a goniomter head and represents a modified Merrill-Bassett cell.

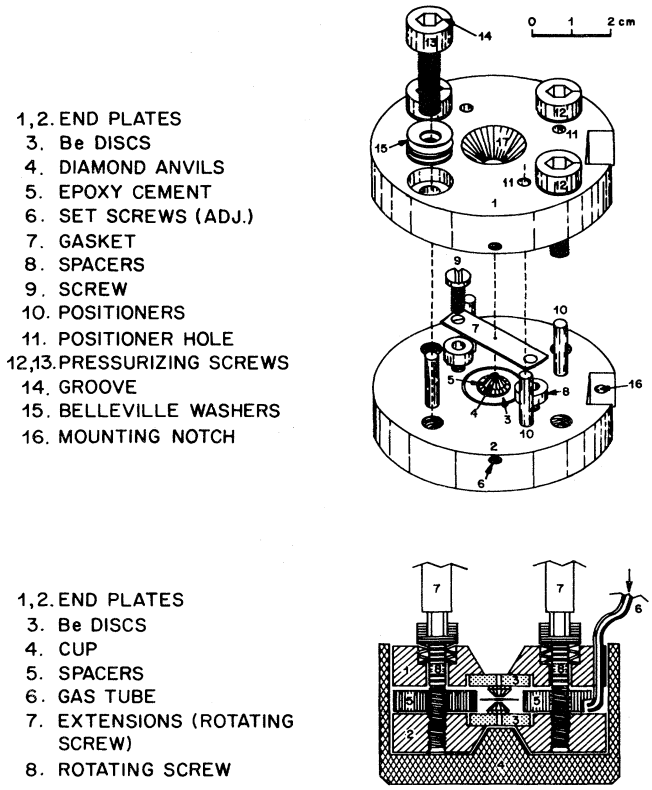

FIG. 16. Miniature DAC for x-ray diffraction studies of condensed gases. Cryogenic loading shown in the lower part of the figure (after Mao and Bell, 1980).

tometry. It is based on the single-crystal Merrill-Bassett cell and can be mounted on a goniometer for four-circle diffractometry. Hazen and Finger have incorporated a heater assembly into the above cell for work at high temperatures up to 450°C and 30 kbar. In this cell, disks of boron carbide are used for the diamond seat in place of the Be disks. A miniature resistance element made of Pt-Pt 10% Rh thermocouple wire is used to concentrate the heat on the sample, and this operates alternately as a heating element and as a thermocouple. An Inconel X750 foil of 250-μm thickness with a hole 300 μm in diameter serves as the gasket.

For cryogenic loading, Mao and Bell (1980) have modified the Merrill-Bassett cell which is shown in Fig. 16. The main body of this cell is made of maraging steel (Vascomax-250) because of its suitability for low-temperature applications. The diamond anvils are cemented to the Be disks with a low-temperature epoxy cement. The cell is assembled and transferred to the cryostat for loading with the desired sample and pressurized to approximately 10 kbars. After the gasket hole is sealed, the cell is removed from the Dewar and warmed to room temperature for mounting on the four-circle goniometer. The ruby chip introduced into the gasket hole during the preloading procedure serves to measure the pressure.

Another useful device for single-crystal work that has some desirable features is due to Keller and Holzapfel (1977) and is shown in Fig. 17. The special shape of the Be supports for the diamonds reduces the problem of the x-ray absorption corrections in Be to a constant factor. The steel backings have wide conical apertures for the transmission of the diffracted x-rays over a wide angle. Also, provisions are available in this cell for centering and parallel alignment of the anvil flats with set screws. The cell is a miniaturized version of the Holzapfel optical cell and can be mounted on a four-circle goniometer for x-ray

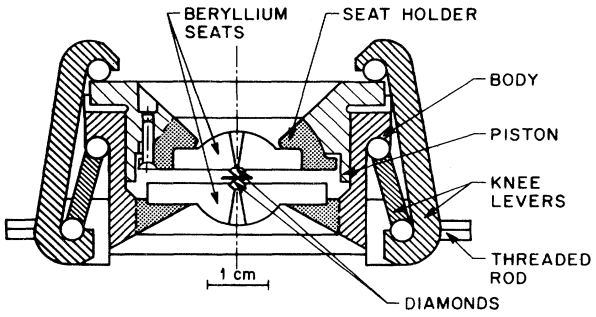

FIG. 17. Modified Holzapfel cell for single-crystal x-ray diffraction to 100 kbar (after Keller and Holzapfel, 1977). Beryllium seats allow for large-angle x-ray data collection.

diffractometry. It is also adapted to fit the Phillips PW-1100 four-circle diffractometer (Denner *et al.*, 1978). The device is capable of generating pressures of 100 kbar.

Limitation in pressure for single-crystal studies is imposed by the load that can be applied, by the strength of the Be or boron carbide supports, and by the solidification of the fluid pressure medium: 105 kbar for 4:1 methanol-ethanol mixture. With the possibility of using He and H_2 as pressure media, the working pressure range for single-crystal work could be raised by a factor of 2.

2. Powder x-ray diffraction with the DAC

All types of DAC's are suited for powder diffraction work. Table II summarizes the capabilities of the different types of DAC's for high-pressure x-ray diffraction studies. Film techniques have dominated earlier work (Bassett and Takahashi, 1974; Jayaraman *et al.*, 1974) and still is a powerful method to measure compressibilities, to detect phase transitions, and to identify simple crystal structures. Currently, however, energy dispersive x-ray diffraction (EDX) is the best general method available for powder studies and it is fast. The EDX technique and the DAC were first coupled, independently, by two groups (Buras *et al.*, 1977; Skelton *et al.*, 1977), and the advantages of having a fixed angle with the DAC were demonstrated. The EDX enables rapid collection of diffraction data with a solid-state detector and further there is no need for a large conical opening in the backing plates of the diamond anvils. Buras *et al.* (1977) were the first to combine DAC with synchrotron radiation for high pressure x-ray diffraction and more recently Ruoff and Baublitz (1981), Baublitz, Arnold, and Ruoff (1981), Spain *et al.* (1981), and Manghnani *et al.* (1981) have demonstrated that with a powerful synchrotron as the x-ray source, powder diffraction data can be collected in a matter of seconds with the DAC. Fujii *et al.* (1980) have used a position sensitive detector (PSD) with the DAC and Mo$K\alpha$ radiation and have shown that the method combines rapid data collection capability with a high signal-to-noise discrimination. For quantitative intensity determination the PSD may be the best.

Extended x-ray absorption fine structure measurements using DAC have been reported (Ingalls, Garcia, and Stern, 1978; Ingalls *et al.*, 1980, 1981; Werner and Hochheimer, 1982).

TABLE II. DAC's for high-pressure x-ray diffraction.

Call type	Pressure limit (kbar)	Ref.
NBS (modified design)	>350 (40)[a]	Piermarini and Block (1975)
Basset cell	~400	Jayaraman (1972)
Mao-Bell cell	~1000	Mao *et al.* (1978), Mao and Bell (1979c)
Holzapfel cell	~400	Werner, Hochheimer, Jayaraman, and Leger (1981)
	(100)	Keller and Holzapfel (1977)
Merrill-Bassett	(100)	Merrill and Bassett (1974) Hazen and Finger (1977)
Schiferl cell	(50)	Schiferl (1977)

[a]Numbers in parentheses refer to pressure limit for single-crystal high-pressure x-ray diffraction studies.

E. Spectroscopy with the DAC

Historically, the DAC was conceived at the NBS for infrared spectroscopy at high pressures, and early infrared (ir) absorption measurements were carried out with the NBS cell by Lippincott and co-workers at the University of Maryland. Improved techniques for near- and mid-ir absorption spectroscopy were later developed by Ferraro and Basile (1974), and by Adams and Sharma (1977b, 1979). The main difficulty about ir absorption measurements with the DAC is the small aperture, dictated by the anvil face. The bulk of the early work was done in ungasketed geometry, which suffers from the presence of large pressure gradients. Results obtained in ungasketed geometry were found to differ significantly from those obtained with gasketed geometry (Adams and Sharma, 1979). However, with gasketing the aperture is further reduced and this makes ir spectroscopy with the DAC experimentally a challenging problem. Welber (1976, 1977), Adams and Sharma (1977a, 1977b, 1979), and Syassen and Sonnenschien (1982) have developed microspectroscopy techniques for carrying out absorption and reflectivity measurements. Adams and Sharma (1977a, 1977b, 1979) have introduced into the optics a beam condenser made of KBr lenses for mid-ir absorption studies. With a 0.4-mm-diameter hole in the gasket, good spectra were obtained up to 17 kbar in the DAC, in the mid-ir region (Adams and Sharma, 1979). In operating the DAC in the gasketed geometry, the ratio of the hole size to the diamond flat anvil face should not be less than 1:2. For mid-ir spectroscopy, a gasket hole diameter of 0.3 mm and thickness of 0.1 mm are required and this dictates using at least a 0.7-mm anvil face. Then the upper limit of pressure for mid-ir spectroscopy with the improved techniques could go as high as 300 kbar. If a pressure-transmitting medium is used, a ratio recording instrument is called for; otherwise, transmission through the area not covered by the sample would vitiate the results. Far-ir studies are even more challenging, since one must focus enough energy on the sample and detect extremely weak outputs. Some crucial design considerations of optics for ir spectroscopy are set out by Adams and Sharma (1977a, 1977b). Welber (1976) has used a large parabolic mirror to condense the beam and the microspectroscopic system is good for measurements of absorption from near ir to near uv in the 1—200 kbar range. Precision optical absorption measurements in the range above ~4 eV are beset with problems, and some of these are discussed in two recent studies on solid Xe (Asaumi, Mori, and Kondo, 1982; Makarenko *et al.*, 1982).

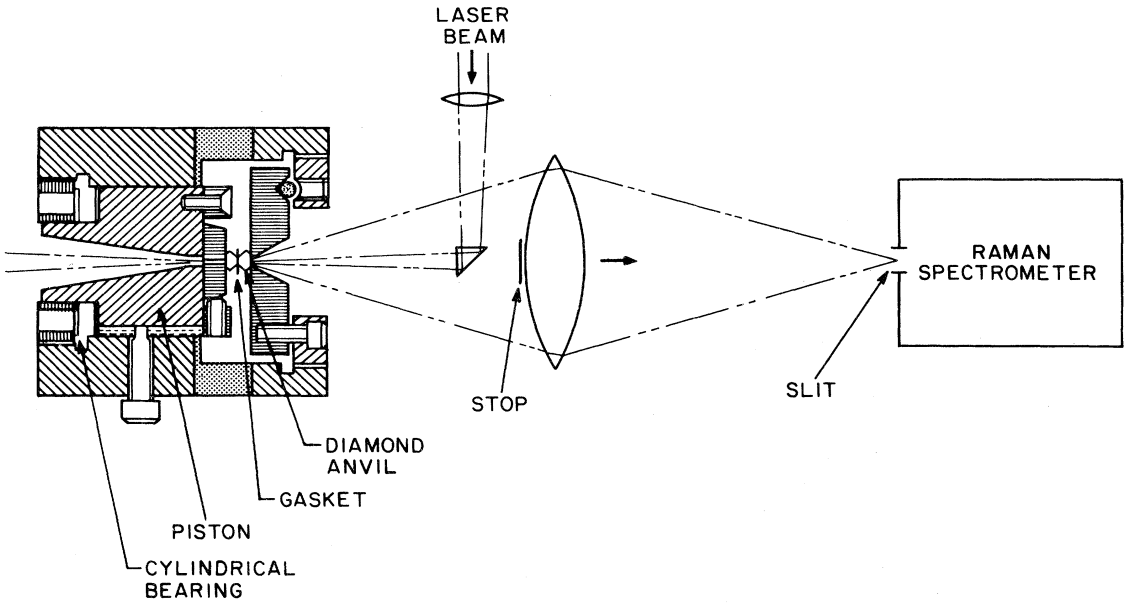

FIG. 18. Schematic for Raman scattering studies with the DAC in the backscattering geometry. The laser beam should be focused to a fine spot ~30—50 μm. The DAC of Nakamura *et al.* (1979) is shown.

1. Raman scattering

The first Raman studies with the DAC were reported by Brasch, Melveger, and Lippincott (1968) and Postmus *et al.* (1968), employing forward scattering geometry (0°). Adams, Payne, and Martin (1973) first found that good Raman spectra are obtainable with backscattering geometry (180°). Raman measurements to pressures over 100 kbar in a gasketed cell with a pressure-transmitting medium was first carried out by Weinstein and Piermarini (1975), who investigated the phonon frequencies in Si and GaP as a function of pressure. Very useful experimental details are given in the paper. In Fig. 18 the optical arrangement for Raman scattering with the DAC is shown (Nakamura *et al.*, 1979) for backscattering geometry. The laser beam is focused to a fine spot (30—40 μm) by the lens. A small right-angle prism or mirror deflects the focused beam on the sample placed inside the DAC. The scattered light is focused onto the slit of a Raman spectrometer by the collecting lens, whose focal length is between 75 to 130 mm, with f value $f/1$ to $f/2$, or by an off-axis ellipsoidal mirror in both 0° and 180° scattering geometries (Adams, Sharma, and Appleby, 1977). A double monochromator with conventional photon counting is quite satisfactory for detecting the Raman signal.

Almost any DAC is suitable for Raman spectroscopy, provided the conical opening behind the exit diamond is adequate (40° or larger). Hirsch and Holzapfel (1981) have modified the Holzapfel cell by providing a sapphire backing for the diamond to increase the angular aperture for the scattered light. The sapphire block is about 10 mm in diameter and 10 mm high, c-axis oriented, and surrounded by a slightly tapered sleeve. This assembly is press fitted into the backing plate of the DAC so that the sapphire is somewhat supported. The combined windows (sapphire and the angular opening in the back plate) provide an effective aperture of $f/1.4$ outside the cell for the scattered light. The laser beam enters through one of the

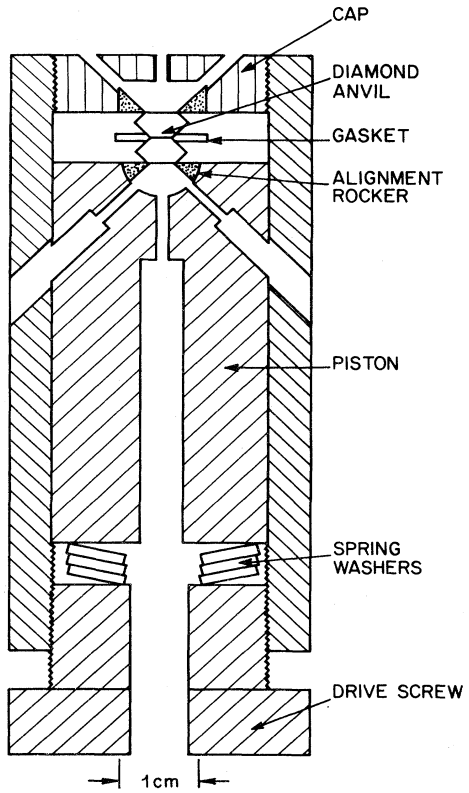

FIG. 19. Bassett's "LUP" series DAC for Raman scattering in right-angle geometry (after Whitfield, Brody, and Bassett, 1976). Also useful for Brillouin scattering experiments.

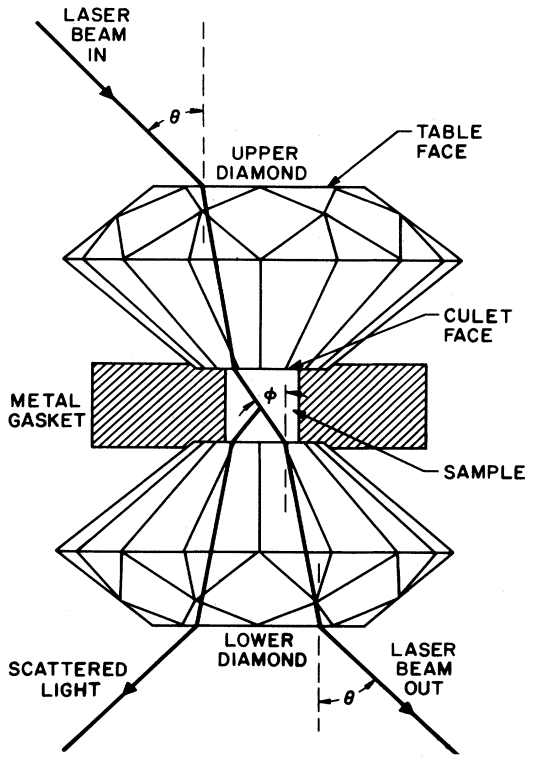

FIG. 20. The ray paths through the diamonds and the gasket hole in right-angle geometry (after Whitfield, Brody, and Bassett, 1976).

small symmetrically located slits in the backing plate at an outside angle of 30°—35° and exits through the other. This helps to eliminate much of the scattered light from the front, thereby enabling regions close to the laser line to be scanned. The sapphire-backed DAC are limited in pressure by the maximum uniaxial stress the sapphire can withstand before cracking. With a brilliant-cut 0.6 carat anvil and an anvil face of 0.6 mm, the pressure reduction at the back of the anvil (table of 4 mm is 25:1). Hirsch and Holzapfel claim to have reached 500 kbar. Therefore, it appears that the sapphire backing will withstand a uniaxial stress in the neighborhood of 20 kbar without cracking. One of the advantages of the Holzapfel cell is that a simple cryostat with optical windows can be used for low-temperature operation, down to 77 K (Hirsch and Holzapfel, 1981). The Mao-Bell cell has been extensively used for Raman spectroscopic studies, and with H_2, Raman spectra have been obtained at pressures as high as 623 kbar (Sharma, Mao, and Bell, 1980a). Whitfield, Brody, and Bassett (1976) have modified the Bassett cell for Raman scattering to permit ±45° optical access to the sample, in addition to direct access. This cell, shown in Fig. 19, has been used both in Raman and Brillouin scattering very effectively. The cell has two opposing $\frac{1}{3}$ carat gem quality diamonds with 1.0-mm octagonal anvil face and is provided with mechanisms for centering and alignment of the diamond faces. Figure 20 shows the ray path through the diamonds and the gasket, for right-angle scattering geometry. The latter geometry is also useful for Brillouin scattering experiments with the DAC. Right-angle geometry minimizes greatly the elastically scattered light and enables scanning to within 6 cm^{-1} of the laser line.

2. Brillouin scattering

Brillouin scattering experiments in the DAC enable the measurement of sound velocities as a function of pressure even in very small samples, and the elastic constants can be calculated from these velocities, once the density is known. Whitfield, Brody, and Bassett (1976) were the first to use the DAC for Brillouin scattering studies. They modified the Merrill-Bassett cell and studied NaCl, for the density of NaCl as a function of pressure is well known (Decker, 1971). In later experiments (Bassett and Brody, 1977; Bassett *et al.*, 1979) the cell shown in Fig. 19 was used. Figure 21 illustrates the geometrical conditions employed.

A hypersonic wave traveling through a crystal produces a periodic modulation of the refractive index in the form of planes of higher and lower refractive index. Light can be scattered from these planes, in a manner analogous to Bragg's law. However, since the planes are nonstationary, the scattered light undergoes a Doppler shift in frequency, depending on the velocity of the hypersonic wave and the geometry of interaction of the light, given by

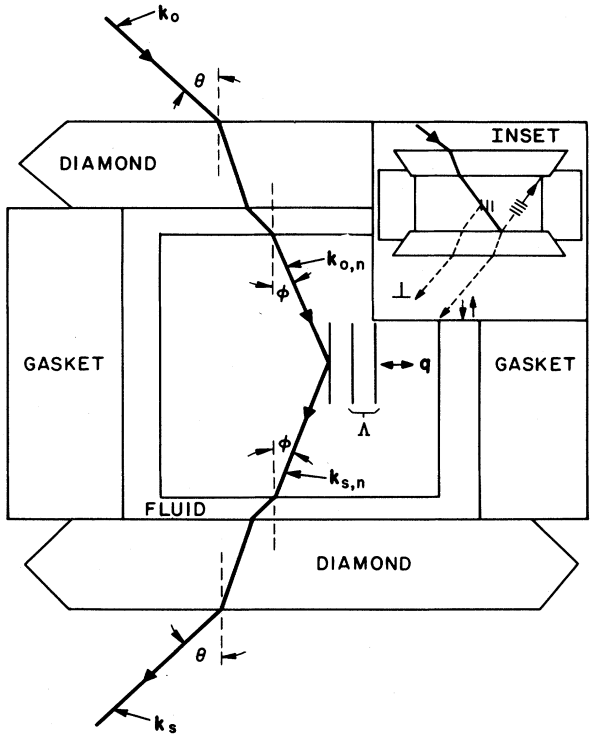

FIG. 21. The Bragg-reflected Brillouin component by sound waves shown schematically. In this geometry the refractive index n cancels out. Inset shows the origin of a second signal that arises due to backscattering from the laser light reflected from the exit diamond's inner face (after Whitfield, Brody, and Bassett, 1976).

$$\Delta\nu = 2U_S n \sin\theta/\lambda_0 , \quad (2)$$

where U_S is the sound wave velocity, n the refractive index of the substance, θ the angle of incidence of the light with respect to the phonon wave front, and λ_0 the laser wavelength. If the interfaces crossed by the light rays are parallel and if the set of emerging angles equals the set of entering angles as shown in Fig. 21, Snell's law can be used to eliminate the refractive index, and the above equation becomes

$$\Delta\nu = 2U_S \sin\theta/\lambda_0 . \quad (3)$$

If the angle θ is 45° ($2\theta = 90°$), the equation becomes

$$U_S = \Delta\nu\lambda_0/\sqrt{2} . \quad (4)$$

The simplicity of Eq. (4) is due to the parallel surfaces and symmetry of the right-angle geometry. The refractive indices of the diamond, the fluid medium, and the sample drop out, because of the substitution of the angle θ and external wavelengths λ_0 and λ_S for the internal angle ϕ and the internal wavelengths. In backscattering geometry, knowledge of the refractive indices would be necessary to compute $U_S^* = \Delta\nu^*\lambda_0/2n$, where n is the refractive index. With the diamond cell in the 90° geometry, the laser beam reflected from the inner surface of the exit diamond serves as an incident beam for giving a backscattered signal, from which the refractive index n of a fluid or an isotropic medium can be obtained using the relation $\Delta\nu/\Delta\nu^* = 1/\sqrt{2n}$. This geometric condition was taken advantage of by Shimizu *et al.* (1981) in measuring the refractive index of H_2 to 200 kbar.

F. Electrical and other measurements

1. Resistance measurements

Electrical resistance measurement with the DAC is a challenging experimental problem, but several attempts have been made. Mao and Bell (1976a) have measured the pressure variation of the resistance of highly insulating samples in ungasketed geometry. Block, Forman, and Piermarini (1977) have described a technique to perform two-lead resistance measurements under hydrostatic pressure. In this, an insulating layer sandwiched between two gasket elements isolated them electrically so that they could serve as electrodes to the sample. The semiconductor to the metallic transitions in GaP and ZnS were measured. In a variation of the method the gasket was coated with a ceramic paint, and a tungsten wire laid on it served as one of the electrodes. But the method works only with highly insulating samples. Metallic samples are difficult to measure because of their small resistance as against a large contact resistance. More recently Mao and Bell (1981b) have devised a four-lead arrangement which uses extremely fine lead wires (12—5-μm-diameter wires) of tungsten, chromel, or alumel, supported by a prepressed MgO disk, with the sample pressed against them. Pressure generated was measured with ruby powder embedded in MgO. Suitably placed Mylar templates provide insulation for the wires from contacting the anvil supporting metallic blocks. Mao and Bell were able to measure the α-ε transition in Fe with the above arrangement. The

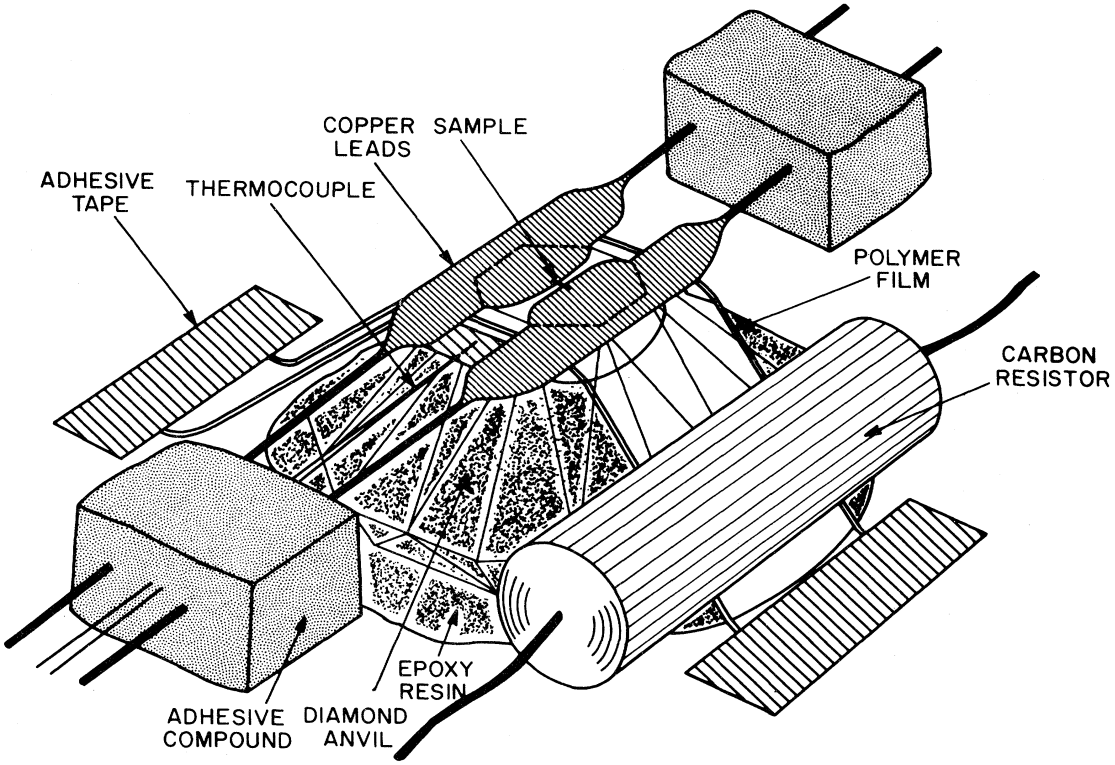

FIG. 22. Electrical resistance measurement in a DAC. Shows the arrangement of leads (from Sakai *et al.*, 1982). The carbon resistor serves as thermometer for low-temperature measurement.

technique can also be adapted for gasketed geometry. In this case the gasket is coated with a ceramic substance for insulation and the lead assembly supported on it, while the sample is suspended in the hydrostatic medium in the gasket hole.

For electrical resistance measurements at high pressure (up to 250 kbar) and at low temperatures down to 2 K, Sakai *et al.* (1982) have described a four-lead arrangement (Fig. 22). In this, thin Cu or Pb lead wires are used as electrical leads, and two layers of thin polymer films (Saran wrap of 0.05-mm total thickness) inserted between the leads and the anvils serve as the pressure medium for the sample wire. Helium gas pressure was applied to generate the load. Pressure was calibrated using Bi, Pb, ZnS, and GaP as fixed points. The insulator to metal transitions in iodine and Si:H films were observed, and the high-pressure phases were tested for superconductivity.

All the above-mentioned techniques have limited use and limited precision. Precise electrical resistance measurement in the DAC is a difficult problem. In this connection it should, however, be mentioned that Dunn and Bundy (1977, 1980, and 1981) and Bundy and Dunn (1979) have made extensive resistance measurements of apparent precision on several elements (S, Ca, Sr, Ba, Eu, Se, Te) to 400–500 kbar and at 5 K, using a supported taper cell with sintered diamond pistons in the anvil configuration.

2. Other measurements

The DAC has been adapted for magnetic susceptibility, microwave resonance, and absorption measurements (Spain, Skelton, and Rachford, 1980). Among the applications in nuclear physics, Huggins, Mao, and Virgo (1975) adapted the DAC for Mössbauer studies at high pressures and Hensley, Bassett, and Huizenga (1973) measured the pressure dependence of the radioactive decay constant of Be^7 up to 270 kbar and found a sizable effect. Viscosity of liquids has been measured by Piermarini, Forman, and Block (1978) utilizing the falling-sphere method. Because of the smallness of pressurized volume compared to the volume of the sphere, corrections for the contribution to the drag on the sphere from the walls of the cell become important. These have been analyzed using equations of hydrodynamics in the low Reynolds number limit (Munro, Block, and Piermarini, 1979). Measurement of viscosity enables one also to determine the glass transition pressure, which can be independently verified by ruby R line broadening (Munro, Piermarini, and Block, 1979).

Ves and Cardona (1981) have recently reported that uniaxial stress up to 30 kbar can be applied on thin films deposited directly onto the diamond anvil. To do this, the pressure medium 4:1 methanol-ethanol is frozen into a solid by cooling the DAC to 100 K and then applying stress. Under these conditions the applied stress is found to remain uniaxial up to 30 kbar. This was verified by observing the spin-orbit-split exciton in CuCl and CuBr. Above 30 kbar the pressure becomes increasingly more hydrostatic. This technique opens up a new application for the DAC and for investigating the effect of large uniaxial stresses on the optical properties of thin films.

III. SPECTROSCOPIC MEASUREMENTS

A. Optical absorption studies

The transparency of the diamond over a broad spectral range and the evolution of microspectroscopic techniques (Welber, 1976, 1977; Adams and Sharma, 1977a, 1977b; Syassen and Sonnenschein, 1982) have stimulated quantitative absorption and reflectivity studies with the DAC to very high pressures. The shifts in the energy gap with pressure in Ge (Welber *et al.*, 1977), GaAs (Welber *et al.*, 1975), InP (Müller, Trommer, *et al.*, 1980; Kobayashi *et al.*, 1981), $ZnSiP_2$ (Shirakawa and Nakai, 1981), CuCl (Müller, Ves, *et al.*, 1980; Ves *et al.*, 1981), and CdS (Batlogg *et al.*, 1981) from optical absorption measurements have been recently determined. Luminescence under pressure has been reported for CuCl (Blacha *et al.*, 1982), GaAs (Yu and Welber, 1978; Olego, Cardona, and Müller, 1980), and some other systems.

1. Ge and InP

In most III-V compounds, the direct (Γ) minimum is the lowest energy gap and this increases with pressure. At some high pressure, the direct minimum crosses the L or X minimum and then the material becomes an indirect gap semiconductor. These band-crossing effects are reflected in the optical absorption and luminescence. In GaAs the direct gap increases at the rate of ~ 10 meV kbar^{-1} and the X-conduction band becomes the lowest minimum at about 40 kbar. In InP the direct gap moves to higher energies at the rate of 6.35 meV kbar^{-1} and the Γ-X crossing occurs at about 90 kbar (Müller, Trommer, *et al.*, 1980; Kobayashi *et al.*, 1981). At pressures greater than >180 kbar in GaAs and >100 kbar in InP, a pressure-induced phase transition occurs, which more or less terminates the absorption measurements.

In Ge the pressure dependence of the direct gap has been measured by Welber *et al.* (1977) to 104 kbar. (Ge is an indirect-gap semiconductor with the lowest gap at the L point, but the direct edge dominates the absorption and hence can be observed.) At higher pressures the material is reported to turn opaque, as a result of a phase transition to the metallic tin structure. Some of the pertinent data related to pressure studies are given in Table III. Figure 23 shows the shift in the absorption edge as a function of pressure for InP. The development of the tail in the absorption edge signifies the influence of the (X) conduction band, which moves down in energy with pressure. The direct energy-gap change (dE_g/dP), when plotted against pressure, exhibits a marked sublinearity in all cases, but becomes linear in the case of InP when plotted against the lattice parameter change. However, in the case of both Ge and GaAs a small sublinearity still

TABLE III. Mode Grüneisen parameters for some diamond/zinc-blende crystals (Trommer *et al.*, 1980). The original sources of the data are cited in Trommer *et al.* (1980).

	LO	TO	TA(X)	TA(L)	Transition pressure (kbar)[a]
C	0.98±0.04	0.98±0.04	0.4 ±0.9		
Si	1.04±0.01	1.04±0.01	−1.4 ±0.2	−1.3 ±0.3	125±5
Ge[b]	1.12±0.02	1.12±0.02	−1.53± .05		80±5
GaP	0.95±0.02	1.09±0.03	−0.72±0.03	−0.81±0.07	220±10
GaAs	1.23±0.02	1.39±0.02	−1.62±0.05	−1.72±0.15	172±7
GaSb	1.21±0.02	1.23±0.02			80
InP	1.24±0.02	1.44±0.02	−2.08±0.1	−2.00±0.1	100
AlSb	1.27±0.05	1.23±0.05			77
ZnS	0.95±0.1	1.85±0.2	−1.55±0.2	−1.0 ±0.2	150±5
ZnSe	0.9 ±0.1	1.4 ±0.1	−1.30±0.2	−1.5 ±0.2	137±3
ZnTe	1.2 ±0.1	1.7 ±0.1	−1.55±0.2	−1.5 ±0.2	100

[a]Pressure at which the diamond/zinc-blende lattice becomes unstable. The data are mainly from Piermarini and Block (1975) and Ruoff and Baublitz (1981).
[b]Olego and Cardona (1982).

remains. Welber *et al.* (1975, 1977) have shown that this sublinearity is reproduced in calculations using the method of pseudopotential and that it is consistent with the theory.

Luminescence studies yield information about the direct-gap change with pressure and the results are consistent with absorption measurements. The luminescent intensity begins to drop sharply at the Γ-X band crossing and thus is a good indicator to determine the band crossing. The luminescence and absorption data for InP are plotted against lattice parameter change in Fig. 24(a), while Fig. 24(b) shows the rapid fall in the luminescence, near the band crossing.

2. CuCl

CuCl exhibits several phase transitions under pressure, among which the reported semiconductor-to-metallic transition at about 45 kbar (Chu *et al.*, 1978) has attracted much attention. However, recent optical absorption measurements to 150 kbar (Müller, Ves, *et al.*, 1980; Ves *et al.*, 1981), structural and microscopic studies to 125

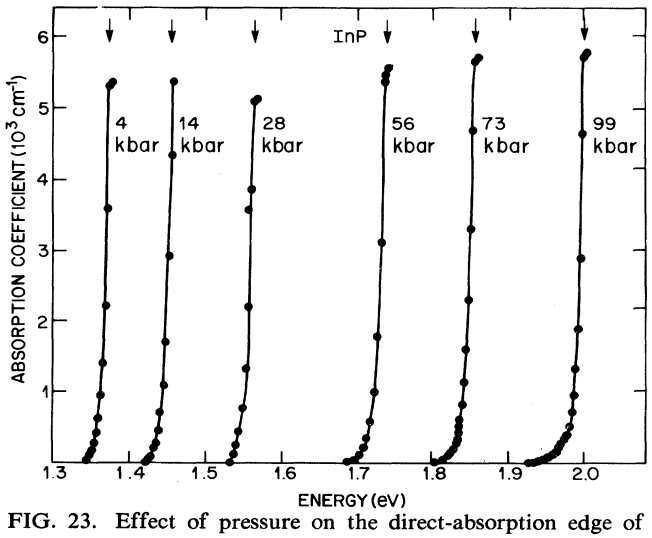

FIG. 23. Effect of pressure on the direct-absorption edge of InP. The development of the tail at high pressures signifies the influence of the indirect edge (after Trommer *et al.*, 1980).

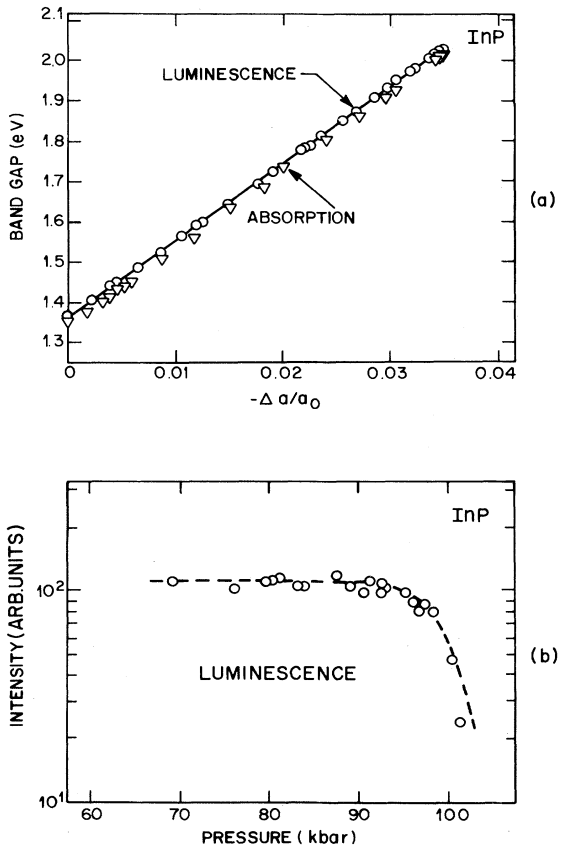

FIG. 24. (a) Band-gap change of InP plotted against lattice parameter change, from luminescence and absorption measurements. (b) Shows the luminescence intensity vs pressure. Sharp change is due to the onset of phase transition (after Trommer *et al.*, 1980).

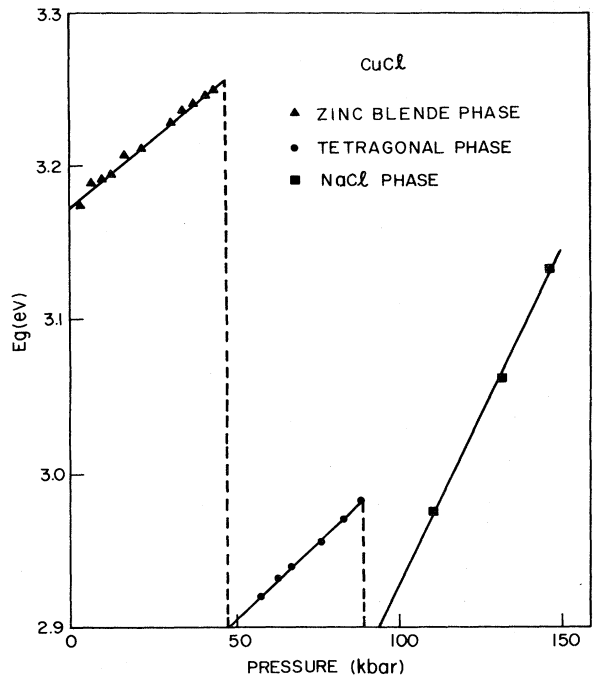

FIG. 25. The band-gap variation in CuCl with pressure. The discontinuities are due to first-order phase transitions (after Müller, Ves, *et al.*, 1980).

kbar, and resistance measurements in the DAC (Piermarini *et al.*, 1979) give no support for a transition to the metallic state. The structure changes from the zinc-blende to the tetragonal structure near 45 kbar and from the latter to the rock-salt-type structure near 80 kbar are clearly seen in the x-ray powder studies, in qualitative optical transmission studies under the microscope, and in quantitative optical absorption measurements. The pressure dependence of the energy gap from optical absorption data is reproduced in Fig. 25. The abrupt changes are due to the first-order pressure-induced phase changes to the above-mentioned structures. There is some evidence that nonhydrostatic pressure leads to decomposition when CuCl is in the NaCl phase. More recent optical investigations on very high-purity CuCl (Batlogg and Remeika, 1980) have shown that the evidence presented in an earlier study for the existence of a smaller indirect gap in CuCl (in support of a transition to the excitonic superconducting state) does not exist in the pure material.

3. As_2S_3 and GeS_2

In these systems high-pressure optical absorption and refractive index measurements have been reported for both the crystalline and amorphous forms. The results have been used to derive information regarding the network dimensionality in the amorphous state. Crystalline As_2S_3 (Besson *et al.*, 1981) as well as As_2S_3 glass (Weinstein, Zallen, and Slade, 1980) and amorphous GeS_2 (Zallen, Weinstein, and Slade, 1981) exhibit an unusually large decrease in the energy gap (red shift) with pressure. Figures 26(a) and (b) show the pressure dependence of both the gap and the refractive index for two crystalline forms of GeS_2, namely, $2d$-GeS_2 and $3d$-GeS_2, and the amorphous α-GeS_2. The $3d$-GeS_2 is quartzlike in structure, and $2d$-GeS_2 has a layer structure. By comparing the refractive-index behavior under pressure, Weinstein *et al.* (1982) concluded that the amorphous form closely resembles $2d$-GeS_2 and hence it has a molecular structure with dimensionality less than 3. From the response to hydrostatic pressure of the optical absorption and refractive index and from the main Raman band of As_2S_3 glass, it is concluded that the latter is composed of discrete macromolecules.

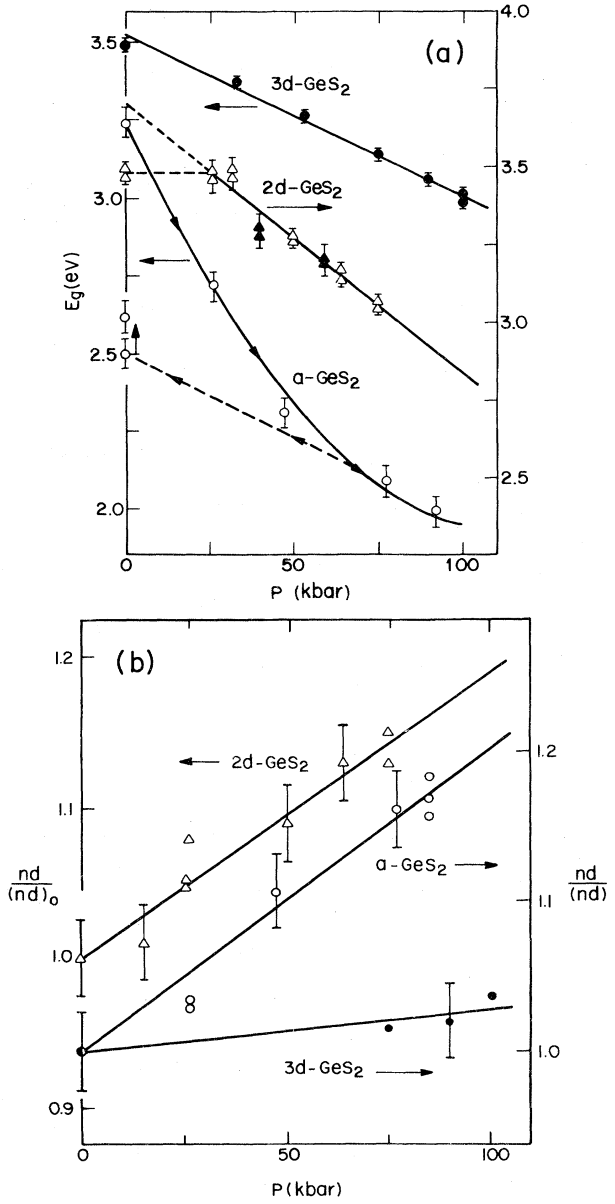

FIG. 26. (a) Band-gap variation in different crystalline states of GeS_2 with pressure; $3d$ is quartzlike, $2d$ has a layer structure, and a is amorphous. (b) The normalized refractive index change with pressure for the three forms. The a-GeS_2 slope closely resembles $2d$-GeS_2, hence has dimensionality <3 (after Weinstein *et al.*, 1982).

B. Optical reflectivity measurements

Optical reflectivity measurements are useful to derive information on the electronic structure of highly absorbing and metallic systems. While quantitative reflectivity measurements are not difficult to carry out under ambient conditions, it becomes a challenging problem to carry out such measurements in the DAC. Bassett, Takahashi, and Stook's (1967) optical observations and the measurement of the reflectance change accompanying the α to ε-Fe transition seem to be the first reported reflectivity measurement with the DAC. They used a simple optical setup and found that the brighter yellowish appearance of ε-Fe was due to a rising reflectance edge near 650 nm. In recent years microspectroscopic techniques have been devised for quantitative measurements by Welber (1977) and by Syassen and Sonnenschein (1982). The latter have devised a microoptic double-beam system which overcomes some of the difficulties of the single-beam system of Welber. Using these systems, quantitative reflectivity measurements on SmSe (Welber and Jayaraman, 1979) and more recently on I, Cs (Syassen *et al.*, 1981a), and anthracene (Sonnenschein, Syassen, and Otto, 1981) have been performed to elucidate the electronic structure changes that take place in these materials under pressure.

SmSe undergoes a continuous $4f$-electron delocalization and valence change with pressure (Jayaraman *et al.*, 1970a, 1970b). With increasing pressure the sample goes through a sequence of color changes from black, steel blue, deep purple, and a copperlike metallic color to bronze-yellow metallic. A quantitative study of this phenomenon has been carried out to 70 kbar by Welber and Jayaraman (1979). From the reflectivity the plasma frequency ω_p, τ the relaxation time, and $\sigma(0)$ the static conductivity were evaluated by fitting to the three-parameter Drude expression

$$\varepsilon(\omega)=\varepsilon_\infty-\frac{\omega_p^2}{\omega(\omega+i/\tau)}=\varepsilon_1+i\varepsilon_2\,, \tag{5}$$

where ε's are the dielectric constants. The observed deviations from the Drude theory are regarded as evidence for interband contributions to the dielectric constant, which determine the characteristic metallic colors in rare-earth monochalcogenides.

1. Cesium

Cesium is believed to undergo a $6s$-$5d$ electronic transition under pressure, and all the anomalous physical properties under pressure are attributed to this electronic transition. Also, recent band-structure calculations by Glötzel and McMahan (1979) have given support to such a change in the electronic structure. Syassen *et al.* (1981a) have recently measured the reflectivity of Cs to 136 kbar, with a view to obtaining spectroscopic evidence for the $6s$-$5d$ transition. Cesium undergoes several phase transitions in the 1—50 kbar range: bcc→fcc at 22.5 kbar, fcc I→fcc II at 42.5 kbar, fcc II—Cs IV at 43.7 kbar (Jayaraman, Newton, and McDonough, 1967). The reflectivity of bcc and fcc I-CS are shown in Figs. 27(a) and (b). Figure 28 shows a plot of the optical conductivity obtained from a Kramers-Kronig analysis of the optical reflectivity data at two pressures. The deviation from Drude behavior of the optical conductivity and the large peak in σ are interpreted as evidence for s-d transition. From the pressure dependence of the reflectivity it is believed that a $6s$-$5d$ transition occurs continuously from the beginning, as well as discontinuously near 42 kbar in Cs.

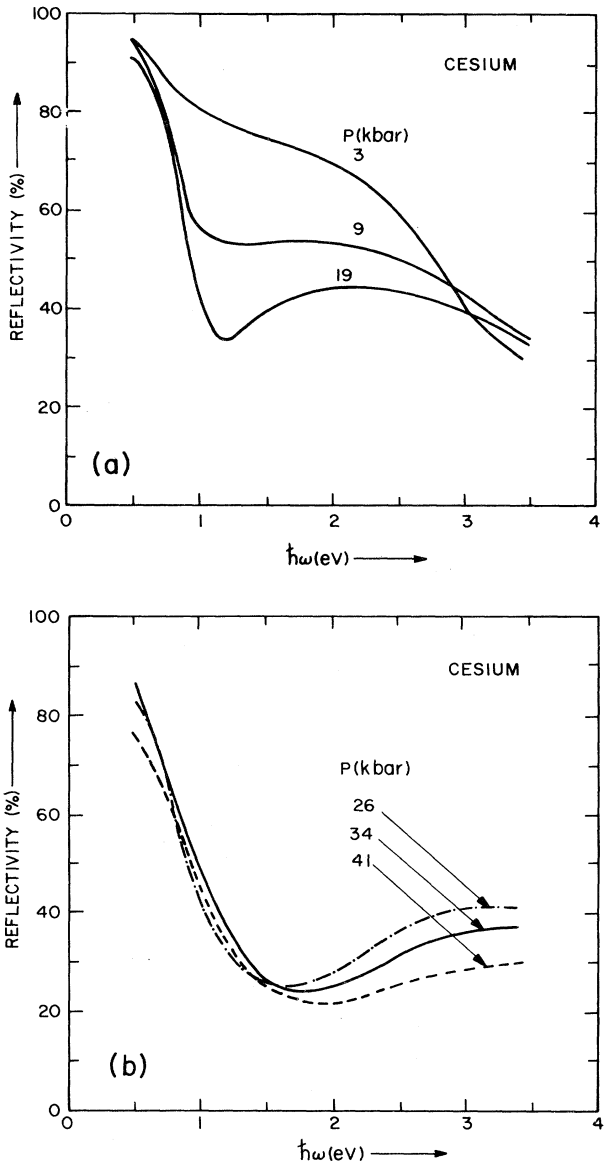

FIG. 27. Reflectivity data for Cs at different pressures. (a) Reflectivity in the bcc phase. (b) In the fcc phase (after Syassen *et al.*, 1981a).

2. Iodine

The optical reflectivity of I under pressure has been studied up to 300 kbar by Syassen *et al.* (1981a). Figure

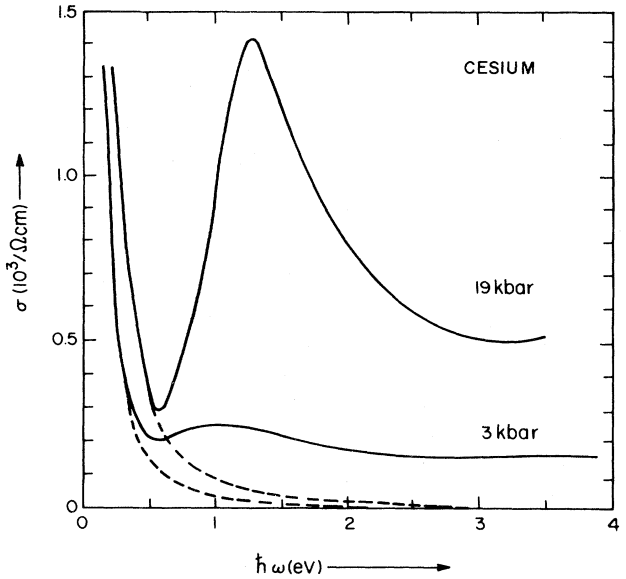

FIG. 28. Optical conductivity of Cs extracted from the reflectivity data. The dashed lines correspond to Drude-type conductivity. Anomalies explained on the basis of *s-d* crossing (after Syassen *et al.*, 1981a).

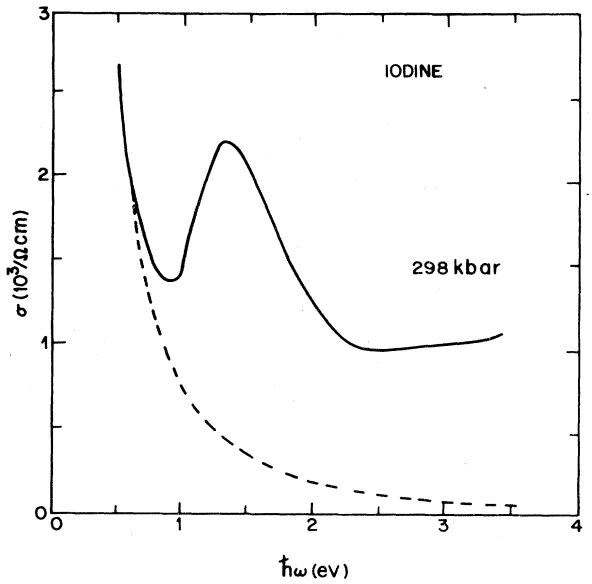

FIG. 30. Optical conductivity of iodine at 298 kbar, extracted from the reflectivity data. The dotted line is the Drude-type conductivity. The anomaly is due to 5*p*-5*d* interband absorption (after Syassen *et al.*, 1981a).

29 shows the reflectivity data and Fig. 30 the optical conductivity data extracted from a Kramers-Kronig analysis of the reflectivity. The molecular-to-monatomic transition at about 210 kbar is reflected in the first occurrence of a low-energy structure in the curve for 210 kbar. The increasing reflectivity between 1.5 and 3 eV in the high-pressure curves is regarded as evidence for higher electronic density in the monatomic phase of iodine and is evidence that it is a *p*-band metal. The 1.3-eV peak is attributed to an interband absorption due either to transitions in the 5*p* subbands, or to transitions from 5*p* to the bottom of the excited 5*d* band. (See Sec. V.B.)

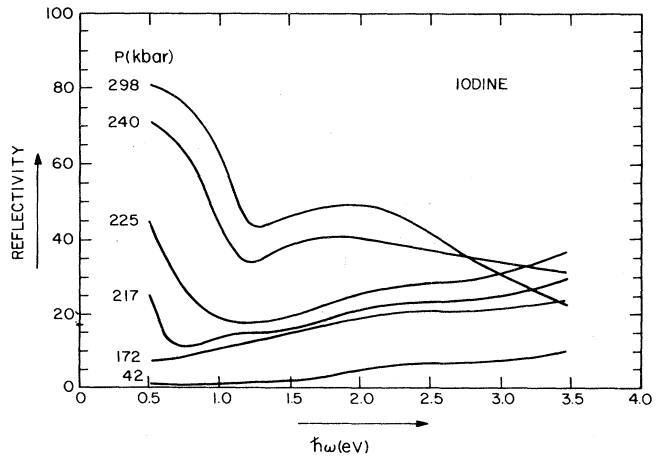

FIG. 29. Optical reflectivity of iodine in the pressure range 42—298 kbar. The dip near 1.3 eV in the monatomic metallic phase (225, 240, 298 kbar curves) is ascribed to 5*p*-5*d* interband absorption (after Syassen *et al.*, 1981a).

C. Raman scattering studies on solids at high pressure

Raman scattering experiments in the DAC provide a convenient way of investigating the effect of pressure on the optical phonons in crystalline solids to several hundred kilobars. From the pressure-induced shifts in the phonon energies, information on interatomic binding forces in crystals, charge transfer effects, and structural instabilities can be extracted. The volume dependence of the phonon dispersion can provide a testing ground for the lattice-dynamical models, as it is difficult to obtain the dispersion and the mode Grüneisen parameters without a knowledge of both the long- and short-range forces in crystalline solids. Structural instabilities are reflected in the phonon dispersion as phonon softening, and a new phonon spectrum appears when a phase change occurs. Charge transfer effects are seen in the so-called LO-TO splittings. The intermolecular interactions are strongly enhanced by pressure in molecular crystals. In recent years a number of semiconductors crystallizing in the diamond/zinc-blende structure and some ternary compounds with the related chalcopyrite structure, as well as several molecular crystals, have been studied in the DAC, and a variety of interesting data have been gathered (Weinstein and Zallen, 1982). Some of these results will be discussed.

1. General considerations

a. Mode Grüneisen parameter

The phonon dispersion under pressure is described in terms of the mode Grüneisen parameters γ_i defined by

$$\gamma_i = -\frac{\partial \ln \omega_i}{\partial \ln V} = \frac{1}{\beta \omega_i}\left[\frac{\partial \omega_i}{\partial P}\right], \tag{6}$$

where ω_i is the phonon frequency, β is the isothermal compressibility, V is the volume of the crystal, and P is the pressure. The dimensionless quantity γ_i is obtained from the measured pressure dependence of the mode frequency ω_i and the isothermal compressibility β_T of the substance. γ_i is usually positive, since vibrational frequencies almost always increase with compression. Weighted averages of the γ_i enter into the theories of thermal expansion and equation of state of solids. In order to construct a simple theory of thermal expansion $(\alpha)_V$, Grüneisen assumed all the the γ_i to be equal, whence

$$(\alpha)_V = \gamma \beta C_V . \tag{7}$$

C_V is the specific heat at constant volume. For three-dimensional network crystals, the Grüneisen approximation is a useful idea of reasonable validity. The optical phonons in the covalently bonded Ge family and III-V semiconductors exhibit γ close to unity. For II-VI semiconductors the pressure variation of the optical phonon frequencies corresponds to γ of about 2, while for alkali halides γ is about 3 (see Zallen, 1974). However, the Grüneisen approximation breaks down in the case of molecular crystals. Whereas the intermolecular modes are roughly in agreement with it, the intramolecular modes are grossly in disagreement (see Sec. III.C.6).

b. $d\omega/dT$

The temperature dependence $d\omega/dT$ in crystals consists of two contributions: (1) due to the effect of temperature on the vibrational excursions of the atoms about their equilibirum positions ("explicit" term), and (2) due to the volume change, via the thermal expansion ("implicit" term). These two contributions can be expressed by the relation

$$\left[\frac{d\omega}{dT}\right]_P = \left[\frac{\partial \omega}{\partial T}\right]_V - \left[\frac{\alpha_V}{\beta}\right]\left[\frac{d\omega}{dP}\right]_T , \tag{8}$$

where $(\alpha)_V$ and β are the volume thermal expansion and compressibility, and $(\alpha_V/\beta)(d\omega/dP)$ the "implicit" term. Since $(d\omega/dP)_T$ is available from pressure experiments, the relative importance of these two contributions can be determined. The fraction of total temperature coefficient, which can be attributed to the "explicit" contribution $(\partial\omega/\partial T)_V$, is denoted by θ (Zallen and Slade, 1978)

$$\theta = \frac{(\partial\omega/\partial T)_V}{(\partial\omega/\partial T)_P} = 1 - \left[\frac{dT}{dP}\right]_\omega \left[\frac{\beta}{\alpha_V}\right]^{-1} . \tag{9}$$

From the measured value of α and β, θ can be computed using the above expression. If θ_i is small, the volume-driven ("implicit") contribution is dominant, and if it is closer to 1, the "explicit" term is the dominant one.

c. Transverse charge e_T^*

Another effect of pressure on the phonon frequencies is the LO-TO splitting. The LO-TO splitting $\omega_{LO}-\omega_{TO}$ is related to the microscopic theory through Born's transverse dynamical charges e_T^* (Born and Huang, 1954, Chap. 2)

$$\omega_{LO}^2 - \omega_{TO}^2 = 4\pi e_T^{*2}/MV\varepsilon_\infty , \tag{10}$$

where V is the volume of the unit cell, M the reduced mass $[1/M=(1/M_a+1/M_b)]$, and ε_∞ the infrared dielectric constant for frequencies well above the highest ω_L and below the electronic absorption edge. The theory can be generalized to a primitive cell with more than two atoms to yield

$$\omega_{LO}^2 - \omega_{TO}^2 = \frac{4\pi N}{\varepsilon_\infty}\sum_i \left[\frac{e_i^* n_i}{M_i^{1/2}}\right]^2 , \tag{11}$$

where l/N is the volume of the primitive cell, e_i^*'s are the transverse dynamical charges on the ion, M_i is the atomic mass, and $\hat{n}_i$ are the eigenvectors of the ir-active modes under consideration.

The splitting can be calculated if the dynamical charges and the eigenvectors are known. The dynamical charges for a given tetrahedral bond can be calculated from the bond-orbital model for tetrahedral semiconductors (Harrison, 1980). This model gives the transverse charge in units of electronic charge

$$e_T = -\Delta Z + \tfrac{20}{3}\alpha_P - \tfrac{8}{3}\alpha_P^3 , \tag{12}$$

where ΔZ is one-half the difference in core charges between the anion and the cation and α_P is the polarity or ionicity of the bond, as defined by Harrison (1980). The charges thus obtained [from Eq. (12)] have been compared with Born's transverse charge calculated from Eq. (10) and the experimental LO-TO splittings in some studies (Carlone, Olego, *et al.*, 1981). Also, Eq. (12) has been used to get the α_P dependence on the lattice parameter, from the charges derived from Eq. (10) (Trommer *et al.*, 1980).

2. Diamond zinc-blende semiconductors

Because of the high symmetry of the diamond/zinc-blende lattice, the Raman spectra of substances crystallizing in these structures are simple to understand in terms of the vibronic properties of the two atoms in the unit cell. With the diamond-structure-type elemental substances, there is only one Raman line appearing in the first order because of the degeneracy of the LO and TO phonon energies. In the zinc-blende structured materials, the LO-TO phonons are split because of the positive and negative charges on the two ions in the unit cell, giving rise to two Raman lines in the first-order spectrum. In fact, charge transfer under pressure has been determined from the LO-TO splitting in a number of systems.

The second-order Raman spectrum of diamond/zinc-blende crystals is a broad spectrum with some sharp

features (critical points), comprising of overtones and combinations. Since the entire Brillouin zone (BZ) contributions to the second-order Raman scattering intensity, the spectrum is broad, but the zone-boundary phonons have a high density of states which lead to the so-called critical points. The sharp features associated with these critical points can be followed as a function of pressure and this enables one to determine the phonon dispersion of many of the zone-boundary acoustic and optical phonons. In several diamond/zinc-blende-type crystals the pressure shift of the TA phonon has been determined from their second-order spectra, and it has been shown that the TA phonons exhibit a negative Grüneisen γ, a feature that has been related to the occurrence of pressure-induced phase transitions in these lattices (see Klement and Jayaraman, 1967; Pistorius, 1976).

a. Si, GaP, InP

Raman scattering measurements under pressure on Si and GaP (Weinstein and Piermarini, 1975), Ge (Asaumi and Minomura, 1978; Olego and Cardona, 1982), GaAs (Trommer, Anastassakis, and Cardona, 1976), ZnS, ZnSe, ZnTe (Weinstein, 1977), and InP (Trommer *et al.*, 1980) have been reported up to their phase transition pressure. The energy gap increases with pressure in most of the diamond/zinc-blende group of semiconductors. Consequently, some of them become more transparent to laser radiation at high pressure than at atmospheric pressure, yielding good Raman spectra. GaAs is a particularly good example of this situation. Also, since the energy gap changes with pressure, pressure experiments offer the possibility of observing resonance Raman effects (Weinstein, Renucci, and Cardona, 1973; Trommer *et al.*, 1980).

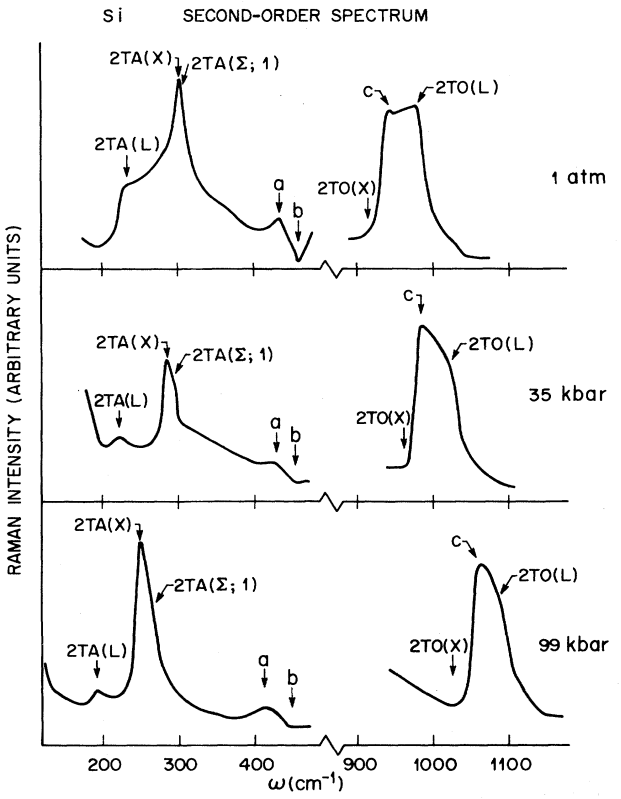

FIG. 32. The second-order Raman spectrum of Si at different pressures (from Weinstein and Piermarini, 1975). The shift in the peak positions (critical points) can easily be followed. The assignment of the peaks follows from neutron work.

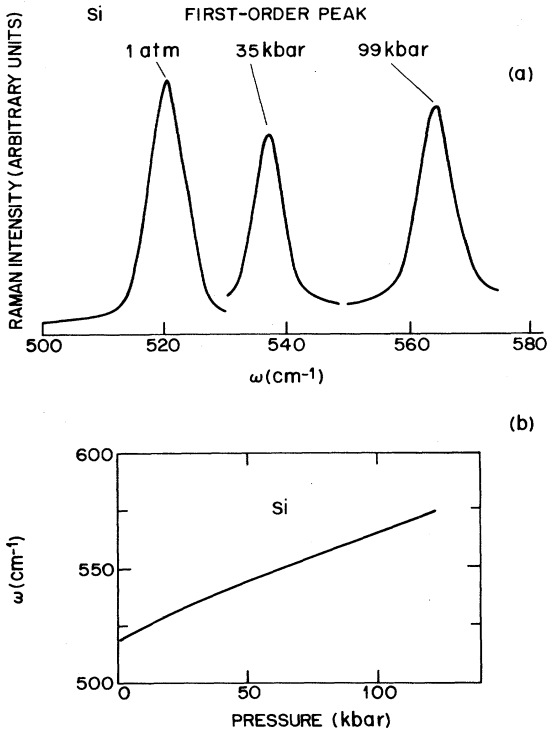

FIG. 31. Shift of the first-order Raman line in Si with pressure. (a) shows the peaks, and (b) the shift with pressure (after Weinstein and Piermarini, 1975).

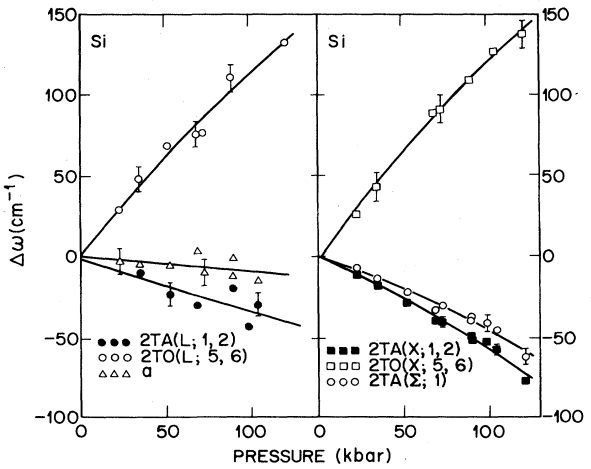

FIG. 33. The shifts of the critical points of the second-order Raman spectrum of Si plotted against pressure. The softening of the TA mode is to be noted, for it signifies a phase transition (after Weinstein and Piermarini, 1975).

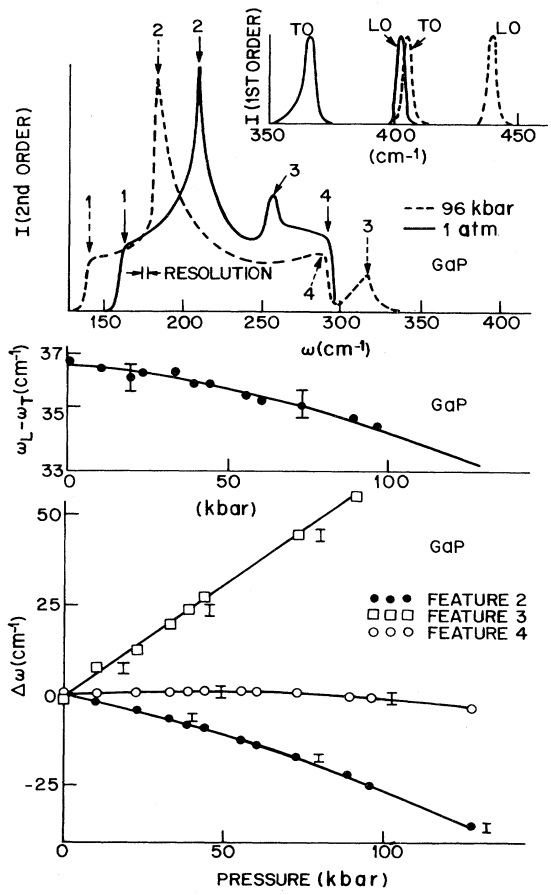

FIG. 34. The first- and second-order Raman peaks of GaP at 1-atm pressure (solid line) and 96 kbar (dotted line). The variation of the LO-TO splitting with pressure is shown in the middle, while at the bottom the shifts of critical points in second-order Raman spectrum are plotted against pressure (after Weinstein and Piermarini, 1975).

The pressure dependence of the phonons in group-IV elements, and in III-V and II-VI compounds, is illustrated with Si, GaP, InP, and ZnS as examples, from the studies of Weinstein and Piermarini (1975) and from Trommer *et al.* (1980). In Fig. 31 the pressure-induced shift of the first-order Raman peak of Si is shown and in Fig. 32 the second-order Raman peak of Si at three pressures is shown. Figure 33 is a plot of the shift in the frequency with pressure of the critical points in the two-phonon spectrum, identified from the critical-point assignments (as due to 2TA, 2TO phonons associated with the L and X points in the BZ).

In Fig. 34 the pressure effect on the first- and second-order Raman spectrum of GaP is shown. Similar data for InP are reproduced in Figs. 35 and 36. In both cases the LO and TO phonons shift to higher frequency. Pressure dependences of the sharp features of the second-order spectrum are plotted in Figs. 34 and 36 (bottom) for GaP and InP. The labeling of these features also follows from the critical-point assignments from neutron scattering results (see Weinstein and Piermarini, 1975).

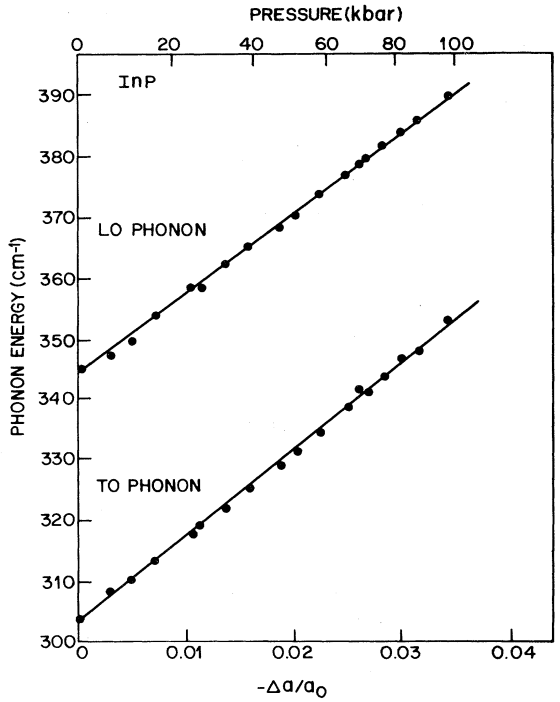

FIG. 35. The LO-TO phonon shift in InP with pressure and lattice parameter change (after Trommer *et al.*, 1980).

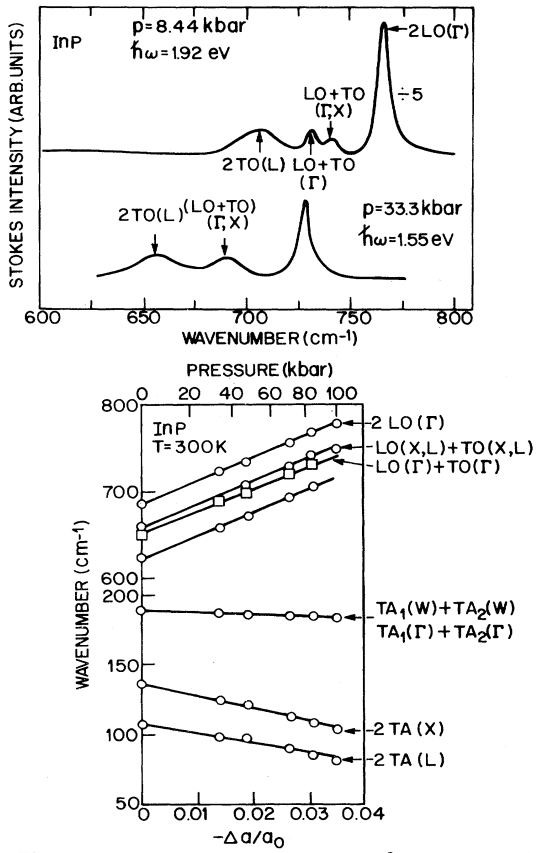

FIG. 36. The second-order Raman spectrum of InP at two different pressures. Bottom figure shows the effect of pressure and lattice parameters on the second-order Raman features (critical points) in InP (after Trommer *et al.*, 1980).

b. Zn chalcogenides

The phonon dispersion in ZnS obtained from high-pressure Raman measurements near the transition pressure of 150 kbar (Weinstein, 1977) is shown in Fig. 37. The curves are based on high-pressure Raman data interpolated between critical points, according to the shape of the one-atmosphere phonon dispersion curves obtained from neutron measurements. The latter are also shown in Fig. 37 as squares, triangles, and circles. The justification for drawing full phonon dispersion curves from Raman data limited to critical points is that so long as pressure remains hydrostatic, the phonon dispersion curves remain analytic. The phonons in Zn chalcogenides behave similarly under pressure, with only the magnitude of the effects varying from one material to the other.

The mode Grüneisen parameters for a number of diamond/zinc-blende semiconductors are given in Table III. The compressibilities needed to calculate the γ_i were usually obtained through the use of the Murnaghan's equation of state and elastic constant data. A comparison of the experimentally obtained γ_i with the theoretically predicted γ_i has been made by Weinstein and Piermarini (1975), finding that the predicted γ_i are substantially different from the measured values; in particular, the largest discrepancy is for the TA mode that softens under pressure. According to Olego and Cardona (1982), recent microscopic theoretical calculations for Ge and Si (Wendel and Martin, 1979; Soma, Matsuo, and Saitoh, 1981a, 1981b) have yielded γ_i which are in much better agreement with the measured values. Also to be noted are the *ab initio* calculations of Yin and Cohen (1980, 1981) for Si and Ge, which yield excellent agreement with the measured γ_i, and also predict the pressure-induced phase transitions in these materials in good agreement with experiment.

The increase of the LO-TO phonon frequency and the softening of the lowest acoustic branch (TA) with pressure in the diamond/zinc-blende semiconductors is now a well-established pressure effect. It has been shown that the TA mode softening is indicative of the weakening of noncentral forces of long-range origin needed to stabilize the tetrahedral lattice against the short-wavelength shear distortion (Weber, 1974). Therefore, it is conjectured that the zone-boundary TA phonon softening is a likely driving mechanism for the pressure-induced phase transition, ubiquitous in the diamond/zinc-blende materials. A relationship between negative γ_i of the TA modes and the pressure-induced transitions in diamond/zinc-blende semiconductors was first suggested by Weinstein (1977). The data of Trommer *et al.* (1980) and Olego and Cardona (1982) also support this suggestion. Although the phase transitions occur at pressures far below the pressures at which the TA mode frequencies would be driven to zero, it is believed that the relationship suggested by Weinstein has some appeal. The plot of $\gamma\mathrm{TA}(X)$ against the observed transition pressure is presented for a number of cases in Fig. 38. The linear relationship is not strictly obeyed, as is evident from Fig. 38.

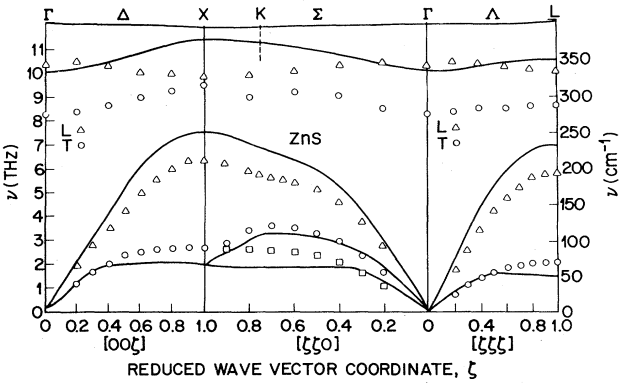

FIG. 37. The phonon dispersion relation (solid line) in ZnS at 150 kbar from the shifts of the second-order Raman features. The data points are from 1 atm phonon dispersion curves from neutron data. High-pressure Raman data interpolated according to the shape of the 1-atm data (after Weinstein, 1977).

c. Charge transfer

In Fig. 39 the LO-TO splitting as a function of pressure as well as lattice parameter change is shown for InP. The splitting decreases with increasing pressure and is characteristic of zinc-blende-type materials. From the experimental splittings the transverse charges have been calculated by Trommer *et al.* (1980) via Eq. (10), and a plot

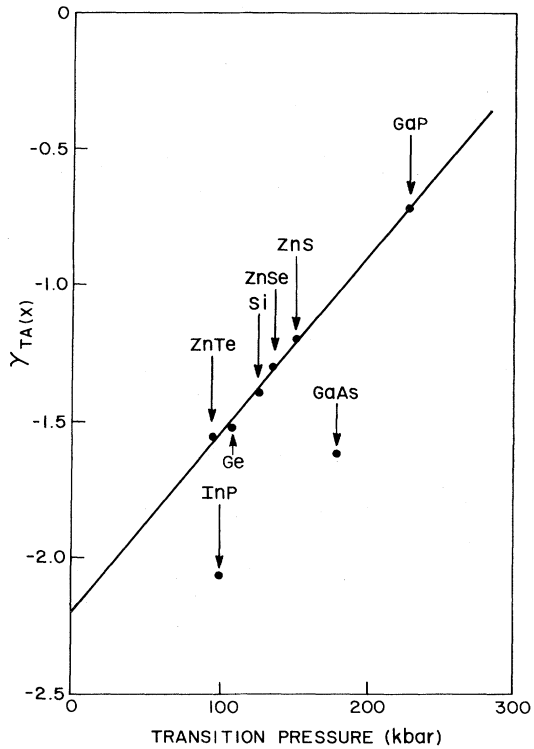

FIG. 38. A plot of the Grüneisen parameter against transition pressure for a number of diamond/zinc-blende-type semiconductors (Trommer *et al.*, 1980). The Ge point is included (after Olego and Cardona, 1982).

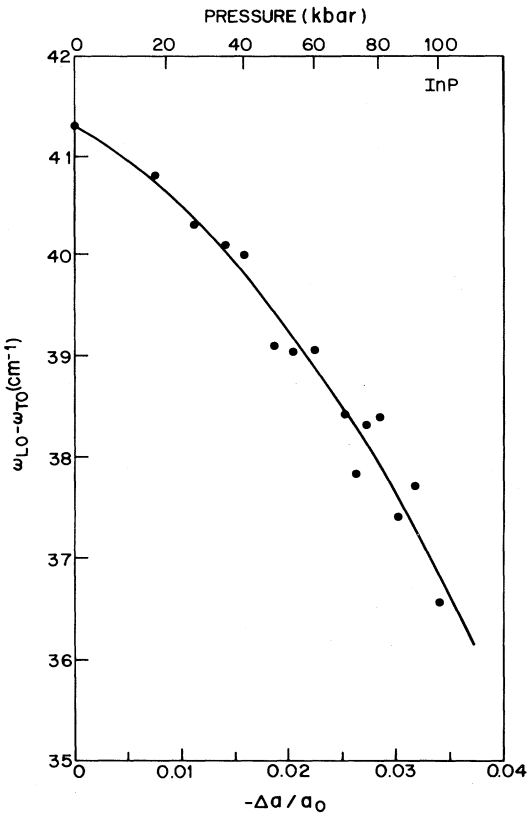

FIG. 39. Plot of the LO-TO splitting as a function of pressure and lattice parameter change for InP (after Trommer *et al.*, 1980).

of this against pressure, as well as the lattice parameter change, is shown for InP and GaAs in Figs. 40(a) and 40(b), respectively. In the plot, the transverse charges obtained from two other methods by Trommer *et al.* (1980) are also shown. In the one designated as $V_2 \propto a^{-2}$, the polarity α_P was calculated from the relation $\alpha_P = V_3/(V_2^2+V_3^2)^{1/2}$ (Harrison, 1976), where V_2 represents a covalent energy gap and V_3 is an ionic contribution to the gap, assumed to be independent of a. With this assumption and $V_2 \propto a^{-2}$, the α_P calculated was used in Eq. (12) to obtain e_T^* as a function of the lattice parameter. Trommer *et al.* (1980) have indicated another possible approach which uses the microscopic pseudopotential expression for e_T^*. In this approach e_T^* is expressed in terms of the Bloch states and energies of the crystal; the latter are obtained from a pseudopotential energy-band calculation (Vogl, 1978). The results of this calculation for InP and GaAs indicate a stronger pressure dependence of e_T^* than the experimentally obtained values. Trommer *et al.* (1980) conclude that both types of calculations predict the sign and magnitude of the observed effects reasonably well.

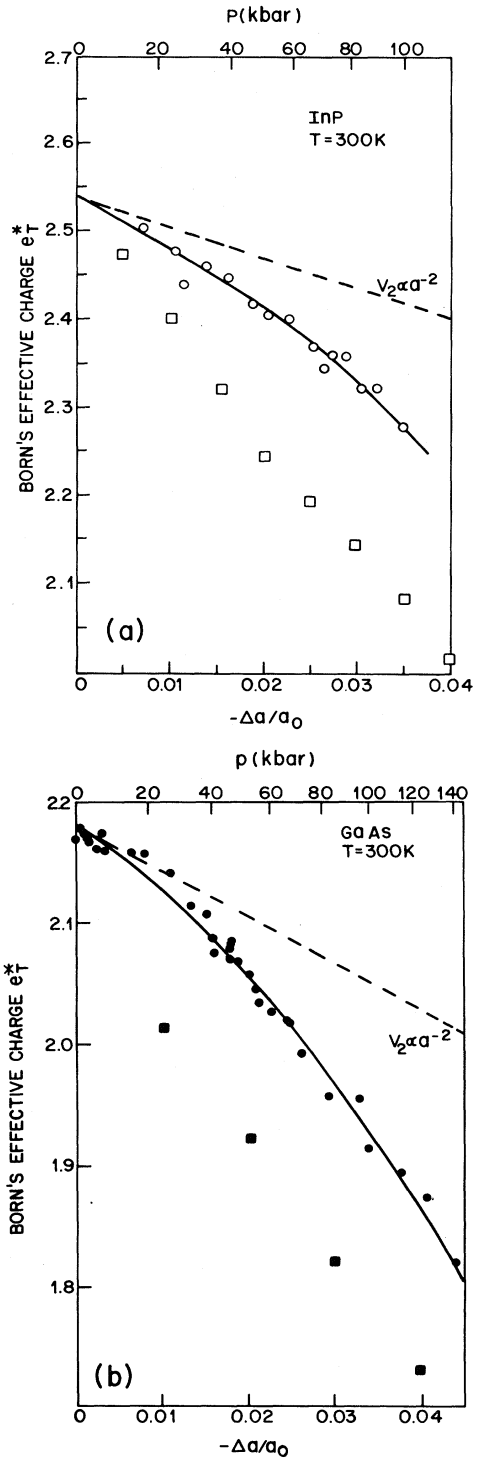

FIG. 40. (a) Born's transverse charge as a function of pressure and lattice parameters (for InP) calculated from LO-TO splitting, using Eq. (10). The squares represent the pseudopotential calculation. For the dotted line see text. (b) The same plot for GaAs (after Trommer *et al.*, 1980).

3. SiC

The effect of pressure on the first- (to 220 kbar) and second-order (to 110 kbar) Raman spectrum of SiC has recently been reported (Olego, Cardona, and Vogl, 1982; Olego and Cardona, 1982). Contrary to behavior in the diamond/zinc-blende materials, the LO-TO splitting in-

creases with pressure in 3C-SiC, indicating that the e_T^* increases with pressure. This has been attributed to a charge transfer from Si to C. Whereas the diamond/zinc-blende materials become less ionic on compression, 3C-SiC becomes more ionic upon compression. Olego, Cardona, and Vogl (1982) have shown that the local pseudopotential expression for e_T^* (for SiC the expression reduces to $e_T^* = 2.81 - 14.1\Delta a/a_0$) predicts an increase in charge with compression, consistent with the measurement. In Fig. 41 the e_T^* calculated is compared with the experiment, which shows a qualitative but not a quantitative agreement. On the other hand, the bond orbital model predicts even the sign wrongly ($e_T^* = 1.69 + 2.97\Delta a/a_0$), as is clear from Fig. 41. This failure is attributed to the neglect of the volume dependence of the ionic contribution to the effective gap, which enters in the definition of α_P. The Grüneisen parameters of several optical and acoustic phonons of 3C-SiC have been obtained from a study of the critical points in the second-order Raman spectrum with pressure.

4. $CuGaS_2$ and $AgGaS_2$

$CuGaS_2$ and $AgGaS_2$ crystallize in the chalcopyrite structure, which is related to the zinc-blende one. It can be regarded as a superlattice of the zinc-blende lattice, with the cations alternating. The pressure dependence of the Raman modes in $CuGaS_2$ and $AgGaS_2$ have been studied up to 200-kbar pressure recently (Carlone, Olego, *et al.*, 1981). The interest in these compounds is because of the pressure-induced phase transitions that occur in them. The chalcopyrite structure is also based on tetrahedral bonding and hence is vulnerable to high pressure (Werner, Hochheimer, and Jayaraman, 1981).

The Raman spectrum of chalcopyrite-structured compounds is rich in lines, and a majority of them have been followed as a function of pressure. The modes have been identified by applying group-theoretical analysis (Bettini, 1974). As in the diamond/zinc-blende materials, the lowest acoustic mode softens with pressure in $CuGaS_2$ and $AgGaS_2$ and therefore has a negative Grüneisen γ. The pressure dependence of the observed phonons in $AgGaS_2$ from Carlone, Olego, *et al.* (1981) are shown in Fig. 42. This a good example to show the effect of phase transitions on the phonon spectrum. Two phase transitions occur in this compound; a subtle phase transition near 42 kbar to a hexagonal lattice (Werner, Hochheimer, and Jayaraman, 1981) and a further change to the rock-salt structure near 120 kbar. Both these transitions are reflected in the Raman spectrum as abrupt changes in the peak positions, intensity, and number of peaks. The different phases are marked as I, II, and III, respectively,

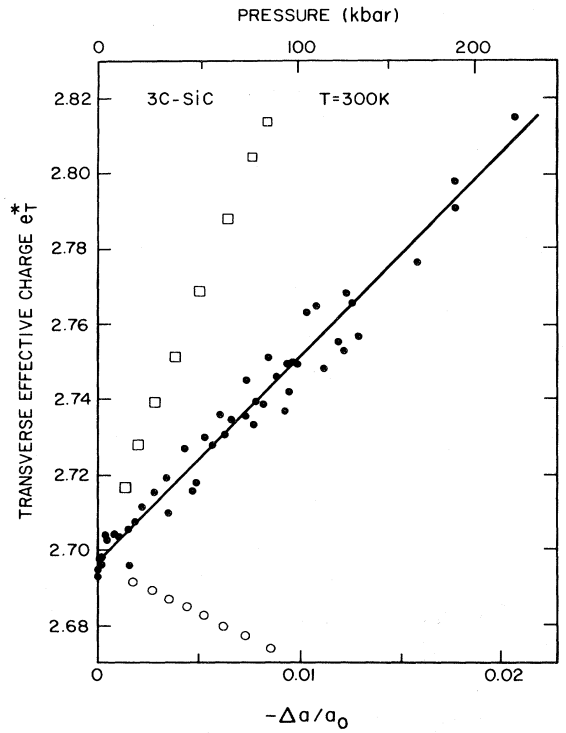

FIG. 41. Born's transverse charge obtained from experimental LO-TO splitting for 3C-SiC. Solid line is a fit to the data into $e_T^* = (2.697 \pm 0.004) - (5.45 \pm 0.10)\Delta a/a_0$. The squares are the results of pseudopotential calculation, and open circles are the predictions of the band-orbital model [Eq. (12)] (after Olego, Cardona, and Vogl, 1982).

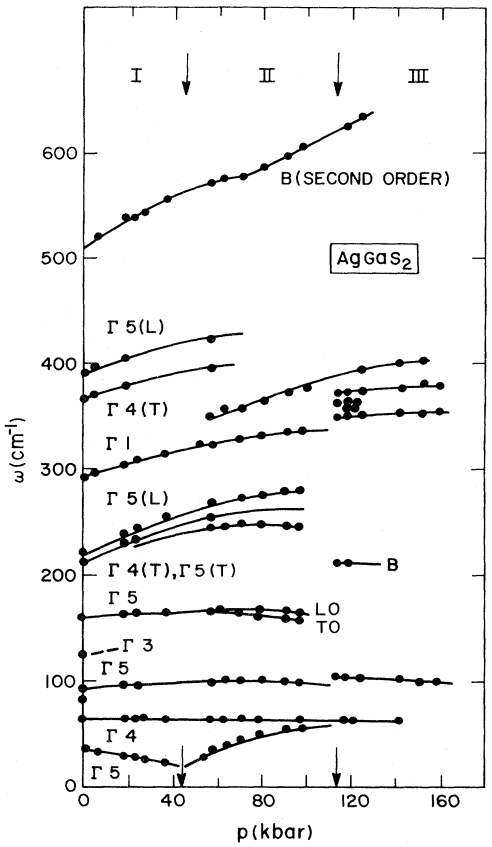

FIG. 42. The first-order Raman line shifts with pressure in $AgGaS_2$. The lowest-mode frequency softens. Phase changes occur near 42 and 120 kbar, and the Raman data reflect these (after Carlone, Olego, *et al.*, 1981b).

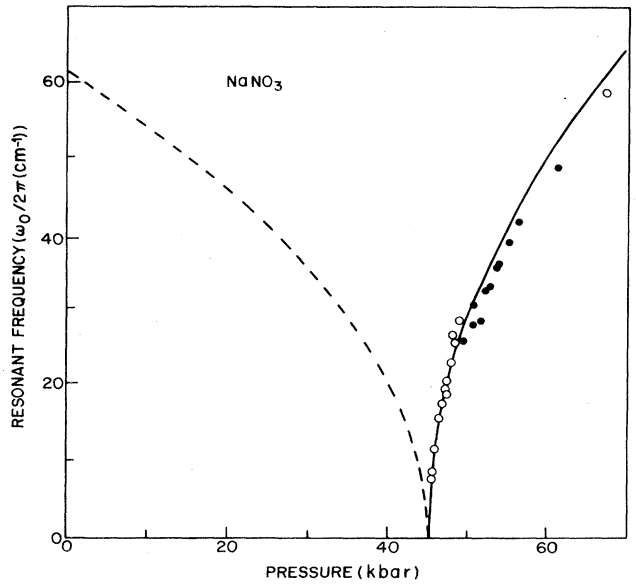

FIG. 43. Pressure dependence of the soft mode in $NaNO_3$. The A_1 symmetry mode inactive in the paraelectric phase becomes active in the high-pressure ferroelectric phase due to loss of the inversion symmetry. The solid curve is a least-squares fit using mean-field theory (see text) (after Lettieri, Brody, and Bassett, 1978).

in Fig. 42 to show their regions of stability. $CuGaS_2$ transforms from the chalcopyrite structure to the rock-salt structure (Werner, Hochheimer, and Jayaraman, 1981) at about 160-kbar pressure. Again, the Raman lines disappear at high pressure and the sample turns dark because of an abrupt change in the energy gap due to the phase transition to the rock-salt structure.

5. $NaNO_3$

$NaNO_3$ undergoes a pressure-induced transition to ferroelectric state. The soft-mode behavior under hydrostatic pressure in $NaNO_3$ has been studied by Lettieri, Brody, and Bassett (1978) by Raman measurements in a gasketed DAC, using 90° scattering geometry. In the paraelectric phase the soft mode is Raman inactive, but in the ferroelectric phase, due to the loss of inversion symmetry, the soft mode (A_1 symmetry) is Raman active. The pressure dependence of this mode is shown in Fig. 43. The solid curve is a least-square fit using a mean-field expression of the form

$$\frac{\omega_0}{2\pi} = A(P - P_c)^{1/2}, \quad P > P_c \tag{13}$$

in the ferroelectric phase, where ω_0 is the resonant angular frequency, P is the pressure, $P_c = 45.0 \pm 0.5$ kbar is the critical pressure, and $A = 13 \pm 1$ $cm^{-1}\,kb^{-1/2}$ (kb=kilobar). For the paraelectric form

$$\frac{\omega}{2\pi} = A/\sqrt{2}(P_c - P)^{1/2} . \tag{14}$$

The results show that a simple damped oscillator model is an appropriate phenomenological description of the soft-mode behavior in $NaNO_3$ transition and that there is no departure from mean-field behavior.

6. Molecular crystals

a. General description

In molecular crystals, the intramolecular bonding is strong, while the intermolecular bonding is weak. Because of this, there is a hierarchy of force constants in the crystal, and this is reflected in the Raman spectra. In a typical molecular crystal, one finds the Raman peaks from the intramolecular modes distinctly segregated (to high frequencies) from the low-frequency Raman peaks of the intermolecular modes. In general, molecular crystals exhibit a rich and complex Raman spectrum, but the above distinction helps in separating and understanding the pressure effects. Because molecular crystals are highly compressible, application of modest pressures strongly enhances the intermolecular interactions. Consequently, the frequencies of the intermolecular modes increase rapidly with pressure, while the effect of pressure on the internal mode frequencies is much weaker. Thus pressure differentiates the strength of the bonds in the system. Recent pressure studies on molecular crystals (Zallen, 1974; Zallen and Slade, 1978; and Chattopadhyay *et al.*, 1981, 1982) have yielded several interesting results which will be discussed.

In Fig. 44 the pressure dependences of the observed

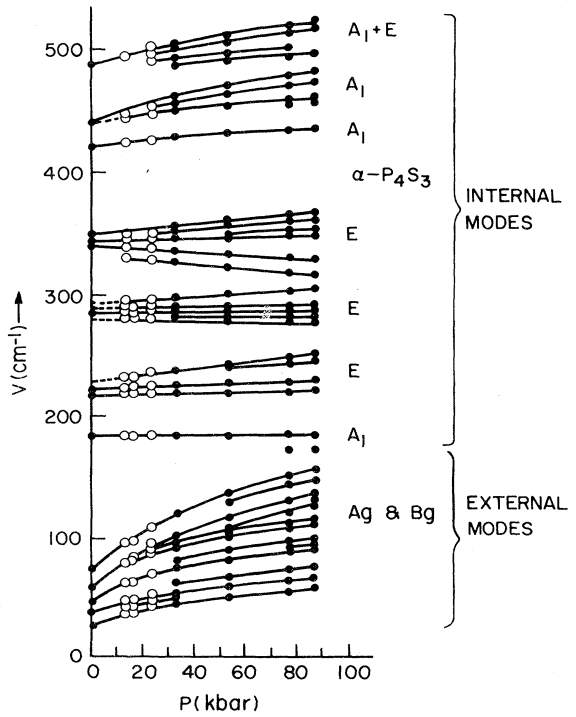

FIG. 44. Pressure dependence of the Raman frequencies in α-P_4S_3. The external modes are more sensitive to pressure than the internal ones. Open circles represent data obtained on releasing pressure (after Chattopadhyay *et al.*, 1981).

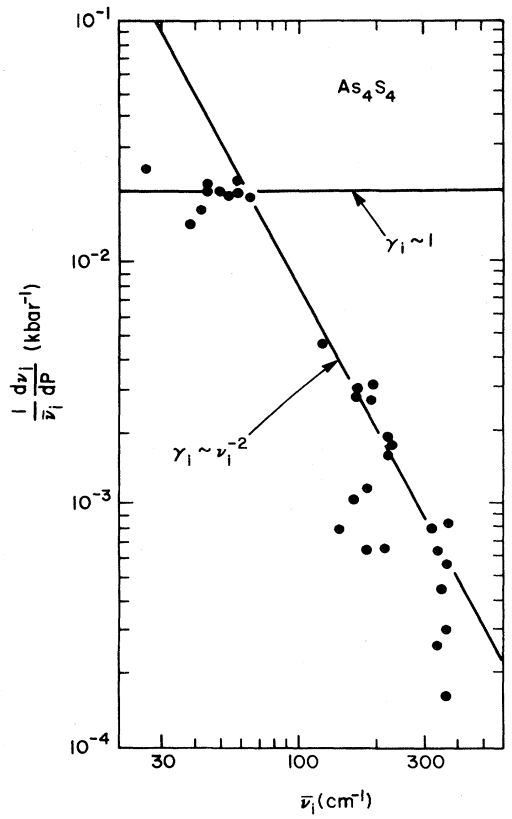

FIG. 45. A log-log presentation of phonon mode frequency shift with pressure (initial shifts) against mode frequency, to exhibit the vibrational scaling behavior in molecular crystals. The simple scaling law holds for external modes but not for internal modes, reflecting the disparity in bonding forces (after Zallen and Slade, 1978).

internal and external mode Raman frequencies from the measurements of Chattopadhyay *et al.* (1981) for α-P_4S_3 are shown. The external modes are well separted from the internal ones at low pressure, but at high pressures they get closer. The strong sensitivity to pressure of the external modes is clear. It may also be noted that within the grouping the higher-frequency Raman peaks are more strongly affected by pressure than the lower-frequency ones, resulting in spectral expansion with increasing pressure. In the high-pressure spectra many more lines are seen, especially in the internal-mode region and these are the Davydov splittings. The increased intermolecular interaction at high pressure and the spectral expansion referred to earlier conspire to reveal the Davydov splittings of the internal-mode frequencies, which are not resolved in ambient pressure and room-temperature spectra.

A special representation of the pressure Raman data was first suggested by Zallen (1974) (see also Zallen and Slade, 1978) for molecular crystals, shown for As_4S_4 in Fig. 45. Each point in Fig. 45 corresponds to a zone-center phonon which has been followed under presssure, with the horizontal axis set by zero-pressure Raman frequency and the vertical coordinate provided by the initial logarithmic pressure derivative $(1/\omega)(d\omega/dP)$. A log-log presentation is used for compactness.

b. Vibrational scaling behavior

The Grüneisen parameter γ_i connects the volume dilation $\Delta V/V$ with the fractional change in frequency by

$$\Delta\omega_i/\omega_i = -\gamma_i(\Delta V/V) = \gamma_i \beta P \ , \tag{15}$$

where ω is the frequency, P the pressure, and β the compressibility. In the Grüneisen approximation, all γ_i are assumed to be equal. This amounts to a scaling law in which the frequency spectrum uniformly expands as the crystal contracts

$$\omega \sim V^{-\gamma} \ . \tag{16}$$

Zallen (1974) first pointed out that such an approximation while still good for a single-bond-type solid fails in the case of molecular crystals. Since $d(\ln\omega_i)/dP$ is $\beta\gamma_i$, Grüneisen's approximation predicts a set of points, all lying on or near a horizontal line in a plot of $\log[1/\omega_i(d\omega_i/dP)]$ against $\log\omega_i$. Zallen and Slade (1978) demonstrated for the first time that, in such a plot for S_8, As_4S_4, and S_4N_4, although the Grüneisen approximation works for the external modes, it breaks down drastically in the intramolecular regime. Figure 45 shows the behavior for As_4S_4. For α-P_4S_3 the behavior is quite similar. In the external-mode region the points fall on the indicated horizontal line, while in the internal-mode region $d(\ln\omega)/dP$ rapidly decreases. In this connection Zallen (1974) has proposed a bond-scaling relationship which connects bond stiffness with bond length, $k \sim r^{-6\gamma}$, where k is the force constant, r the bond length, and γ a bond scaling exponent of the order of unity, applicable to both intramolecular and intermolecular bonds.

In the simplest model (Zallen and Slade, 1978) of a molecular crystal the bond-stiffness—bond-length scaling parameter γ is related to the external-mode Grüneisen parameter $\gamma_i \sim 2\gamma$ and $\gamma_0 \sim (k_1/k_0)2\gamma$, where k_1/k_0 is the intermolecular-to-intramolecular force constant ratio. The bond-stiffness—bond-length parameters γ and γ_i differ only by a geometry-determined factor of the order of unity, while the internal-mode Grüneisen parameter γ_0 is drastically reduced by the factor $k_1/k_0 \ll 1$. Qualitatively, γ_i is of the order of unity and is of normal size, but γ_0 is reduced to values of the order of 10^{-2}. Zallen and Slade (1978) have pointed out that the above-mentioned modification to the scaling law expresses the existence of disparate forces existing in a molecular crystal.

The latter authors have also justified the slope in Fig. 45 observed for the internal modes, invoking an inverse-square correlation between γ_i and mode frequency $\gamma_i \sim \omega_i^{-2}$, the latter following $\omega_i \sim k_i^{1/2}$ and $\gamma_i \sim k_i^{-1}$. The slope for α-P_4S_3 only approximately justifies the above. However, the overall features of the α-P_4S_3 pressure data support the ideas that have been advanced by Zallen and Slade to explain the vibrational spectrum of molecular crystals under pressure.

7. Two- and one-dimensional materials

The layer-structured compound As_2S_3 (Besson *et al.*, 1981) has been studied, and in some sense its behavior is not unlike that of molecular crystals. The results of both optical absorption and Raman studies show that interlayer interaction increases strikingly under pressure in crystalline As_2S_3 and that there is a smooth transition from two-dimensional to three-dimensional behavior.

The Raman spectrum of the quasi-one-dimensional systems $TCNQ^0$, TTF^0, K(TCNQ), $CS_2(TCBQ)_3$, perylene-TCNQ, and phenazine-TCNQ has been investigated to 70-kbar pressure by Carlone, Hota, *et al.* (1981). The Grüneisen parameters obtained range over several orders in magnitude. From the pressure- and gas-phase data it is concluded that the low-frequency modes in these compounds have a mixed character, and that a clear separation into external and internal modes is not possible, as in the case of P_4S_3 or As_4S_3. The log-log plot of the Grüneisen parameter against the phonon frequency shows a continuous variation. Both TTF^0 and $TCNQ^0$ undergo a change in color from yellow to dark red with increasing pressure and become opaque at about 80 kbar. These organic compounds are of interest because superconductivity has been observed under pressure and in chemically substituted members at ambient pressure. It is therefore important to understand how pressure influences the inter- and intramolecular forces.

IV. CONDENSED GASES

The quest for metallic hydrogen has stimulated the development of cryogenic and other filling techniques to trap condensed gases in the DAC for pressurization and study. As a result, the high-pressure behavior of N_2, O_2, H_2, He, and rare-gas solids has been investigated using Raman and Brillouin scattering, optical microscopy, and x-ray structure analysis. In several cases their equations of state have been determined and compared with theory. Pressure-induced phase transformations have been reported in N_2, O_2, and H_2. Another by-product of these studies is that H_2, He, and Xe are found to be excellent hydrostatic pressure media up to several hundred kilobars, even though they are solids at these pressures (Mao, Mao, and Bell, 1982). Their usefulness as pressure media is briefly stated in the earlier section. In this section Raman, Brillouin, and *P-V-T* measurements will be presented and discussed.

A. Hydrogen and deuterium

Hydrogen and deuterium have been the focus of attention for high-pressure studies in the DAC, for they carry the prediction of a transition to the metallic state at high densities and high-temperature superconductivity (Ashcroft, 1968; Ross and Shishkevish, 1977; Ross and McMahan, 1976, 1981). The properties of solid molecular H_2 are extensively discussed by Silvera (1980). In a diatomic molecular crystal like H_2, metallization can occur in two ways: (1) the molecular lattice is insulating but at some very high pressure breaks down to a monatomic metal, or (2) a gradual transition to the metallic state occurs in the molecular crystal before it becomes a monatomic solid. Recent calculations predict 3.1—3.6 Mbar (Ross and McMahan, 1976) for the former and 2.1 Mbar for the latter, according to Friedli and Ashcroft (1977), and 3.4 Mbar, according to Herzfield's theory (Ross and McMahan, 1982). Ashcroft (1981) and Mon, Ashcroft, and Chester (1980) have pointed out that in certain high-density ranges metallic hydrogen and deuterium may have a liquidlike ground state, in which case they are describable as quantum liquid metals, obeying either Fermi-

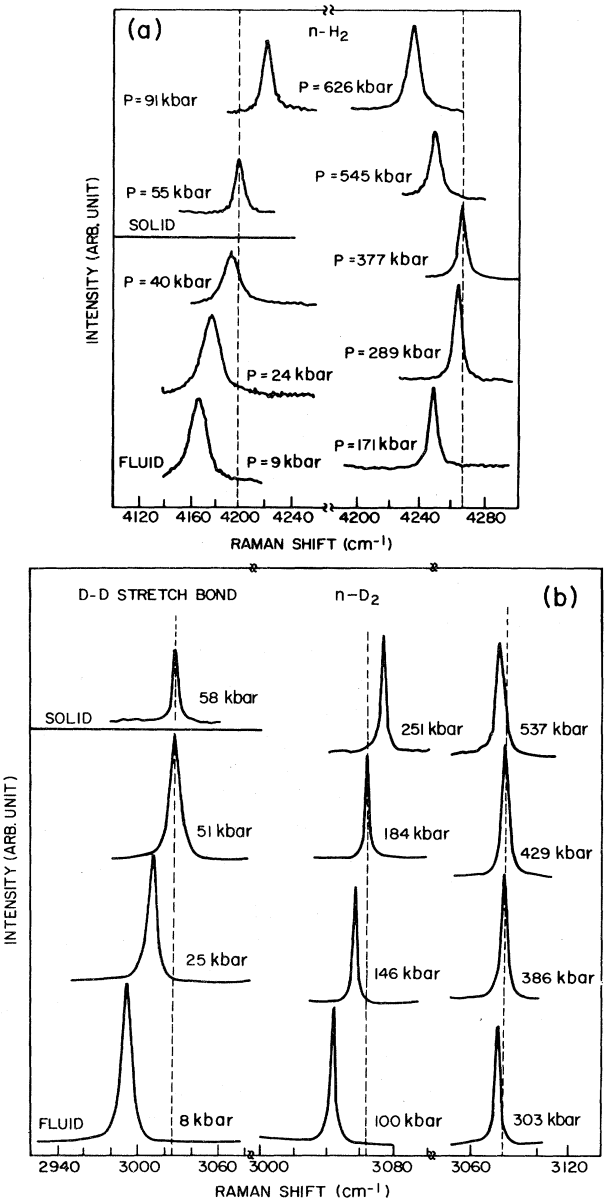

FIG. 46. (a) The vibrational $Q_1(1)$ mode Raman peak of n-H_2, (b) $Q_1(2)$ mode of n-D_2 at different pressures (after Sharma *et al.*, 1980a, 1980b).

Dirac or Bose-Einstein statistics. In both H_2 and D_2 there is the likelihood of superconductivity, and in deutronic fluid superfluidity through Bose condensation. While these exciting possibilities and predictions make hydrogen and deuterium worthy of attention, the predicted pressure range for driving hydrogen to the metallic state and observing its exotic properties appears to be still very much outside the range of static pressures that are presently attainable with the DAC. Nevertheless, some very interesting experiments have been carried out on H_2 and D_2 in the DAC, which have a bearing on the metallic hydrogen problem.

1. Molecular dynamics

Mao and Bell's (1979b) first optical observation in the DAC showed that hydrogen solidifies near 57 kbar at 298 K to a clear transparent solid, and remains that way up to the 500 kbar reached in that study. Further, from observations on the refractive index change with pressure, Mao and Bell concluded that the density of hydrogen must have increased to 0.6—0.7 $g\,cc^{-1}$ at 360 kbar. Encouraged by these results, Raman scattering investigations on H_2 and D_2 in the DAC were undertaken by the Geophysical Lab group to probe the intra- and intermolecular interactions as a function of pressure (Sharma, Mao, and Bell, 1980a, 1980b). Hydrogen and D_2 were studied in the ranges 20—630 and 8—537 kbar, respectively, at room temperature. Both rotational and the H-H, D-D bond stretching vibrations were followed as a function of pressure. In the fluid phase the rotational lines broaden and progressively become diffuse, while shifting slightly to higher frequency with pressure. At the solidification pressure they become unobservable in H_2, for the Rayleigh tail overlaps the rotational lines, but with D_2 they are seen up to 146 kbar. The H-H stretching vibration frequency $Q_1(1)$ 4155.2 cm^{-1} has been followed up to 626 kbar and the D-D stretching vibration $Q(2)$ 2987.23 cm^{-1} to 537 kbar. These are shown in Figs. 46(a) and (b). In both H_2 and D_2 this peak broadens with pressure in the fluid phase and suddenly sharpens at the solidification pressure. However, before freezing, the width of the D_2 peak is much sharper than that of H_2 (8 cm^{-1} compared to 15 cm^{-1}). The sharpening at the solidification pressure is believed to be due to a reduction in the collision-induced broadening in the solid. With increasing pressure, the $Q_1(1)$ band of H_2 sharpens up to about 175 kbar and then broadens. Similar behavior is observed in D_2. Figure 47 shows the effect of pressure on the linewidth in D_2. Figure 48 is plot of the $\Delta\nu_R/\nu_0$ (percentage change) of the $Q_1^H(1)$ and $Q_1^D(2)$ against pressure. The remarkable feature in Fig. 48 is the leveling off near 300 kbar and then the decrease of $\Delta\nu_R$ with pressure, indicating a softening of the H—H and D—D bond. The initial increase in the frequency of vibration is the direct response of H_2 and D_2 to compression, which is usually observed in molecular crystals. In Table IV some of the relevant parameters are given. The changes observed in the Raman spectrum of n-D_2 and n-H_2 with pressure closely resemble each other but with two significant differences. (1) In both fluid and solid phases the D-D stretching band is narrower than the H-H stretching band at the corresponding pressure, and (2) the frequency ratio ν_D/ν_H increases gradually with increasing pressure in both fluid and solid phases. The changes in the above ratio imply (1) a difference in the force constants of D_2 and H_2 molecules or (2) a small difference in the compressibility of n-D_2 and n-H_2, or both. The softening of the H-H band with pressure is indicative of a gradual shift toward instability. Although one is quite far away from the predicted metallic state of hydrogen, the results of Raman study indicate that high pressure is making it less molecular, which is in the right direction.

Silvera and Wijngaarden (1981) have reported a second-order phase transition in *ortho*-D_2, based on a Raman scattering study in the DAC to 540 kbar at liquid-He

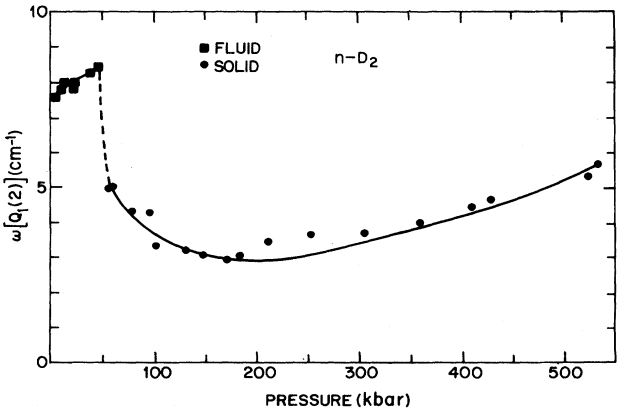

FIG. 47. Pressure dependence of the halfwidth (w) of the $Q_1(2)$ peak in n-D_2 (after Sharma *et al.*, 1980b).

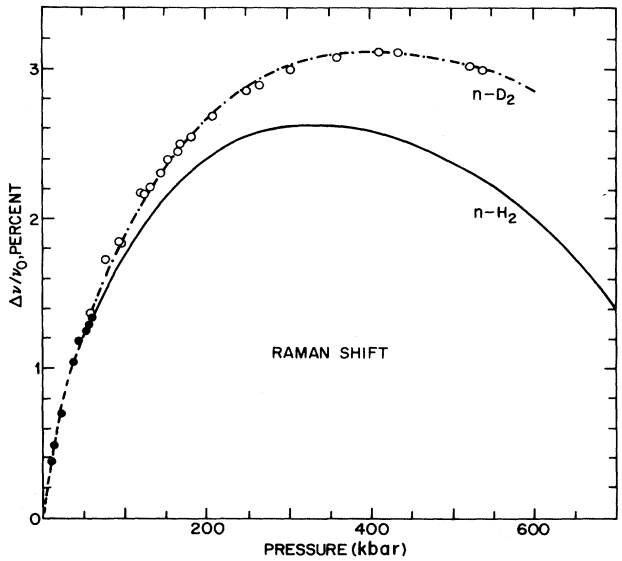

FIG. 48. The shift of $[Q_1](2)$ ($\Delta\nu/\nu_0$ in percentage) as a function of pressure in n-D_2 and n-H_2 at 300 K. The softening of this frequency at high pressures is to be noted (after Sharma *et al.*, 1980b).

TABLE IV.[a] Frequencies in inverse centimeters of Raman bands of hydrogen at various pressures and room temperature (vw, very weak; w, weak; m, medium; bd, broad; sh, shoulder; ω, full width at half maximum height).

	Pure rotational bands			Vibrational bands	
Pressure	$S_0(0)$	$S_0(1)$	$S_0(2)$	$S_0(3)$	$Q_1(1)$
1—2 bars	354.381	587.055	814.406	1034.651	4155.201
5 kbar	355.0,m ($\omega=12.0$)	590.8,s ($\omega=13.0$)	817.4,w ($\omega=11.6$)	1036.3,w ($\omega=10.6$)	4136.3,m
9 kbar	357.0,m ($\omega=12.1$)	592.4,s ($\omega=28.8$)	820.9,w ($\omega=20.2$)	1040.0,w ($\omega=20.7$)	4165.5,m
24 kbar	354.8,m 369.0,vw(sh)	529.5,w 564.5,vw(sh) 596.2,s	824.7,w ($\omega=22.7$)	1044.4,w ($\omega\sim20$)	4183.8,m ($\omega=13.1$)
40 kbar	360.7 ($\omega=27.3$)	601.5,s ($\omega=51.5$)	832.0,w ($\omega=33.8$)	1051.2 ($\omega=32.3$)	4200.7,m ($\omega=14.1$)
55 kbar	vw,bd	~602,w,bd	~832,vw,bd	vw,bd	4205.0,m ($\omega=5.7$)

[a]From Sharma, Mao, and Bell (1980).

temperatures. They studied o-D_2, as well as p-H_2, but found evidence for the transition only in o-D_2. The $J=2$ rotational band undergoes a remarkable broadening in the pressure range 200—278 kbar and then splits at higher pressures. The splitting is attributed to a phase transition in which the spherically symmetric molecules of o-D_2 enter into an orientationally ordered state at low tempera-

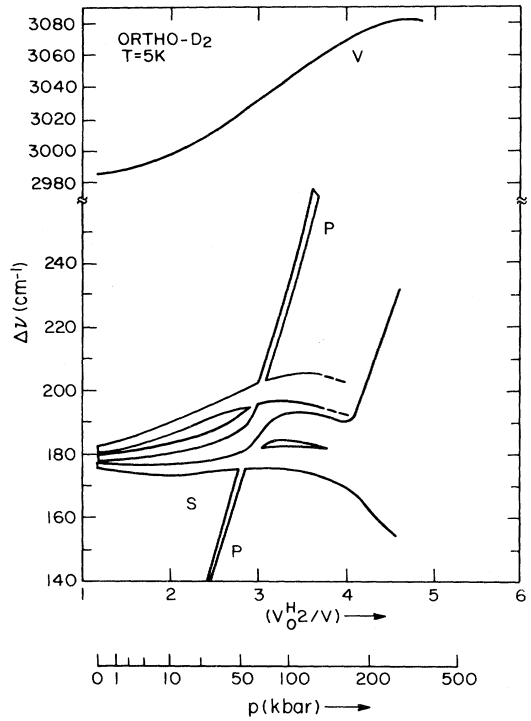

FIG. 49. Raman frequency shifts in crystalline H_2-D_2 as a function of volume and pressure. V represents the vibrational frequency of the stretching mode, P the phonons and some rotational modes. The width of the branches represents the linewidth of the transitions. The splitting at about 278 kbar is due to a phase transition due to an orientational ordering of the D_2 molecules (after Silvera and Wijngaarden, 1981).

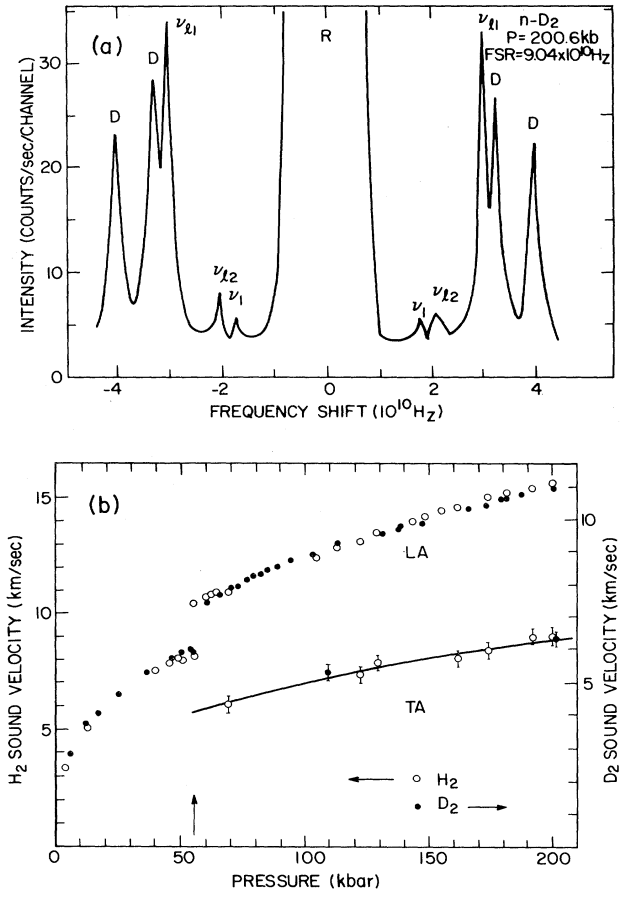

FIG. 50. (a) Brillouin spectrum of solid n-D_2 at 200 kbar and 300 K. ν_{l1} and ν_t are signals corresponding to LA and TA. ν_{l2} is the backscattered signal from LA mode. Peaks marked D are the Brillouin-scattered signals from the diamond. (b) Sound velocity variation of n-H_2 and n-D_2 with pressure. The vertical scale for n-H_2 velocity is $\sqrt{2}$ times that for the n-D_2. LA and TA stand for longitudinal and transverse acoustic modes. Vertical arrow indicates the freezing point at ~55 kbar (after Shimizu *et al.*, 1981).

tures, and the broadening is a precursor effect. Figure 49 shows the effect of pressure on the Raman frequencies observed in o-D_2 at 5 K.

2. Equation-of-state studies

Establishing the correct experimental equation of state for H_2 and D_2 for a large pressure range is of immense importance for calculating their high-pressure properties. Although shock data exist for D_2 up to 800 kbar and for H_2 to 100 kbar (Nellis and Mitchell, 1982), they are beset with the problem of high temperatures, unavoidable in shock compression. The DAC offers the best possible way to obtain the pressure-volume or the pressure-density relationship to very high pressures under static conditions. To this end, Brillouin scattering measurements to 200 kbar at room temperature (Shimizu *et al.*, 1981) and direct measurement of the volume to 370 kbar at liquid-He temperatures (van Straaten, Wijngaarden, and Silvera, 1982) have been made in the DAC. A typical Brillouin scattering spectrum obtained in solid n-D_2 at 200 kbar and 300 K for 90° scattering geometry is shown in Fig. 50(a). The sound velocity $U_S=\Delta\nu_S\lambda_0/\sqrt{2}$ calculated from the frequency shifts is shown in Fig. 50(b). For the 90° geometry used, the refractive index drops out (see Sec. II.E.2). At solidification the velocity splits into longitudinal acoustic (LA) and transverse acoustic (TA) components. The density ρ at pressure P was obtained through the relation

$$\rho(P_B)-\rho(P_A)=\int_{P_A}^{P_B}(\gamma_S/U_S^2)dP\ , \tag{17}$$

where $\gamma_S=C_P/C_V$ is the ratio of the specific heats at constant pressure to constant volume. Using values of $\gamma_S=1.07$ for n-H_2 and $\gamma_S=1.10$ for n-D_2 for the fluid, the density was calculated, and the data are shown in Fig. 51. For the solid region the adiabatic sound velocities were averaged to get

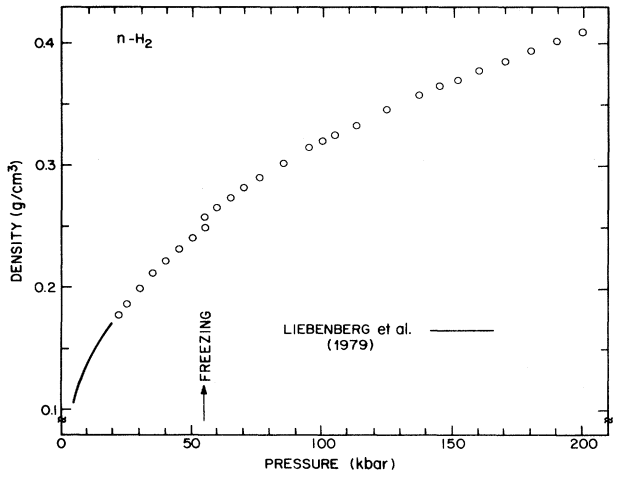

FIG. 51. Density of n-H_2 as a function of pressure. Open circles are the data of Shimizu *et al.*, 1981, and solid line is after Liebenberg, Mills, and Bronson (1979).

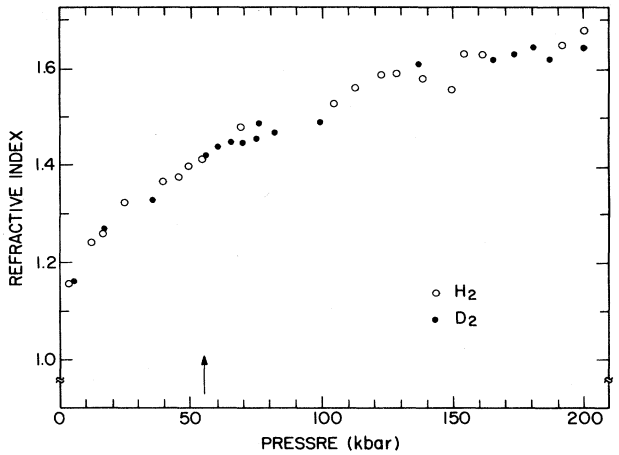

FIG. 52. Refractive index of n-H_2 and n-D_2 as a function of pressure (after Shimizu *et al.*, 1981).

$$U_S=(U_{LA}^2-\tfrac{4}{3}U_{TA}^2)^{1/2}\ . \tag{18}$$

With $\gamma_S=1$, $\rho(P)$ was calculated using Eq. (17) and is plotted in Fig. 51. The equations of state obtained for $55<P<200$ kbar are

$$\rho(P)=0.0734P^{0.334}-0.0214 \tag{19}$$

for solid n-H_2 and

$$\rho(P)=0.148P^{0.334}-0.0627 \tag{20}$$

for solid n-D_2. The elastic moduli were also calculated from ρU_{LA}^2 and ρU_{TA}^2 for both n-H_2 and n-D_2 near 95 kbar, yielding $C_{11}=4.82\times10^{11}$ dyn cm^{-2} and $C_{44}=1.27\times10^{11}$ dyn cm^{-2}. These values are comparable to that of NaCl at 1 bar, which shows that n-H_2 and n-D_2 are soft solids.

The Brillouin-scattered signal from 90° scattering $\Delta\nu$ and the backscattered signal $\Delta\nu*$ (from the exit diamond's inner surface reflected laser beam) were used to obtain the refractive index n through the relationship $\Delta\nu/\Delta\nu*=1/\sqrt{2}n$ (see Fig. 52). From n and V the polarizability α was calculated using the Lorenz-Lorenz relationship

$$\frac{n^2-1}{n^2+2}=\frac{4\pi N\alpha}{3V}\ , \tag{21}$$

where N is the Avagadro number and V the molar volume. Polarizability α appears to be insensitive to pressure in the fluid phase, with a value of 8.17×10^{-25} cm^3. However, α abruptly decreased by about 4.5% on solidification and thereafter gradually decreased with pressure, attaining a value of 7.12×10^{-25} cm^3 at 200 kbar. This decrease is attributed to a resistance of the molecule to deform at high pressure.

The low-temperature (5-K) equation of state for D_2 and H_2 to 370 kbar was experimentally determined by van Straaten, Wijngaarden, and Silvera (1982). They have obtained the volume as a function of pressure by measuring the area and the thickness of the gasket hole that contained the H_2 or D_2. While the area measurement was

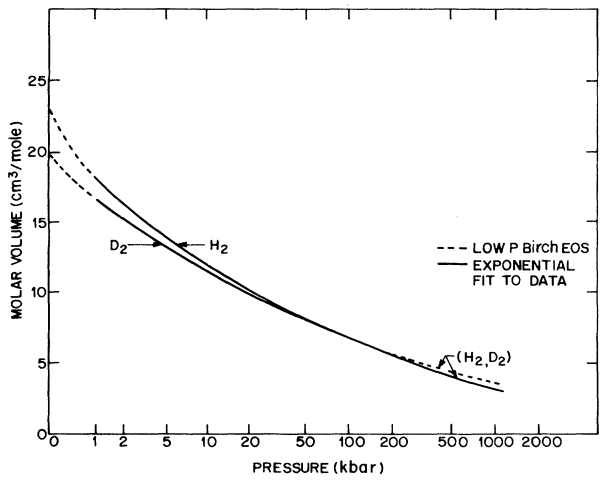

FIG. 53. The $T=5$ K isotherms for H_2 and D_2 (see text) (after van Straaten, Wijngaarden, and Silvera, 1982). The dotted line is from the equation of state Birch (Driessen, deWall, and Silvera, 1979).

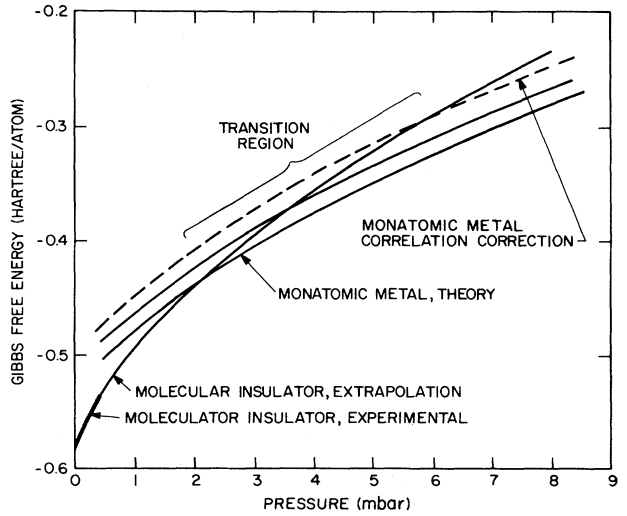

FIG. 54. Gibbs free energy as a function of pressure for monatomic metallic and molecular insulating hydrogen. Metallization occurs at the intersection of the two curves (after van Straaten, Wijngaarden, and Silvera, 1982).

straightforward, the thickness had to be evaluated from the refractive index, which in turn was measured using well-known optical interference conditions. The refractive index data were fitted with the Lorenz-Lorenz relationship to a curve $n(P)$, given by

$$n=-0.7+0.0009P+1.83(1.37+P)^{0.03}\ . \qquad (22)$$

These values of n vs P were then used to determine the thickness d using the interference condition for the fringe separation. The experimentally determined P and V have been fitted to an equation of state with validity for $T=0$ K limit. The pressure is obtained from $P=-\partial F/\partial V$, where $F=F_S+F_g$ is the free energy consisting of the lattice energy F_S and zero-point energy F_g. For the lattice energy a simplified form given by Silvera and Goldman (1978) was used. The data and calculations are shown in Fig. 53, and the data are given in Table V. From the good agreement of the results with the proposed equation of state, it is suggested that the effective pair potential is a valid approximation for solid H_2, at least up to 400 kbar. From the free energies calculated using the above-mentioned equation of state for the insulating phase of molecular hydrogen, and by comparing it with the spread of Gibb's free energies for the metallic phase from Ross and McMahan (1976), it is predicted that the transition pressure for metallic hydrogen lies between 1.9 and 3.6 Mbar, with full correlation energy taken into account. However, it can be as high as 5.6 Mbar, if the correlation

TABLE V. Pressure-volume data for H_2 and D_2 at $T=5$ K from van Straaten, Wijngaarden, and Silvera (1982).

V	Pressure (kbar) Present work			
(cm^3 $mole^{-1}$)	D_2	H_2	H_2[a]	H_2[b]
10	20.0	22.7	22.6	22.9
9	31.2	34.6	35.1	35.3
8	49.9	54.1	56.3	56.6
7	82.5	87.8	93.8	94.3
6	142	149	165	167
5	262	271	312	320
4	528	537	656	702
3	1216	1220	1614	1854
2	3513	3482	5151	6940
1.6	5972	5892		

[a]Silvera and Goldman (1978).
[b]Birch equation of state (Driessen, deWall, and Silvera 1979).

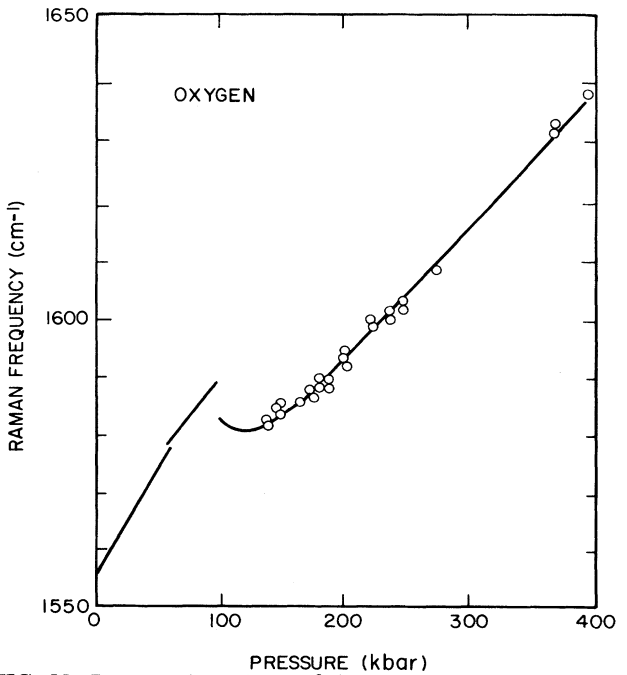

FIG. 55. Pressure dependence of the stretching vibration in oxygen. The breaks in slope represent phase changes. Data points are for ε-O_2 (after Syassen and Nicol, 1981).

energy is reduced by a factor of 2. The results of these calculations by van Straaten *et al.* are shown in Fig. 54.

B. Oxygen

Oxygen has been studied up to 400 kbar by Raman and electronic absorption spectroscopy (Nicol, Hirsch, and Holzapfel, 1979; Syassen and Nicol, 1981) and by x rays to determine the structure at 68 kbar and 298 K (Schiferl, Cromer, and Mills, 1981; d'Amour, Holzapfel, and Nicol, 1981). At 298 K, phase transiton from liquid oxygen to β-O_2 near 59 kbar, β- to α-O_2 near 96 kbar, and α- to ε-O_2 near 99 kbar have been reported from discontinuities observed in the pressure dependence of the Raman band of the O_2 internal mode (Nicol, Hirsch, and Holzapfel, 1979), shown in Fig. 55, and from optical observation. Dramatic changes in color are also observed at pressures above 100 kbar. The so-called β, α, and γ forms are low-temperature phases of O_2. Their phase boundaries in the 1—10 kbar range have been determined. d'Amour, Holzapfel, and Nicol (1981) have drawn the phase boundaries for β-α and α-ε in the high-pressure region, using the determinations by Nicol, Hirsch, and Holzapfel (1979) and other unpublished observations by the same authors. This diagram is shown in Fig. 56. The *P-T* diagram is not complete, for the low-pressure region is not yet connected to the high-pressure region. The structure of ε-O_2 has not yet been resolved, but it appears to be a new high-pressure form. Other than the small abrupt changes mentioned above (see Fig. 55), the Raman shift of the internal mode of O_2 does not show any abnormal behavior up to 400 kbar. The ε-O_2 absorbs light strongly at high pressures, making it look dark in transmission. The transmission spectra of ε-O_2 near 120 kbar show weak, structureless shoulders near 700 and 500 nm, and by 160 kbar a strong absorption edge moves in and cuts off the visible spectrum. These changes are attributed to strong electronic absorption due to transitions between Π Π^* configurations. Evidently, the behavior of oxygen under high pressure is novel and our understanding of the high-pressure properties is bound to advance in the future. We can especially expect the breakdown of the molecular structure as well as a transition to the metallic state.

C. Nitrogen

Nitrogen has been studied in the DAC by Raman spectroscopy to 400 kbar (LeSar *et al.*, 1979; Schwalbe *et al.*, 1980) and by high-pressure x-ray diffraction near the freezing pressure at room temperature (Schiferl, Cromer, and Mills, 1978) and near 49 kbar at room temperature (Cromer *et al.*, 1981). The pressure dependence of the stretching frequency of N_2 is shown in Fig. 57. Near 49 kbar the stretching mode splits into two components, with the lower-frequency component stronger in intensity by a factor of 3. The intensity of the upper, weaker component decreases above 84 kbar and is lost in the background at about 120 kbar. Nitrogen freezes at about 24 kbar at room temperature but seems to be a good pressure

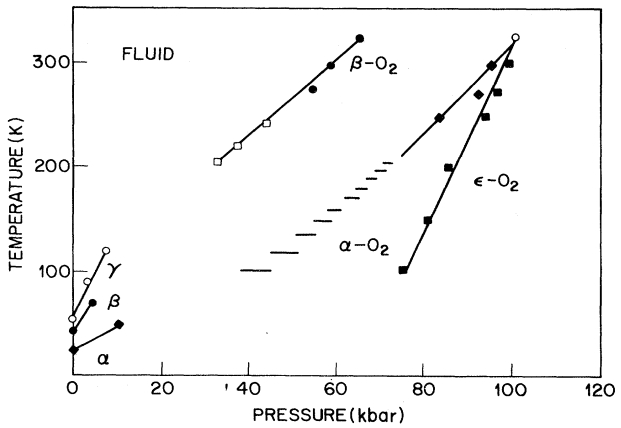

FIG. 56. Partial *P-T* diagram for O_2 (after d'Amour, Holzapfel, and Nicol, 1981).

medium up to 130 kbar as judged by the width of the R_1R_2 ruby lines (LeSar *et al.*, 1979).

The crystal structure of solidified N_2 at room temperature is found to be β-N_2 (Schiferl, Cromer, and Mills, 1978), the same as the one observed when liquid N_2 is cooled below 46 K at ambient pressure. At 49 kbar and 299 K, the single-crystal study of Cromer *et al.* (1981) has shown that the structure of N_2 is of β-F_2 type, which is also the structure of γ-O_2 at 50 K and ambient pressure. Thus single-crystal work confirms the phase change observed in the Raman studies as a splitting of the stretching mode near 50 kbar. It has been suggested that the splitting arises in the β-F_2 phase, because N_2 molecules occupy two sites of different symmetry and are therefore subject to somewhat different intermolecular potentials. The observed intensity ratio of 2.8 between the split Raman components seems to agree with the number of atoms in the two different sites; the occupations are in the same ratio.

The compressibility of N_2 from shock experiments shows a striking deviation from the theoretically calculated Hugoniot (Ross and McMahan, 1981); unusually large and sudden increase above 400 kbar, suggesting a breakdown in the molecular structure. However, qualitative

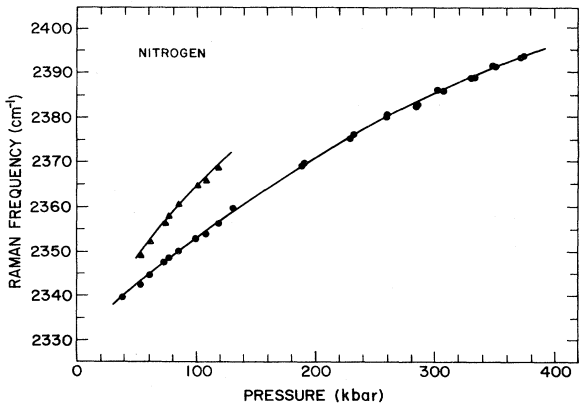

FIG. 57. Stretching vibration of solid N_2 as a function of pressure. The splitting is attributed to a phase transition near 54 kbar (after LeSar *et al.*, 1979).

observations with the DAC to 410 kbar by Schwalbe *et al.* (1980) suggest no anomalous changes in transmission. The effect observed in shock data is presumed to have a thermal origin because of shock heating (Ross and McMahan, 1981).

D. Rare-gas solids

Argon and Ne solidify at 11.5 and 47.5 kbar, respectively, at 293 K. Single crystals can be prepared easily by repeated melting and freezing at room temperature and the crystals have the fcc structure. Pressure-volume data have been obtained by high-pressure x-ray diffraction studies in the DAC (Mao and Bell, 1981a) to 90 kbar by Hazen *et al.* (1980b). Zou *et al.* (1981) have extended the measurements to 145 kbar for Ne. The high-pressure data obtained at 293 K were reduced to 0-K values and fitted to a second-order Murnaghan equation of state. Rare-gas solids are found to be soft at low temperatures and high pressure and have been proposed as pressure media for high-pressure experiments in the DAC.

A metal-insulator transition was reported for Xe by Nelson and Ruoff (1979).[2] They measured the resistance of a thin film of Xe deposited on an interdigited electrode arrangement in a diamond anvil indentor. A sharp drop in resistance was reported near 300-kbar applied pressure, which was attributed to an insulator-to-metal transition in Xe. However, optical observations in the DAC up to 300 kbar by Syassen and to 440 kbar by Schiferl have not produced any evidence for a metallic phase. Solid Xe is found to be clear and transparent at the above pressures, which suggests that the optical energy gap is still over 4 eV. Furthermore, the optical absorption edge has recently been measured up to 440 kbar (Syassen, 1982), 630 kbar (Makarenko *et al.*, 1982), and 550 kbar (Asaumi, Mori, and Kondo, 1982), indicating gap closure probably at pressures in excess of 1 Mbar.

Herzfeld has predicted from simple classical Lorentz oscillator model (see Table VI) metallization of Xe at a volume of 10.2 $cm^3\,mole^{-1}$. Theoretical calculations by Ross and McMahan (1980) predict metallization due to band crossing at about 11 $cm^3\,mole^{-1}$, corresponding to 1.3 Mbar (Hedin-Lundqvist potential), and 9 $cm^3\,mole^{-1}$, corresponding to ~ 2 Mbar when Slater exchange potentials were used. Similar results have been found by Ray *et al.* (1980). Hama and Matsui (1981) have made augmented-plane-wave (APW) calculations for both fcc and bcc Xe and predict that the fcc-to-bcc transition would precede the metallization of Xe. Accordingly, they find that above 620 kbar the bcc has the lower energy and the metallization pressure to be 830 kbar. When spin-orbit coupling is taken into account, the metallization pressure is reduced to 660 kbar. A recent shock compression study of Xe by Nellis, van Thiel, and Mitchell (1982), which would correspond to 600 kbar on the 0-K isotherm, does not show evidence for any insulator-metal transition. The possibility of a hcp structure for Xe at high pressure and the need for band calculations for this structure have been suggested by Ross and McMahan (1981). If Xe goes hcp at high pressure, such a transition should be verifiable by x-ray diffraction studies with the DAC.

TABLE VI.[a] Predicted metallization properties for band overlap. APW stands for augmented plane wave; LMTO, linear muffin-tin orbital.

		APW	LMTO
	V_{Herzfeld} ($cm^3\,mol^{-1}$)	$V_{\text{band theory}}$ ($cm^3\,mol^{-1}$)	$P_{\text{band theory}}$ (Mbar)
He	0.5	0.3	112
Ar	4.2	4.5	5.8
Xe	10.2	11.0	1.3
H_2	2.0	(2.4)[b]	
I_2	40.0		
CsI	24.7		

[a]From Ross and McMahan (1981). According to the Herzfeld criterion a closed-shell atom or molecule becomes metallic when the molar volume V becomes equal to or less than its gas-phase molar refractivity (R), given by $R = 4\pi/3N\alpha$, where N is Avagadro's number. It can be shown that $R = \frac{4}{3}\pi N r^3$ when r is the radius of the atom (Ross and McMahan, 1981).
[b]Friedli and Ashcroft (1977).

V. HIGH-PRESSURE X-RAY DIFFRACTION STUDIES

A. Phase changes and compression of solids

Numerous studies on pressure-induced phase transformations and compression of solids using the DAC have been reported in the literature. Systems of interest to geophysics and geochemistry constitute the bulk of this work, and these have appeared in Carnegie Institute of Washington Year Books over the years, in a conference volume *High Pressure Recearch: Application in Geophysics,* edited by M. H. Manghnani and S. Akimoto (1977), and in journals devoted to geophysical research. We shall confine our attention here to certain systems because of their special interest to the physics of solids at high pressure. Accordingly, the pressure-induced dissociation in a diatomic molecular solid, leading to the metallic state in iodine, $4f$ electron delocalization in rare-earth systems (YbO, Pr, Eu, and Yb) and its consequences, the sequence of phase transitions (hcp-Sm-dhcp-fcc) in Y and Sc, and, finally, the effect of pressure on the crystal structure of actinides (Am, Pu, and Th) will be discussed.

B. Iodine

From the pressure dependence of the resistance and the optical gap, Balchan and Drickamer (1961) and Riggle-

[2]A recent analysis by Chan *et al.* (1982) has revised the presure attained by Nelson and Ruoff (1979) in their experiment on the metallization of Xe with the diamond indentor as exceeding 1 Mbar. In this event, it would appear that Nelson and Ruoff (1979) might actually have produced metallic Xe.

man and Drickamer (1963) showed two decades ago that iodine underwent a continuous pressure-induced transformation to the metallic state. Iodine is a molecular crystal, and it is of great interest to know whether this transition to the metallic state occurs in the molecular crystal due to a continuous conduction-valence band overlap, or whether iodine dissociates to become a monatomic metal, with its metallic character then a consequence of the unfilled 5*p* band. The earlier high-pressure x-ray studies by Lynch and Drickamer (1966) and Kabalkina, Kolobiyana, and Vereshchagin (1967) were unable to resolve the question. Also, shock compression (McMahan, Hord, and Ross, 1977) measurements to 2 Mbar did not reveal any discontinuities, and it was concluded that iodine molecules continuously dissociate under pressure. Some definitive answers to these questions have come out of a recent high-pressure x-ray study by Takemura *et al.* (1980) and a Raman scattering study by Shimomura, Takemura, and Aoki (1982), both carried out with the DAC.

Iodine crystallizes in the orthorhombic space group D_{2h}^{18}-Cmca. According to Shimomura *et al.* (1978), it retains not only the above structure, but also remains a molecular crystal up to 206 kbar, even though it has become metallic above about 170 kbar. This metallization in iodine occurs by band overlap prior to the dissociation. The more recent study by Takemura *et al.* (1980) has shown that iodine transforms to a monatomic lattice around 210 kbar with about 4% change in volume, and that the high-pressure phase has a much simpler structure, namely, a body-centered orthorhombic cell belonging to the space group D_{2h}^{25}-I_{mmm}. Figure 58 illustrates the projections of the structure of iodine at three different pressures. An inspection of Fig. 58 reveals that compression gradually forces the intermolecular distances to approach the intramolecular ones and the intermolecular axes to approach 90°, culminating in the transition to the monatomic lattice at about 210 kbar. The Raman scattering study of I_2 by Shimomura, Takemura, and Aoki (1982) supports the gradual dissociation up to the transition pressure, and the completion of it at the first-order transition, near 210 kbar. Two intramolecular (B_{3g} and A_g) and two intermolecular modes (B_{3g} and A_g) were observed with I_2 and these were followed as a function of pressure up to 210 kbar. The lattice mode A_g exhibited an initial increase in the frequency, leveled off near 150 kbar, and then decreased at higher pressures. The Grüneisen parameter for the A_g mode continuously decreased with pressure, while the B_{3g} changed very little. The two lattice modes which represent intermolecular vibrations grew in intensity with pressure. The continuous decrease of the $\gamma_{(A_g)}$ and the increase in intensity of the lattice modes relative to the stretching frequencies were taken as evidence for a gradual molecular dissociation with pressure.

From the trends in the *a* and *c* lattice parameters in the 210—300 kbar region, it is predicted that iodine will become face-centered tetragonal at about 450 kbar, and fcc at higher pressures. Iodine is now regarded as molecular and semimetallic in the low-pressure phase, and monatomic and metallic in the high-pressure phase above 210 kbar.

The dissociation of iodine under pressure has implications for the pressure-induced transition to the metallic state predicted for hydrogen in the megabar range. It would be of interest to investigate bromine under these high pressures in the DAC, for Br is likely to undergo a transition to the metallic state within the range of static pressure now available with the DAC.

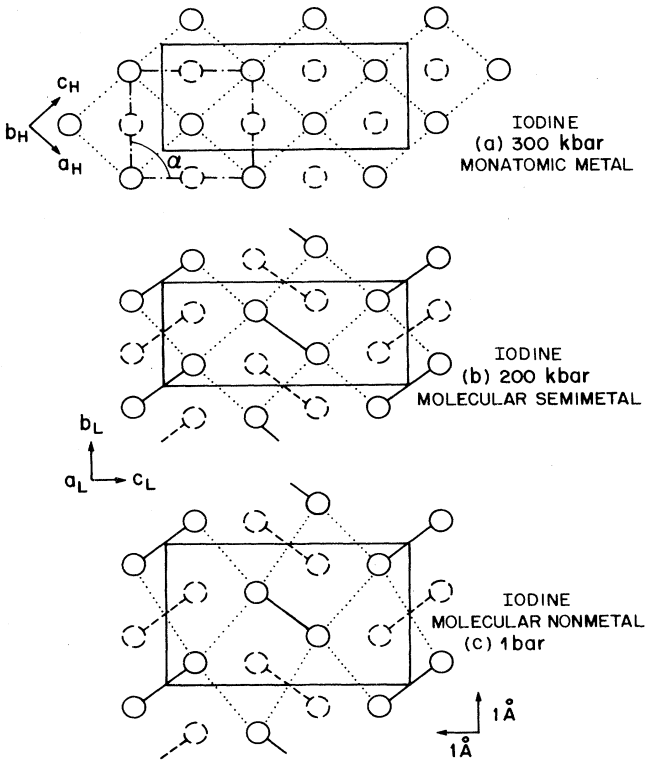

FIG. 58. Projections of the crystal structure of iodine at three different pressures. The atoms represented by solid and dashed lines lie, respectively, at the basal plane and halfway above in a perpendicular plane (after Takemura *et al.*, 1980).

C. Rare-earth systems and valence changes

The DAC has been an invaluable tool in establishing pressure-induced valence changes due to 4*f* electron delocalization in systems involving Sm, Eu, Yb, and Tm by high-pressure x-ray diffraction studies (Jayaraman *et al.*, 1974, 1976; Jayaraman, Maines, and Bucher, 1978; Croft and Jayaraman, 1980; and Werner, Hochheimer, Jayaraman, and Bucher, 1981), and in many instances by simple optical observations of the reflected light from the sample. For instance, SmS undergoes a spectacular change in color from black to gold in reflected light, and SmSe goes through a sequence of color changes as the valence transition proceeds continuously with increasing pressure. Thus a simple optical observation with the DAC enables one to decide whether a system is worthy of study. The valence transitions are isostructural and first order in some systems (SmS, Sm_4Bi_3, Ce), while in others they take

place continuously with pressure, resulting in anomalous compression behavior (most Yb systems). The unusual properties of the so-called intermediate valence state have been discussed extensively [*Valence Instabilities and Related Narrow Band Phenomena,* edited by R. D. Parks (1977); and *Valence Fluctuation in Solids,* edited by L. M. Falicov, W. Hanke, and M. P. Maple (1981)]. From high-pressure x-ray diffraction studies with the DAC, a few systems which exhibit valence changes under pressure have been chosen for discussion here.

1. YbO

Among the Yb monochalcogenides, YbO was successfully synthesized only recently (Leger, Yacoubi, and Loriers, 1979). It has the NaCl structure with $a=4.88$ Å, appears black, and is a semiconductor. The compression behavior of YbO has recently been studied in the DAC to 350-kbar pressure (Werner, Hochheimer, Jayaraman, and Leger, 1981) by high-pressure x-ray diffraction. The results are shown in Fig. 59. The solid line was calculated using the Murnaghan equation of state,

$$P=(B_0/B_0')[(V_0/V)^{B_0'}-1]\,, \tag{23}$$

with $B_0=1300$ kbar and $B_0'=4$, the former obtained from an extrapolation of the Anderson-Nafe plot for divalent rare-earth (RE) monochalcogenides (Jayaraman *et al.*, 1974). The compression anomaly in Fig. 59 is attributed to a continuous valence change commencing near 80 kbar. Optical observations have shown that the color of the material had changed from black to golden yellow near 300 kbar, providing strong additional support for a valence change. The behavior of YbO is rather unusual, for it shows that valence change can be spread over a large pressure range.

2. Praseodymium

Praseodymium was investigated by high-pressure x-ray diffraction with the DAC by Mao *et al.* (1981) to 300-kbar pressure. A phase transition from the dhcp to the fcc at about 50 kbar was known before (see Klement and Jayaraman, 1967). Mao *et al.* (1981) found a transition to a distorted fcc above 70 kbar, which they call Pr III. Apparently, Pr III transforms to a distorted hcp above 210 kbar with $a=5.678$ Å, $C=5.017$ Å. The unit cell volumes for Pr III and Pr IV at the transition are calculated as 349.9 and 140 Å^3, respectively, yielding 21.5 and 17.5 cm^3 for the volume/atom. The recent study of Smith and Akella (1982) suggests that the high-pressure phase of Pr is not hexagonal but rather alpha-U. The large volume decrease ($\sim 19\%$) at the above transition and the resistance-temperature behavior at high pressures noted in a previous study by Wittig (1980) have been interpreted in terms of change in the valence state of Pr from the 3^+ toward the 4^+ state. In this sense, the behavior of Pr at high pressures is regarded as a counterpart of the $4f^1$ delocalization in metallic Ce. Theoretical evidence to support this conclusion comes from Skriver (1981). Praseodymium has a tendency to form the

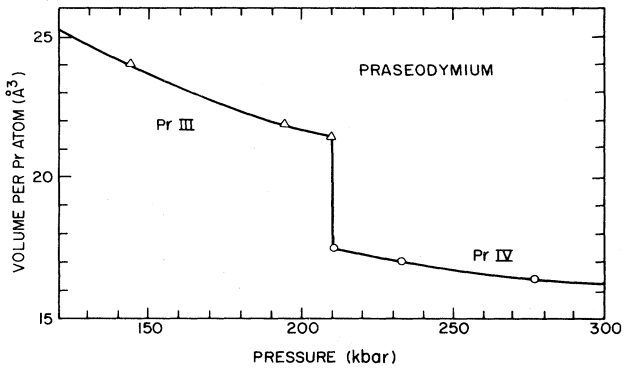

FIG. 60. Volume of Pr atom as a function of pressure. The abrupt change is attributed to a phase transition from distorted fcc to distorted hcp, with valence change from Pr^{3+} toward the Pr^{4+} state (after Mao *et al.*, 1981).

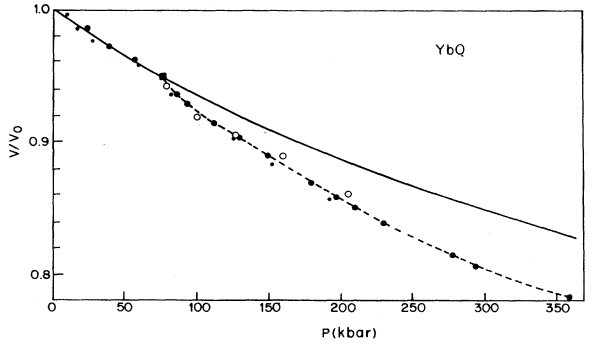

FIG. 59. Pressure-volume relationship for YbO. Solid line calculated using Murnaghan equation of state with $B_0=1300$ kbar and $B_0'=4$. The deviation as shown by the dotted line is due to valence change of Yb^{2+} toward the Yb^{3+} state (after Werner, Hochheimer, Jayaraman, and Leger, 1981).

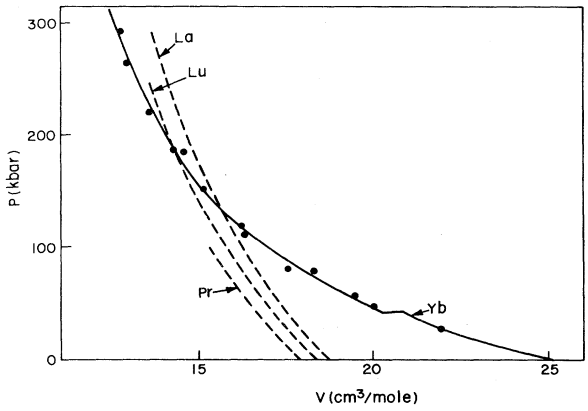

FIG. 61. Pressure-volume relationship for Yb metal. The drop in volume near 40 kbar is the fcc-to-bcc transition. The large compression of Yb is attributed to a continuous valence change over a broad pressure range. Dashed lines show the compression behavior of typical trivalent rare-earth metals (after Syassen and Holzapfel, 1979).

quadrivalent state, as judged from its chemical properties. For instance, PrO_2 exists. Figure 60 shows the compression curve of Pr.

3. Europium and ytterbium

Europium and Yb are divalent metals, with half-filled $4f^7$ and fully filled $4f^{14}$ configuration. The compression of Eu to 200 kbar and Yb to 300 kbar has been measured (Syassen and Holzapfel, 1979; Holzapfel, Ramesh, and Syassen, 1979). In Eu a transition from bcc to the hcp lattice near 145 kbar and a large compressibility at low pressures were noted. Again, in Yb a large compression in the 1—150 kbar range and a transition from bcc to hcp near 200 kbar were observed. The hcp structure of Eu and Yb and a compression behavior characteristic of trivalent rare earths at high pressures are taken as evidence for a gradual transition in Eu and Yb toward the trivalent state at high pressures. The compression curve for Yb is shown in Fig. 61. The scaled compression curves of La, Lu are also shown for comparison. Theoretical calculations of Johansson and Rosengren (1975) predict a valence change for both Eu and Yb in the range of 150—300 kbar.

Syassen *et al.* (1981b) have obtained additional evidence for a valence change in Yb by measuring the LIII x-ray absorption edge of Yb as a function of pressure to 330 kbar with a DAC and a bent crystal x-ray monochromator and a conventional 2-KW x-ray source. In Fig. 62 the shift of the LIII edge with pressure is shown. At 330 kbar a 6.5-eV shift of the LIII edge to higher binding energy has been noted. This experiment strongly supports a pressure-induced valence change in Yb. Figure 63 shows the mean valence evaluated from the absorption data.

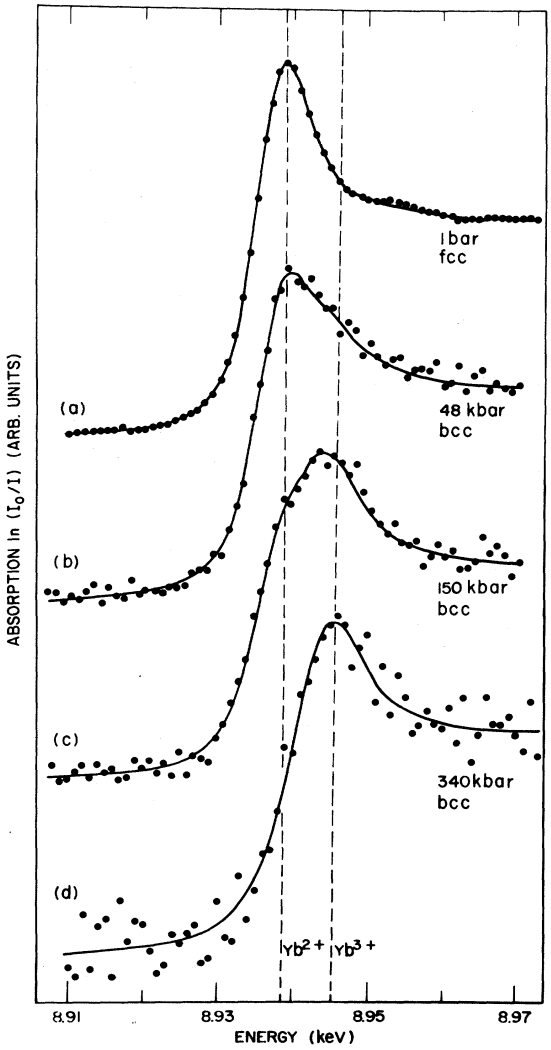

FIG. 62. The LIII absorption spectra of Yb at different pressures. The Yb^{2+} and Yb^{3+} positions are indicated by dotted lines. The solid lines are the least-square fit to the data. The movement of the edge to the 3^+ position is clear (after Syassen *et al.*, 1981b).

4. Yttrium and scandium

Y and Sc are both trivalent and have the hcp structure. Because of their close similarity in chemical properties to those of the rare earths, they are often grouped with the rare earths. Some years ago the occurrence of a sequence of pressure-induced phase transitions from hcp→Sm-type—dhcp-fcc was established for the rare-earth series with increasing pressure (see *Handbook of Physics and Chemistry of Rare Earths,* edited by K. A. Gschneidner, Jr., and L. Eyring, 1978). Johansson and Rosengren (1975) found an empirical correlation between the crystal structure of the lanthanides and the fraction of the atomic volume occupied by ion core. This correlation was later given a quantitative justification by Duthie and Pettifor

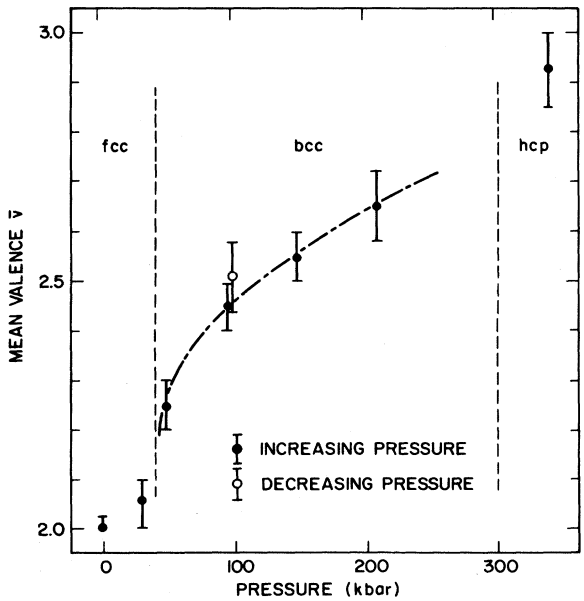

FIG. 63. Pressure dependence of the mean valence of Yb metal in its various phases at room temperature. The dashed lines represent phase boundaries as determined from x-ray diffraction studies.

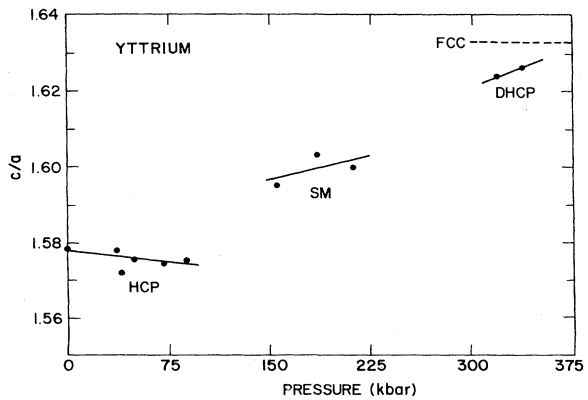

FIG. 64. The normalized c/a ratio for Y plotted against pressure to show the sequence of pressure-induced phase transition from hcp→Sm-type→dhcp-to ultimately fcc (after Vohra *et al.*, 1981).

(1977) in terms of d-band occupancy and its variation with volume. It was suggested that the number of d-electrons per atom controls the relative stability of the various crystal structures. On the other hand, the prevalent view was that $4f$ electrons participate in the binding in rare-earth metals and the observed complex sequences are a consequence of this. Recently, this problem has received a clear-cut answer from the study of Vohra *et al.* (1981) on Y to pressures of 340 kbar. They found that Y, which is a $4d$ transition metal with no $4f$ electrons, undergoes the sequence of transitions hcp→Sm-type→dhcp in the range 1—340 kbar. Figure 64 shows the c/a ratio against pressure and the various pressure-induced phases of Y. This study establishes clearly that the presence of a $4f$ electron is not necessary for explaining the complex stacking sequences and rather that they may be controlled by the number of d electrons. In this connection, it is to be noted that s-d and p-d electron transfer under pressure are predicted for a number of elements, as reviewed by Ross and McMahan (1982). If such transfer occurs, pressure-induced structural changes may be expected in many other systems.

5. Actinides

Theoretical calculations (Skriver, Andersen, and Johannsson, 1980) predict that compressed Am should exhibit a $5f$-delocalization transition near 100 kbar, analogous to those in Ce and Pr. X-ray diffraction investigations in the DAC by Akella, Johnson, and Shock (1980) and Roof *et al.* (1980) have indicated a transition at 110 kbar from fcc to Am III, and yet another transition to Am IV at 150 kbar. However, there is disagreement as to the identity of phases III and IV, and hence the fcc-Am III volume change is not yet known for any definite conclusions to be drawn about the nature of these transitions. DAC x-ray diffraction data for Th up to 300 kbar (Bellussi, Benedict, and Holzapfel, 1981) and Pu up to 200 kbar (Roof, 1981) do not show any transitions, as is to be expected for these early actinides, in which the $5f$ electrons are already delocalized at ambient pressure. A theoretical review of the actinide situation is given by Johansson, Skriver, and Andersen (1981).

D. 2H-$TaSe_2$-P-T diagram

2H-$TaSe_2$ is a layered metallic substance known to undergo transitions to the charge-density wave (CDW) states when cooled to low temperatures. Accordingly, the transition at 122 K is to the incommensurate (CDW) state and the transition at 90 K to the commensurate (CDW) state; in the latter the q vector of the (CDW) locks with the lattice periodicity. McWhan *et al.* (1980) and McWhan, Axe, and Youngblood (1981) have recently investigated the effect of pressure on these transitions, by following the CDW reflections in a Merrill-Bassett DAC. The cell was mounted on a rotation stage in a closed-cycle He refrigerator for bringing the desired plane into the reflection geometry. Since the CDW reflections were 3 orders of magnitude weaker than the Bragg peaks, a high-brilliance rotating anode x-ray generator was used with a projected 0.2×0.2 mm^2 spot. The Mo$K\alpha$ x-rays were focused by a bent crystal arrangement. From a series of

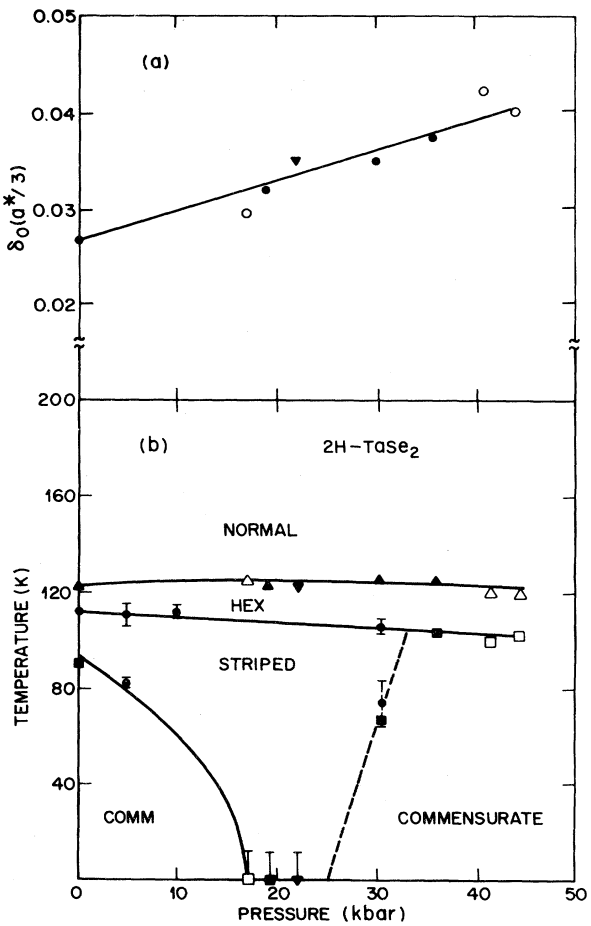

FIG. 65. Pressure-volume diagram for the normal, commensurate, and incommensurate transitions in 2H-$TaSe_2$. The upper figure shows the variation of incommensurability with pressure (after McWhan *et al.*, 1980).

temperature cycles at different pressures, a P-T diagram has been constructed; this is shown in Fig. 65. The incommensurability as a function of pressure is shown in the upper part of the figure. The interesting feature in Fig. 65 is the reentry of the commensurate transition at about 25 kbar. The above study is to show how the DAC has been used to investigate a very subtle phase transition and to reveal an extremely interesting situation.

VI. CONCLUDING REMARKS

Within a short time the DAC has become the most favored device in high-pressure research, and it is needless to emphasize that the introduction of gasketing and the ruby fluorescence method for rapid pressure calibration have triggered this popularity. At present the DAC clearly offers the opportunity to make a variety of rather sophisticated measurements to 500-kbar pressures, and it is conceivable that at least some of these measurements can be extended to the megabar region, but the question, "How accurately do we know the pressures, especially above 300 kbar?" looms in the background. There are, however, hopeful signs on the horizon for a satisfactory solution to this problem. If the sound velocity could be determined from Brillouin scattering, relative volume changes from x-ray diffraction on the same material, and the ruby line shift measured (all the three measurements in the same experiment), it would be possible to calibrate the frequency shift of the ruby fluorescence in an absolute sense via Eq. (17). Recent advances in DAC techniques for light scattering studies should certainly enable one to perform these measurements and we may not be far off from achieving the above-stated goal.

The committee that met during the 8th AIRAPT conference in Uppsala under Bean *et al.* (1982) have recommended the use of the ruby method and the Decker equation of state for NaCl as practial reference standards. They have also recommended that authors fully document how they calculate the pressures and include with the data the measured changes of the pressure indicator, so that pressure can be recalculated as calibration equations, equations of state, or phase transition values evolve.

The possibility of reaching megabar pressures has stimulated band-theory calculations and high-pressure equations of state. McMahan (1982) and Ross and McMahan (1981, 1982) have reviewed results of these calculations and what their implications are for high-pressure research. These calculations predict metallization under pressure, s-d and p-d electronic transitions, pressure-induced crystal-structure changes, and equation-of-state anomalies in several systems, in the range of pressures now accessible with the DAC. While these authors considered primarily elemental materials, pressure-induced metallization due to downward moving d bands has also been predicted for compounds, such as the aklaline-earth monoxides (Bukowinski and Hauser, 1980).

In shock-wave experiments, the s-d and p-d electronic transitions occur due to thermal excitation and are observed as softening of the P-V curve; viz., Xe and I. For both materials, softening of the shock compression P-V curve comes from thermal excitation of electrons from the $5p$ to the $5d$ bands. In static experiments these transitions should occur by transfer to degenerate electronic states, as is exemplified in the case of Cs. The s-d transitions in La and Ba are less dramatic, since they involve a smaller fraction of the valence electrons. However, in the Hugoniot of both La and Ba, a clear change of slope is seen due to s-d transition-related effects.

With increasing pressure, the occurrence of electron transfer to unoccupied d bands is expected to induce structural phase transitions in a variety of elements. Thus first-principles total energy calculations of Moriarty and McMahan (1982) predict transition-metal-like sequences of stable crystal structures for simple metals like Na, Mg, and Al. The calculations suggest hcp-bcc-hcp in Na, hcp-bcc-fcc in Mg, and fcc-hcp-bcc in Al, with increasing pressure. For Mg and Al these transitions are certainly attributable to lowering and partial filling of the initially unoccupied $3d$ band, as the metal is compressed. The first of the above-mentioned transitions are expected to take place near 10, 570, and 1300 kbar at zero temperature, corresponding to V/V_0 of 0.86, 0.56, and 0.58 in the case of Na, Mg, and Al, respectively (Moriarty and McMahan, 1982). Also, rare-gas solids are expected to undergo structural phase transitions after metallization (McMahan, 1982).

Recently, Yin and Cohen (1980) have calculated the zero-temperature energy differences between various phases of compressed silicon using the *ab initio* pseudopotential method. They have found the diamond to β-tin structural transition pressure, volume, and mode Grüneisen parameters in very good agreement with experiments. Furthermore, their calculations for the higher-energy bcc, fcc, and hcp phases are found to agree closely with calculations by an entirely different technique (McMahan, Yin, and Cohen, 1982). In addition, these calculations predict a further structural phase transition in compressed silicon, from the β-tin to the hcp structure at pressures below 1 Mbar. It is tempting to interpret the sequence of transitions in Si as involving a total conversion from covalent to metallic bonding. This is also believed to occur in Ge and C (Yin and Cohen, 1982). The predicted effects are within the range of the DAC, and future studies in this area may be expected to yield interesting results.

Attempts to interface the DAC with synchrotron sources have already proved successful, and this is bound to usher in a new era for high-pressure crystallography with the DAC. Because of the very high source intensity, exposure times can be reduced by several orders of magnitude, making continuous monitoring of the structure of a material possible as pressure is varied. It will be possible to determine the phase diagram of a substance in the P-T plane by changing the pressure and temperature, even when the temperature is of transient nature, as with laser heating. Kinetic studies and observation of transient phenomena will also become possible. Already EXAFS experiments have been successfully carried out using the

DAC, yielding information about interatomic distances. Besides these purely structural aspects, x-ray absorption spectroscopy with the DAC is an attractive proposition and becomes especially relevant for the study of electronic transitions such as those discussed.

The DAC is the tool *par excellence* for optical spectroscopy, and it is in this area that its maximum utility will be realized in the future. Absorption and luminescence studies on organic systems using the DAC are yet to be exploited. Charge transfer under pressure and the pressure-induced shifts of the electronic energy levels can be studied by following luminescence characteristics, as well as by following the electronic absorption features. Drickamer (1981) has discussed some typical examples. We may expect increasing use of the DAC in the study of organic systems, where exciting possibilities for pressure-induced effects exist. The DAC has already proved its usefulness in high-pressure Raman and Brillouin scattering. We may expect a rapid growth in light scattering studies under high pressure.

Hydrogen, helium, and xenon are found to be soft even at very high pressures, and their usefulness as a hydrostatic pressure medium (H_2 up to 700 kbar) has been demonstrated. There is no doubt they will be increasingly used as pressure transmitters, especially when the samples are reactive to normally used pressure media.

Precise resistivity measurement with the DAC is a very difficult problem, and attempts in this area have led to only limited success. However, it is possible to follow superconducting T_c as a function of pressure, or an insulator-to-metal transition with the DAC. A Squid magnetometer can be used in conjunction with the DAC for detecting large and especially abrupt changes in the magnetic characteristics of pressurized samples.

In this article the geophysical applications of the DAC have been left out, as this aspect has been reviewed in several recent articles (Bassett, 1979; Manghnani, Ming, and Jamieson, 1980). Many systems of interest to geophysics and geochemistry have been studied using the DAC to characterize pressure-induced phase transitions, to obtain the equations of state of materials, and to roughly map the P-T diagrams. Although the present capabilities of the DAC in terms of pressure and temperature would correspond to depths of the core-mantle boundary ($\sim$2800 km), the uncertainties involved in pressure calibration at high temperatures (obtained through laser heating) make the phase transformation studies at best only qualitatively useful. Use of synchrotron radiation for rapid and *in situ* determination of phase equilibrium are expected to increase the precision of these studies and to provide a better view of the Earth's interior.

I would like to conclude with a quotation from *Hamlet,* act I, scene V—"And therefore as a stranger give it welcome. There are more things in Heaven and Earth, Horatio, than are dreamt of in your philosophy."

ACKNOWLEDGMENTS

I wish to express my sincere thanks to Dr. G. J. Piermarini for many helpful discussions tracing the evolution of the DAC and for supplying so generously a catalogued set of all publications on the subject from the National Bureau of Standards. My grateful thanks are due to several colleagues in the high-pressure community for their ready response to my request for their publications, which saved me a lot of time, and for supplying me in some instances with figures. They are, in alphabetical order, Dr. W. A. Bassett, Dr. J. M. Besson, Dr. C. W. Chu, Dr. R. M. Hazen, Dr. W. B. Holzapfel, Dr. R. Jeanloz, Dr. M. H. Manghnani, Dr. H. K. Mao, Dr. A. K. McMahan, Dr. R. L. Mills, Dr. S. Minomura, Dr. M. Nicol, Dr. A. L. Ruoff, Dr. D. Schiferl, Dr. S. K. Sharma, Dr. I. F. Silvera, Dr. K. Syassen, and Dr. B. A. Weinstein. I wish to thank Dr. D. B. McWhan for critically reading the manuscript. The two referees made some very constructive suggestions, and I am indebted to them. My associate R. G. Maines helped me in several ways in the preparation of the manuscript and figures, and I am very much indebted to him. Mrs. Ellen Nagle expertly handled the job of typing the manuscript, and I wish to express my thanks to her.

REFERENCES

Adams, D. M., S. J. Payne, and K. M. Martin, 1973, Appl. Spectrosc. **27**, 377.
Adams, D. M., and S. K. Sharma, 1977a, J. Phys. **10**, 10.
Adams, D. M., and S. K. Sharma, 1977b, J. Phys. E **10**, 838.
Adams, D. M., and S. K. Sharma, 1979, Appl. Opt. **18**, 594.
Adams, D. M., S. K. Sharma, and R. Appleby, 1977, Appl. Opt. **16**, 2572.
Akella, J., O. Johnson, and R. N. Shock, 1980, J. Geophys. Res. **85**, 7056.
Asaumi, K., and S. Minomura, 1978, J. Phys. Soc. Jpn. **45**, 1061.
Asaumi, K., T. Mori, and Y. Kondo, 1982, Phys. Rev. Lett. **49**, 837.
Ashcroft, N. W., 1968, Phys. Rev. Lett. **21**, 1748.
Ashcroft, N. W., 1981, in *Physics of Solids Under High Pressure,* edited by J. S. Schilling and R. N. Shelton (North-Holland, Amsterdam), p. 155.
Balchan, A. S., and H. G. Drickamer, 1961, J. Chem. Phys. **34**, 1948.
Barnett, J. D., S. Block, and G. J. Piermarini, 1973, Rev. Sci. Instrum. **44**, 1.
Bassett, W. A., 1979 Annu. Rev. Earth Planet. Sci. **7**, 357.
Bassett, W. A., and E. M. Brody, 1977, in *High Pressure Research: Applications in Geophysics,* edited by M. H. Manghnani and S. Akimoto (Academic, New York), p. 519.
Bassett, W. A., and T. Takahashi, 1965, Am. Mineral. **50**, 1576.
Bassett, W. A., and T. Takahashi, 1974, in *Advanced High Pressure Research,* edited by R. H. Wentorf, Jr. (Academic, New York), Vol. 4, p. 165.
Bassett, W. A., T. Takahashi, and P. W. Stook, 1967, Rev. Sci. Instrum. **38**, 37.
Bassett, W. A., D. R. Wilbrun, J. A. Hrubec, and E. M. Brody, 1979, in *High Pressure Science and Technology,* edited by K. D. Timmerhaus and M. S. Barber (Plenum, New York), Vol. 2, p. 75.
Batlogg, B., and J. P. Remeika, 1980, Phys. Rev. Lett. **45**, 1126.
Batlogg, B., A. Jayaraman, J. E. Van Cleve, and R. G. Maines (to be published).

Baublitz, M. A., V. Arnold, and A. L. Ruoff, 1981, Rev. Sci. Instrum. **52**, 1616.
Bean, V. E., S. Akimoto, P. M. Bell, S. Block, W. B. Holzapfel, J. C. Jamieson, M. H. Manghnani, M. F. Nicol, G. J. Piermarini, and S. M. Stishov, 1982, in *High Pressure in Research and Industry,* Proceedings of the 8th AIRAPT Conference, Uppsala, edited by C. M. Backman, T. Johannisson, and L. Tegner (ISBN, Sweden), Vol. I, p. 144.
Bell, P. M., and H. K. Mao, 1975, in Carnegie Institution of Washington Year Book **74**, p. 399.
Bellussi, G., U. Benedict, and W. B. Holzapfel, 1981, J. Less-Common Met. **78**, 147.
Besson, J. M., J. Cernogora, M. L. Slade, B. A. Weinstein, and R. Zallen, 1981, Physica B **105**, 319.
Besson, J. M., and J. P. Pinceaux, 1979, Science **206**, 1073.
Bettini, M., 1974, Ph.D. dissertation, University of Stuttgart.
Blacha, A., M. Cardona, N. E. Christensen, S. Ves, and H. Overhof, 1982, Solid State Commun. **43**, 183.
Block, S., R. A. Forman, and G. J. Piermarini, 1977, in *High Pressure Research: Applications in Geophysics,* edited by M. H. Manghnani and S. Akimoto (Academic, New York), p. 503.
Block, S., and G. J. Piermarini, 1976, Phys. Today **29**, 44.
Block, S., C. E. Weir, and G. J. Piermarini, 1965, Science **148**, 947.
Born, M., and K. Huang, 1954, *Dynamical Theory of Crystal Lattices* (Clarendon, Oxford).
Brasch, J. W., A. J. Melveger, and E. R. Lippincott, 1968, Chem. Phys. Lett. **2**, 99.
Bukowinski, M. S. T., and J. Hauser, 1980, Geophys. Res. Lett. **7**, 689.
Buras, B., J. Staun, S. Olsen, L. Gerward, G. Will, and E. Hinze, 1977, J. Appl. Crystallogr. **10**, 431.
Bundy, F. P., and K. J. Dunn, 1979, J. Chem. Phys. **71**, 1550.
Carlone, C., N. K. Hota, H. J. Stolz, M. Ebert, and H. D. Hochheimer, 1981, J. Chem. Phys. **75**, 3220.
Carlone, C., D. Olego, A. Jayaraman, and M. Cardona, 1981, Phys. Rev. B **22**, 3877.
Chan, K. S., T. L. Huang, T. A. Grzybowski, T. J. Whetten, and A. L. Ruoff, 1982, J. Appl. Phys. (in press).
Chattopadhyay, T., C. Carlone, A. Jayaraman, and H. G. v. Schnering, 1981, Phys. Rev. B **23**, 2471.
Chattopadhyay, T., C. Carlone, A. Jayaraman, and H. G. v. Schnering, 1982, J. Phys. Chem. Solids **43**, 277.
Chu, C. W., A. P. Rusakov, S. Huang, S. Early, T. H. Geballe, and C. Y. Huang, 1978, Phys. Rev. B **18**, 2116.
Croft, M., and A. Jayaraman, 1980, Solid State Commun. **35**, 203.
Cromer, D. T., R. L. Mills, D. Schiferl, and L. A. Schwalbe, 1981, Acta Crystallogr. Sect. B **37**, 8.
d'Amour, H., H. B. Holzapfel, and M. Nicol, 1981, J. Phys. Chem. **85**, 130.
Decker, D. L., 1971, J. Appl. Phys. **42**, 3239.
Denner, W., W. Dieterich, H. Schulz, R. Keller, and W. B. Holzapfel, 1978, Rev. Sci. Instrum. **49**, 775.
Diatschenko, V., and C. W. Chu, 1981, Science **212**, 1393.
Drickamer, H. G., 1965, in *Solid-State Physics,* edited by F. Seitz and D. Turnbull (Academic, New York), Vol. 17, p. 1.
Drickamer, H. G., 1966, in *Solid-State Physics,* edited by F. Seitz and D. Turnbull (Academic, New York), Vol. 19, p. 135.
Drickamer, H. G., 1981, in *Physics of Solids Under High Pressure,* edited by J. S. Schilling and R. N. Shelton (North-Holland, Amsterdam), p. 3.
Driessen, A., J. A. deWall, and I. F. Silvera, 1979, J. Low Temp. Phys. **34**, 255.
Dunn, K. J., and F. P. Bundy, 1977, J. Chem. Phys. **67**, 5048.
Dunn, K. J., and F. P. Bundy, 1980, J. Chem. Phys. **72**, 2936.
Dunn, K. J., and F. P. Bundy, 1981, Phys. Rev. B **24**, 1643.
Duthie, J. C., and D. G. Pettifor, 1977, Phys. Rev. Lett. **38**, 564.
Falicov, L. M., W. Hanke, and M. P. Maple, Eds., 1981, *Valence Fluctuations in Solids* (North-Holland, Amsterdam).
Ferraro, J., and L. J. Basile, 1974, Appl. Spectrosc. **28**, 505.
Finger, L. W., R. M. Hazen, G. Zou, H. K. Mao, and P. M. Bell, 1981, Appl. Phys. Lett. **39**, 892.
Forman, R. A., G. J. Piermarini, J. D. Barnett, and S. Block, 1972, Science **176**, 284.
Friedli, C., and N. W. Ashcroft, 1977, Phys. Rev. B **16**, 662.
Fujii, Y., O. Shimomura, K. Takemura, S. Hoshino, and S. Minomura, 1980, J. Appl. Crystallogr. **13**, 284.
Fujishiro I., G. J. Piermarini, S. Block, and R. G. Munro, 1982, in *High Pressure in Research and Industry,* Proceedings of the 8th AIRAPT Conference Uppsala, edited by C. M. Backman, T. Johannisson, and L. Tegner (ISBN, Sweden) Vol. II, p. 608.
Glötzel, D., and A. K. McMahan, 1979, Phys. Rev. B **20**, 3210.
Gschneider, K. A., Jr., and L. Eyring, Eds., 1978, *Handbook of Physics and Chemistry* (North-Holland, Amsterdam).
Hama, J., and S. Matsui, 1981, Solid State Commun. **37**, 889.
Harrison, W. A., 1976, Phys. Rev. B **14**, 702.
Harrison, W. A., 1980, in *Electronic Structure and the Properties of Solids,* edited by P. Renz and K. Sargent (Freeman, San Francisco), p. 218.
Hazen, R. M., and L. W. Finger, 1977, in Carnegie Institution of Washington Year Book **76**, 655.
Hazen, R. M., and L. W. Finger, 1981, Rev. Sci. Instrum. **52**, 75.
Hazen, R. M., H. K. Mao, L. W. Finger, and P. M. Bell, 1980a, Appl. Phys. Lett. **37**, 288.
Hazen, R. M., H. K. Mao, L. W. Finger, and P. M. Bell, 1980b, in Carnegie Institution of Washington Year Book **79**, 348.
Hensley, W. K., W. A. Bassett, and J. R. Huizenga, 1973, Science **181**, 1164.
Hirsch, K. R., and W. B. Holzapfel, 1981, Rev. Sci. Instrum. **52**, 52.
Holzapfel, W. B., T. G. Ramesh, and K. Syassen, 1979, J. Phys. (Paris) Colloq. E **40**, 130.
Huber, G., K. Syassen, and W. B. Holzapfel, 1977, Phys. Rev. B **15**, 5123.
Huggins, F. E., H. K. Mao, and D. Virgo, 1975, in Carnegie Institution of Washington Year Book **74**, 405.
Ingalls, R., E. D. Cozier, J. E. Whitmore, A. J. Seary, and J. M. Tranquada, 1980, J. Appl. Phys. **51**, 3158.
Ingalls, R., G. A. Garcia, and E. A. Stern, 1978, Phys. Rev. Lett. **40**, 334.
Ingalls, R., J. M. Tranquada, J. E. Whitmore, and E. D. Cozier, 1981, in *Physics of Solids Under High Pressure,* edited by J. S. Schilling and R. N. Shelton (North-Holland, Amsterdam), p. 67.
Jamieson, J. C., A. W. Lawson, and N. D. Nachtrieb, 1959, Rev. Sci. Instrum. **30**, 1016.
Jayaraman, A., 1972, Phys. Rev. Lett. **29**, 1674.
Jayaraman, A., W. Lowe, L. D. Longinotti, and E. Bucher, 1976, Phys. Rev. Lett. **36**, 366.
Jayaraman, A., R. G. Maines, and E. Bucher, 1978, Solid State Commun. **27**, 709.
Jayaraman, A., V. Narayanamurti, E. Bucher, and R. G. Maines, 1970a, Phys. Rev. Lett. **25**, 368.
Jayaraman, A., V. Narayanamurti, E. Bucher, and R. G. Maines, 1970b, Phys. Rev. Lett. **25**, 1430.

Jayaraman, A., R. C. Newton, and J. M. McDonough, 1967, Phys. Rev. **159**, 527.
Jayaraman, A., A. K. Singh, A. Chatterjee, and S. Usha Devi, 1974, Phys. Rev. B **9**, 2513.
Johannson, B., and A. Rosengren, 1975, Phys. Rev. B **11**, 2836.
Johansson, B., H. L. Skriver, and O. K. Andersen, 1981, in *Physics of Solids Under High Pressure,* edited by J. S. Schilling and R. N. Shelton (North-Holland, Amsterdam), p. 245.
Kabalkina, S. S., T. N. Kolobiyana, and L. F. Vereshchagin, 1967, Sov. Phys.—Dokl. **12**, 50.
Keller, R., and W. B. Holzapfel, 1977, Rev. Sci. Instrum. **48**, 517.
Klement, W., Jr., and A. Jayaraman, 1967, in *Progress in Solid-State Chemistry,* edited by H. Reiss (Pergamon, London), Vol. 3, p. 289.
Kobayashi, T., T. Tei, K. Aoki, K. Yamamoto, and K. Abe, 1981, in *Physics of Solids Under High Pressure,* edited by J. S. Schilling and R. N. Shelton (North-Holland, Amsterdam), p. 141.
Lawson, A. W., and T. Y. Tang, 1950, Rev. Sci. Instrum. **21**, 815.
Leger, J. M., N. Yacoubi, and J. Loriers, 1979, in *Rare Earths in Modern Science and Technology,* edited by G. J. McCarthy, J. J. Rhyne, and H. B. Sibler (Plenum, New York), Vol. 2, p. 203.
LeSar, R., S. A. Ekberg, L. H. Jones, R. L. Mills, L. A. Schwalbe, and D. Schiferl, 1979, Solid State Commun. **32**, 131.
Lettieri, T. R., E. M. Brody, and W. A. Bassett, 1978, Solid State Commun. **26**, 235.
Liebenberg, D. H., 1979, Phys. Lett. A **73**, 74.
Liebenberg, D. H., R. L. Mills, and J. C. Bronson, 1979, in *High Pressure Science and Technology,* edited by K. D. Timmerhaus and M. S. Barber (Plenum, New York), Vol. 1, p. 395.
Liebenberg, D. H., R. L. Mills, J. C. Bronson, and L. C. Schmidt, 1978, Phys. Lett. A **67**, 162.
Liu, L. G., and W. A. Bassett, 1975, J. Geophys. Res. **80**, 3777.
Lynch, R. W., and H. G. Drickamer, 1966, J. Chem. Phys. **45**, 1020.
Makarenko, I., G. Weill, J. P. Itie, and J. M. Besson, 1982, Phys. Rev. (in press).
Manghnani, M. H., and S. Akimoto, Eds., 1977, *High Pressure Research: Application to Geophysics,* in Carnegie Institution of Washington Year Book.
Manghnani, M. H., L. C. Ming, and J. C. Jamieson, 1980, in *Nuclear Instruments and Methods* (North-Holland, Amsterdam), Vol. 177, p. 219.
Manghnani, M. H., E. F. Skelton, L. C. Ming, J. C. Jamieson, S. Qadri, D. Schiferl, and J. Balogh, 1981, in *Physics of Solids Under Pressure,* edited by J. S. Schilling and R. N. Shelton (North-Holland, Amsterdam), p. 47.
Mao, H. K., and P. M. Bell, 1976a, in Carnegie Institution of Washington Year Book **75**, 824.
Mao, H. K., and P. M. Bell, 1976b, Science **191**, 851.
Mao, H. K., and P. M. Bell, 1978a, in Carnegie Institution of Washington Year Book **77**, 904.
Mao, H. K., and P. M. Bell, 1978b, Science **200**, 1145.
Mao, H. K., and P. M. Bell, 1979a, in Carnegie Institution of Washington Year Book **78**, 659.
Mao, H. K., and P. M. Bell, 1979b, Science **203**, 1004.
Mao, H. K., and P. M. Bell, 1979c, J. Geophys. Res. **84**, 4533.
Mao, H. K., and P. M. Bell, 1980, in Carnegie Institution of Washington Year Book **79**, 409.
Mao, H. K., and P. M. Bell, 1981a, *Proceedings of the 17th Annual State of the Art Symposium* (American Chemical Society, Washington, D.C.), p. 105.
Mao, H. K., and P. M. Bell, 1981b, Rev. Sci. Instrum. **52**, 615.
Mao, H. K., P. M. Bell, K. J. Dunn, R. M. Chrenko, and R. C. Devries, 1979, Rev. Sci. Instrum. **50**, 1002.
Mao, H. K., P. M. Bell, J. W. Shaner, and D. J. Steinberg, 1978, J. Appl. Phys. **49**, 3276.
Mao, H. K., R. M. Hazen, P. M. Bell, and J. Wittig, 1981, J. Appl. Phys. **52**, 4572.
Mao, H. K., A. Mao, and P. M. Bell, 1982, Abstracts of the 8th AIRAPT Conference, Uppsala, edited by C. M. Backman, T. Johannisson, and L. Tegner (ISBN, Sweden) Vol. II, p. 453.
McMahan, A. K., 1982, in *High Pressure in Research and Industry,* Proceedings of the 8th AIRAPT Conference, Uppsala, edited by C. M. Backman, T. Johannisson, and L. Tegner (ISBN, Sweden) Vol. II, p. 453.
McMahan, A. K., B. L. Hord, and M. Ross, 1977, Phys. Rev. B **15**, 726.
McMahan, A. K., M. T. Yin, and M. L. Cohen, 1982, Phys. Rev. B **24**, 7210.
McWhan, D. B., J. D. Axe, and R. Youngblood, 1981, Phys. Rev. B **24**, 5391.
McWhan, D. B., R. M. Fleming, D. E. Moncton, and F. J. DiSalvo, 1980, Phys. Rev. Lett. **45**, 269.
Merrill, L., and W. A. Bassett, 1974, Rev. Sci. Instrum. **45**, 290.
Mills, R. L., D. H. Leibenberg, and J. C. Bronson, 1975, J. Chem. Phys. **63**, 4026.
Mills, R. L., D. H. Liebenberg, J. C. Bronson, and L. C. Schmidt, 1980, Rev. Sci. Instrum. **51**, 891.
Ming, L., and W. A. Bassett, 1974, Rev. Sci. Instrum. **45**, 1115.
Mon, K. K., N. W. Ashcroft, and G. V. Chester, 1980, Phys. Rev. B **21**, 2641.
Moore, M. J., D. B. Sorenson, and R. C. Devries, 1970, Rev. Sci. Instrum. **41**, 1665.
Moriarty, J. A., and A. K. McMahan, 1982, Phys. Rev. Lett. **48**, 809.
Müller, H., R. Trommer, M. Cardona, and P. Vogl, 1980, Phys. Rev. B **21**, 2641.
Müller, H., S. Ves, H. D. Hochheimer, M. Cardona, and A. Jayaraman, 1980, Phys. Rev. B **22**, 1052.
Munro, R. G., S. Block, and G. J. Piermarini, 1979, J. Appl. Phys. **50**, 6779.
Munro, R. G., G. J. Piermarini, and S. Block, 1979, J. Appl. Phys. **50**, 3180.
Nakamura, T., Y. Tominaga, M. Udagawa, S. Kojima, and M. Takashige, 1979, Solid State Commun. **32**, 95.
Nellis, W. J., and A. C. Mitchell, 1982 (to be published).
Nellis, W. J., M. van Thiel, and A. G. Mitchell, 1982, Phys. Rev. Lett. **48**, 816.
Nelson, D. A., and A. L. Ruoff, 1979, Phys. Rev. Lett. **42**, 383.
Nicol, M., K. R. Hirsch, and W. B. Holzapfel, 1979, Chem. Phys. Lett. **68**, 49.
Noack, R. A., and W. B. Holzapfel, 1979, in *High Pressure Science and Technology,* edited by K. D. Timmerhaus and M. S. Barber (Plenum, New York), Vol. 1, p. 748.
Olego, D., and M. Cardona, 1982, Phys. Rev. B **25**, 1151.
Olego, D., M. Cardona, and H. Müller, 1980, Phys. Rev. B **22**, 894.
Olego, D., M. Cardona, and P. Vogl, 1982, Phys. Rev. B **25**, 3878.
Parks, R. D., Ed., 1977, *Valence Instabilities and Related Narrow-Band Phenomena* (Plenum, New York).
Piermarini, G. J., and S. Block, 1975, Rev. Sci. Instrum. **46**, 973.
Piermarini, G. J., S. Block, and J. S. Barnett, 1973, J. Appl.

Phys. **44**, 5377.
Piermarini, G. J., S. Block, J. D. Barnett, and R. A. Forman, 1975, J. Appl. Phys. **46**, 2774.
Piermarini, G. J., R. A. Forman, and S. Block, 1978, Rev. Sci. Instrum. **49**, 1061.
Piermarini, G. J., F. A. Mauer, S. Block, A. Jayaraman, T. H. Geballe, and G. W. Hull, 1979, Solid State Commun. **32**, 275.
Piermarini, G. J., and C. E. Weir, 1962, J. Res. Natl. Bur. Stand., Sec. A **66**, 325.
Pistorius, C. W. F. T., 1976, in *Progress in Solid-State Chemistry,* edited by H. Reiss (Pergamon, London), Vol. 2, p. 1.
Postmus, C., V. A. Maroni, J. R. Ferraro, and S. S. Mitra, 1968, Inorg. Nucl. Chem. Lett. **4**, 269.
Probst, C., and J. Wittig, 1978, "Superconductivity: metals, alloys and compounds," in *Handbook on the Physics and Chemistry of Rare Earths,* edited by K. A. Gschneider, Jr. and L. Eyring (North-Holland, Amsterdam), Vol. 1, p. 749.
Ray, A. K., S. B. Trickey, R. S. Weidman, and A. B. Kunz, 1980, Phys. Rev. Lett. **45**, 933.
Riggleman, B. M., and H. G. Drickamer, 1963, J. Chem. Phys. **38**, 2721.
Roof, R. B., 1981, in *Advances in X-Ray Analysis,* edited by D. N. Smith, C. Barrett, D. E. Leyden, and P. K. Predecki (Plenum, New York), Vol. 24, p. 221.
Roof, R. B., R. G. Haire, D. Schiferl, L. A. Schwalbe, E. A. Konetho, and J. L. Smith, 1980, Science **207**, 1353.
Ross, M., and A. K. McMahan, 1976, Phys. Rev. B **13**, 5154.
Ross, M., and A. K. McMahan, 1980, Phys. Rev. B **21**, 1658.
Ross, M., and A. K. McMahan, 1981, in *Physics of Solids Under High Pressure,* edited by J. S. Schilling and R. N. Shelton (North-Holland, Amsterdam), p. 161.
Ross, M., and A. K. McMahan, 1982, Phys. Rev. B (in press).
Ross, M., and C. Shishkevish, 1977, ARPA Report No. R-2056.
Ruoff, A. L., 1979, in *High Pressure Science and Technology,* edited by K. D. Timmerhaus and M. S. Barber (Plenum, New York), Vol. 1, p. 754.
Ruoff, A. L., and M. A. Baublitz, Jr., 1981, in *Physics of Solids Under High Pressure,* edited by J. S. Schilling and R. N. Shelton (North-Holland, Amsterdam), p. 81.
Sakai, N., T. Kajiwara, K. Tsuji, and S. Minomura, 1982, Rev. Sci. Instrum. **53**, 499.
Schiferl, D., 1977, Rev. Sci. Instrum. **48**, 24.
Schiferl, D., D. T. Cromer, and R. L. Mills, 1978, High Temp.-High Pressures **10**, 493.
Schiferl, D., D. T. Cromer, and R. L. Mills, 1981, Acta Crystallogr. Sect. B **37**, 1329.
Schiferl, D., J. C. Jamieson, and J. E. Lenko, 1978, Rev. Sci. Instrum. **49**, 359.
Schwalbe, L. A., D. Schiferl, R. L. Mills, L. H. Jones, S. Ekberg, D. T. Cromer, R. LeSar, and J. Shaner, 1980, in *High Pressure Science and Technology,* edited by B. Vodar and P. H. Martean (Pergamon, Oxford), Vol. 2, p. 612.
Sharma, S. K., H. K. Mao, and P. M. Bell, 1980a, Phys. Rev. Lett. **44**, 886.
Sharma, S. K., H. K. Mao, and P. M. Bell, 1980b, in Carnegie Institution of Washington Year Book **79**, 359.
Shaw, R. W., and M. Nicol, 1981, Rev. Sci. Instrum. **52**, 1103.
Shimizu, H., E. M. Brody, H. K. Mao, and P. M. Bell, 1981, Phys. Rev. Lett. **47**, 128.
Shimomura, O., K. Takemura, and K. Aoki, 1982, in *High Pressure in Research and Industry,* Proceedings of the 8th AIRAPT Conference, Uppsala, edited by C. M. Blackman, T. Johannisson, and L. Tegner (ISBN, Sweden), Vol. I, p. 272.
Shimomura, O., K. Takemura, Y. Fujii, S. Minomura, M. Mori, Y. Noda, and Y. Yamada, 1978, Phys. Rev. B **18**, 715.
Shirakawa, T., and J. Nakai, 1981, in *Physics of Solids Under High Pressure,* edited by J. S. Schilling and R. N. Shelton (North-Holland, Amsterdam), p. 149.
Silvera, I. F., 1980, Rev. Mod. Phys. **52**, 393.
Silvera, I. F., and V. V. Goldman, 1978, J. Chem. Phys. **69**, 4209.
Silvera, I. F., and R. J. Wijngaarden, 1981, Phys. Rev. Lett. **47**, 39.
Skelton, E. F., I. Spain, S. C. Yu, C. Y. Liu, and E. R. Carpenter, Jr., 1977, Rev. Sci. Instrum. **48**, 879.
Skriver, H. L., 1981, in *Physics of Solids Under High Pressure,* edited by J. S. Schilling and R. N. Shelton (North-Holland, Amsterdam), p. 149.
Skriver, H. L., O. K. Andersen, and B. Johansson, 1980, Phys. Rev. Lett. **44**, 1230.
Smith, G. S., and J. Akella, J. Appl. Phys. (in press).
Soma, T., H. Matsuo, and Y. Saitoh, 1981a, Solid State Commun. **39**, 913.
Soma, T., H. Matsuo, and Y. Saitoh, 1981b, Solid State Commun. **39**, 1193.
Sonnenschein, R., K. Syassen, and A. Otto, 1981, J. Chem. Phys. **74**, 4315.
Spain, I. L., S. B. Qadri, C. S. Menoni, A. W. Webb, and E. F. Skelton, 1981, in *Physics of Solids Under High Pressure,* edited by J. S. Schilling and R. N. Shelton (North-Holland, Amsterdam), p. 73.
Spain, I. L., E. F. Skelton, and F. Rachford, 1980, in *High Pressure Science and Technology,* edited by B. Vodar and P. M. Martean (Pergamon, Oxford), Vol. 1, p. 150.
Syassen, K., 1982, Phys. Rev. B **25**, 6548.
Syassen, K., and W. B. Holzapfel, 1979, in *High Pressure Science and Technology,* edited by K. D. Timmerhaus and M. S. Barber (Plenum, New York), Vol. 1, p. 223.
Syassen, K., and M. Nicol, 1981, in *Physics of Solids Under High Pressure,* edited by J. S. Schilling and R. N. Shelton (North-Holland, Amsterdam), p. 319.
Syassen, K., and R. Sonnenschein, 1982, Rev. Sci. Instrum. **53**, 644.
Syassen, K., K. Takemura, H. Tups, and A. Otto, 1981, in *Physics of Solids Under High Pressure,* edited by J. S. Schilling and R. N. Shelton (North-Holland, Amsterdam), p. 125.
Syassen, K., G. Wortman, J. Feldhaus, K. H. Frank, and G. Kaindl, 1981, *ibid.* p. 319.
Takemura, K., S. Minomura, O. Shimomura, and Y. Fujii, 1980, Phys. Rev. Lett. **45**, 1881.
Trommer, R., E. Anastassakis, and M. Cardona, 1976, in *Light Scattering in Solids,* edited by M. Balkanski, R. C. C. Leite, and S. P. S. Porto (Flammarion, Paris), p. 396.
Trommer, R., H. Müller, M. Cardona, and P. Vogl, 1980, Phys. Rev. B **21**, 4869.
van Straaten, J., R. J. Wijngaarden, and I. F. Silvera, 1982, Phys. Rev. Lett. **48**, 97.
Van Valkenburg, A., 1965, Conference Internationale Sur-les-Hautes Pressions, LeCreusot, Saone-et-Loire, France.
Ves, S., and M. Cardona, 1981, Solid State Commun. **38**, 1109.
Ves, S., D. Glötzel, M. Cardona, and H. Overhof, 1981, Phys. Rev. B **24**, 2073.
Vogl, P., 1978, J. Phys. C **11**, 251.
Vohra, Y. K., H. Olijnik, W. Grosshans, and W. B. Holzapfel, 1981, Phys. Rev. Lett. **47**, 1065.
Webb, A. W., D. U. Gubser, and L. C. Towle, 1976, Rev. Sci. Instrum. **47**, 59.
Weber, W., 1974, Phys. Rev. Lett. **33**, 371.

Weinstein, B. A., 1977, Solid State Commun. **24**, 595.
Weinstein, B. A., and G. J. Piermarini, 1975, Phys. Rev. B **12**, 1172.
Weinstein, B. A., J. B. Renucci, and M. Cardona, 1973, Solid State Commun. **12**, 473.
Weinstein, B. A., and R. Zallen, 1982, in *Light Scattering in Solids,* edited by M. Cardona and G. Güntherodt (Springer, Berlin) (in press).
Weinstein, B. A., R. Zallen, and M. L. Slade, 1980, J. Non-Cryst. Solids **35-36**, 1255.
Weinstein, B. A., R. Zallen, M. L. Slade, and J. C. Mikkelsen, Jr., 1982, Phys. Rev. B **25**, 781.
Weir, C. E., S. Block, and G. J. Piermarini, 1965, J. Res. Natl. Bur. Stand., Sec. C **69**, 275.
Weir, C. E., E. R. Lippincott, A. Van Valkenburg, and E. N. Bunting, 1959, J. Res. Natl. Bur. Stand., Sec. A **63**, 55.
Welber, B., 1976, Rev. Sci. Instrum. **47**, 183.
Welber, B., 1977, Rev. Sci. Instrum. **48**, 395.
Welber, B., M. Cardona, C. K. Kim, and S. Rodriquez, 1975, Phys. Rev. B **12**, 5729.
Welber, B., M. Cardona, Y. F. Tsay, and B. Bendow, 1977, Phys. Rev. B **15**, 875.
Welber, B., and A. Jayaraman, 1979, J. Appl. Phys. **50**, 462.
Wendel, H., and R. M. Martin, 1979, Phys. Rev. B **19**, 5251.
Werner, A., and H. D. Hochheimer (unpublished).
Werner, A., H. D. Hochheimer, and A. Jayaraman, 1981, Phys. Rev. B **23**, 3836.
Werner, A., H. D. Hochheimer, A. Jayaraman, and E. Bucher, 1981, in *Physics of Solids Under High Pressure,* edited by J. S. Schilling and R. N. Shelton (North-Holland, Amsterdam), p. 295.
Werner, A., H. D. Hochheimer, A. Jayaraman, and J. M. Leger, 1981, Solid State Commun. **38**, 325.
Whitfield, C. H., E. M. Brody, and W. A. Bassett, 1976, Rev. Sci. Instrum. **47**, 942.
Wijngaarden, R. J., and I. F. Silvera, 1980, in *High Pressure Science and Technology,* edited by B. Vodar and P. H. Martean (Pergamon, Oxford), Vol. 1, p. 157.
Wittig, J., 1980, Z. Phys. B **38**, 11.
Yin, M. T., and M. L. Cohen, 1980, Phys. Rev. Lett. **45**, 1004.
Yin, M. T., and M. L. Cohen, 1981, Solid State Commun. **38**, 625.
Yin, M. T., and M. L. Cohen, 1982, Phys. Rev. B **26**, 3259.
Yu, P. Y., and B. Welber, 1978, Solid State Commun. **25**, 209.
Zallen, R., 1974, Phys. Rev. B **9**, 4485.
Zallen, R., and M. L. Slade, 1978, Phys. Rev. B **18**, 5775.
Zallen, R., B. A. Weinstein, and M. L. Slade, 1982, J. Phys. (Paris) (in press).
Zou, G., H. K. Mao, L. W. Finger, P. M. Bell, and R. M. Hazen, 1981, in *Physics of Solids Under High Pressure,* edited by J. S. Schilling and R. N. Shelton (North-Holland, Amsterdam), p. 137.